Distributed Formation Control of Multi-Agent Systems: Theory and Applications

A THESIS SUBMITTED TO THE UNIVERSITY OF MANCHESTER
FOR THE DEGREE OF DOCTOR OF PHILOSOPHY
IN THE FACULTY OF SCIENCE & ENGINEERING

2020

Junyan Hu
Department of Electrical and Electronic Engineering
School of Engineering

Contents

List of Figures **6**

Symbols **10**

Abbreviations **12**

Abstract **13**

Declaration **14**

Copyright Statement **15**

Publications **16**

Acknowledgements **18**

1 Introduction **20**

1.1 Background and Motivation 20

1.2 Thesis Organization 24

2 Preliminaries **27**

2.1 Matrix Theory 27

2.2 Linear System Theory 28

2.3 Lyapunov Stability Theory 29

2.4 Graph Theory 31

3 Distributed Adaptive Group Formation Tracking for Multi-Agent Systems 32

3.1 Introduction 32

3.2 Problem Formulation 35

3.3 Group Formation Controller Design 37

3.4 Application: Multi-Target Surveillance of Nonholonomic Mobile Robots . . 45

3.4.1 Robot Dynamics 46

3.4.2 Group Formation and Tracking 47

3.5 Conclusion 52

4 Two-Layer Fully Distributed Formation-Containment Control Scheme for Multi-Agent Systems 53

4.1 Introduction 53

4.2 Problem Formulation 57

4.3 Formation-Containment Control Protocol Design 59

4.4 Case Studies 71

4.4.1 Formation-Containment of Networked Satellites 71

4.4.2 Experimental Validation Results with Mobile Robots 75

4.5 Conclusions 79

5 Observer-Based Optimal Formation Control of Innovative Tri-Rotor UAVs Using Robust Feedback Linearization 81

5.1 Introduction 81

5.2 Mathematical Modeling 84

5.2.1 System Description 84

5.2.2 Dynamic Model 85

5.3 Control System Design 89

5.3.1 Robust Feedback Linearization 89

5.3.2 Distributed Optimal Formation Protocol Design 93

5.4 Simulation Results 99

5.5 Conclusion 103

6 Cooperative Control of Heterogeneous Connected Vehicle Platoons 105

6.1 Introduction 105

6.2 Technical Background and Problem Formulation 108

6.2.1 Communication Topology 108

6.2.2 Modelling of Heterogeneous Vehicles 108

6.2.3 Problem Formulation 110

6.3 Control Protocol Design 111

6.4 Nonlinear Simulation Results 115

6.5 Experimental Validation 118

6.5.1 Experimental Setup 118

6.5.2 Experimental Results 119

6.6 Conclusions 121

7 Conclusions **123**

7.1 Contributions 123

7.2 Future Works 125

Bibliography **126**

List of Figures

3.1 Group formation tracking control scheme proposed for multi-agent systems. 34

3.2 Interaction topology (a) before 60s and (b) after 60s. 47

3.3 Formation and sub-formation diagrams for the multi-robot system in $X-Y$ plane. 48

3.4 Time evolvement of the positions of the follower robots belonging to (a) Subgroup 1, (b) Subgroup 2, and (c) Subgroup 3. 48

3.5 Variation of the coupling gains c_i with respect to time. 50

3.6 Time-variation of 2-norms of the group formation tracking errors ξ_i. 51

4.1 A visual illustration of the formation containment activity involving six leader robots, two follower robots and a target (the quadrotor): (a) The leader robots have already achieved a hexagonal formation and keep tracking the target while the followers have entered into the sensing range of two right-most leaders; (b) The leaders detect the followers, start communicating with them and finally, make them converged into the convex hull (indicated by Green dotted lines) spanned by the positions of the leaders. 54

4.2 A two-layer multi-agent systems with directed communication topology. . . 72

4.3 Position of the agents at time instants: (a) $t = 0$s; (b) $t = 10$s; (c) $t = 20$s; (d) $t = 40$s. 73

4.4 Trajectory of the formation reference signal. 73

4.5 Variation of the coupling weights with respect to time. 74

4.6 Variations of the 2-norms of the (a) containment error (ς), and (b) formation error (ξ) with respect to time. 75

4.7 The autonomous mobile robot, Mona [1], used in the hardware experiment. 76

4.8 The directed communication topology among the robots considered in the hardware experiment. 76

4.9 Progress of the formation-containment mission being achieved by a team of six mobile robots in real-time hardware experiment. (a) Initial orientation of the robots at $t = 0$s; (b) At $t = 20$s: leader robots are about to attain the desired square formation; (c) At $t = 40$s: leaders have already achieved the formation and two follower robots have also converged into the area spanned by the leaders; (d) At $t = 80$s: the whole assembly of the leaders has moved towards the centre of the arena following the location of the given target along with the followers being surrounded by them – mission accomplished. 77

4.10 Position trajectories of the robots in the XY plane during the course of achieving formation tracking and containment in the hardware experiment under the application of the proposed FCC protocol. In this figure, the circles represent the leaders, the triangles denote the followers and the star indicates the target to be tracked. 78

4.11 Time variation of the 2-norms of (a) formation tracking error $\xi_i(t)$ of the leaders and (b) containment error $\varsigma_i(t)$ of the followers. 78

5.1 Coordinate systems of the tri-rotor UAV [2]. 85

5.2 Control system scheme: Distributed optimal formation control law and robust feedback linearization combining linear and nonlinear parts 92

5.3 Directed interaction topologies 100

5.4 3D trajectories of the tri-rotor swarm 101

5.5 3D shots of the tri-rotor swarm. (a) $t = 0$ s. (b) $t = 5$ s. (c) $t = 10$ s. (d) $t = 15$ s. (e) $t = 25$ s. (f) $t = 50$ s. 102

5.6 Attitude response of the tri-rotor swarm system. (a) Roll angle ϕ. (b) Pitch angle θ. (c) Yaw angle ψ. 103

5.7 Position response of the tri-rotor swarm system. (a) Longitudinal displacement x_v. (b) Lateral displacement y_v. (c) Vertical displacement z_v 103

6.1 A platoon of driverless vehicles in an automated highway system. 106

6.2 Cooperative control architecture of a heterogeneous and connected vehicle platoon in which the vehicle labelled with 0 acts as the leader while the rest $1, 2, \ldots, N$ vehicles are considered as followers. 109

6.3 Variety of communication topologies used in the simulation case study on the platoon control mission. (a) Topology 1: predecessor-following (PF); (b) Topology 2: two-predecessor following (TPF) and (c) Topology 3: to examine the response of the platoon in the event of link failure. 116

6.4 Simulation results shows the performance achieved by the proposed two-layer cooperative control scheme when applied to a platoon of six connected and heterogeneous vehicles of which one acts as the leader while rest five are followers. (a) Position $p_i(t)$, velocity $v_i(t)$, coupling weight $\xi_i(t)$ and spacing error $\varepsilon_i(t)$ for each of the vehicles in the platoon corresponding to Topology 1; (b) $p_i(t)$, $v_i(t)$, $\xi_i(t)$, $\varepsilon_i(t)$ corresponding to Topology 2; (c) $p_i(t)$, $v_i(t)$, $\xi_i(t)$, $\varepsilon_i(t)$ corresponding to Topology 3. 117

6.5 Hardware control loop associated with the experiment. Experimental arena includes overhead camera tracking system, base station (i.e. the desktop), aluminium framed glass platform and the Mona robots. 119

6.6 Experimental results: course of motion of a two-lane platoon containing six connected vehicles, all represented by Mona robots, in the experimental arena. (a) Initial rest position for all vehicles at $t = 0$s; (b) Lead vehicles has acquired the longitudinal motion from rest at $t > 0$; (c) Following vehicles gradually catch the velocity of the leaders and the desired inter-vehicular spacing is restored; and (d) At $t = 45$s, the platoon (both the lanes) reaches the other end of the arena – mission accomplished. 120

6.7 Time evolvement of position $p(t)$, velocity $v(t)$ and spacing error $\varepsilon(t)$ of the leader and following vehicles during the experiment with real Mona robots: (a) For the vehicles in Lane 1; (b) For the vehicles in Lane 2. 121

Symbols

$\lambda_i(A)$ The ith eigenvalue of matrix A; the eigenvalues of matrix A can be arranged as $\lambda_1(A) \leq \lambda_2(A) \leq \cdots \leq \lambda_n(A)$ when A is symmetric

$\mathbb{C}$ The set of complex numbers

$\mathbb{R}$ The set of real numbers

$\mathbb{R}^n$ The set of real vectors of dimension n

$\mathbb{R}^{m\times n}$ The set of real matrices of size $m \times n$

$\mathbb{R}_{>0}$ The set of positive real numbers

$\mathbb{R}_{\geq 0}$ The set of nonnegative real numbers

$\mathbf{0}_n$ A column vectors of size n with all entries equal to zero

$\mathbf{0}_{m\times n}$ A $m \times n$ matrix with all zeros

$\mathbf{1}_n$ A column vector of size n with all entries equal to one

$\mathcal{A}$ The adjacency matrix

$\mathcal{D}$ The in-degree matrix

$\mathcal{G}$ A graph

$\mathrm{diag}\{a_1, a_2, \cdots, a_N\}$ A diagonal matrix with diagonal entries a_1 to a_N

$\ker(A)$ The null space of matrix A

$\max\{\cdot\}$ The maximum elements

$\min\{\cdot\}$	The minimum elements
$\otimes$	The Kronecker product
$\|\cdot\|$	The standard L_2 Euclidean norm of a vector
A^{T}	The transpose of matrix A
$f : \mathbb{A} \to \mathbb{B}$	The function f with domain $\mathbb{A}$ and range $\mathbb{B}$
I_n	The $n \times n$ identity matrix

Abbreviations

ARE Algebraic Riccati Equation.

FCC Formation-Containment Control.

LQR Linear Quadratic Regulator.

MAS Multi-Agent System.

MIMO Multi-Input Multi-Output.

TGFT Time-Varying Group Formation Tracking.

UAV Unmanned Aerial Vehicle.

The University of Manchester

Junyan Hu
Doctor of Philosophy
Distributed Formation Control of Multi-Agent Systems: Theory and Applications
April 7, 2020

Formation control of networked multi-agent systems has earned significant research interest over the past two decades due to its potential applications in multi-disciplinary engineering problems, such as precision agriculture, space and planetary exploration, multi-target surveillance, cooperative transportation, etc. In contrast to a single specialized agent, a multi-agent system offers flexibility, scalability, reliability, robustness to faults and cost-effectiveness in solving complex and challenging tasks.

Firstly, two novel formation control techniques are proposed for linear multi-agent systems with directed communication topology. (i) A distributed adaptive group formation tracking protocol is proposed. In the proposed approach, the followers are distributed into several subgroups and each subgroup can track a desired sub-formation surrounding the respective leaders. When multiple leaders exist in a subgroup, the sub-formation attained by that subgroup keeps tracking a convex combination of the states of the leaders. Towards the end, a case study on multi-target surveillance operation is taken up to show an application of the proposed adaptive control technique. (ii) A two-layer fully distributed formation-containment control scheme is designed, where the states of the leaders attain a pre-specified time-varying/stationary formation and the states of the followers converge into the convex hull spanned by the states of the leaders. To achieve formation-containment, a set of fully distributed control protocols is developed utilizing the neighbouring state information, which enables the proposed scheme operate without using global information about the entire interaction topology. Simulation and experimental results are provided to demonstrate the feasibility and effectiveness of the proposed framework.

Secondly, a hierarchical control system is proposed for a novel Unmanned Aerial Vehicle (UAV) platform based on a three rotor configuration, where the three propellers can be tilted independently to obtain full force and torque vectoring authority. A robust feedback linearization controller is first developed to deal with this highly coupled and nonlinear dynamics of the proposed tri-rotor UAV, which linearizes the dynamics globally using geometric transformations. A distributed formation control tracking protocol and an optimal observer are then proposed to control a swarm of tri-rotor UAVs. The effectiveness of the designed control strategy is illustrated in a realistic virtual reality simulation environment based on real hardware parameters from a physical construction.

Finally, an automatic cruise control scheme is developed to maintain the string stability of a heterogeneous and connected vehicle platoon moving with constant spacing policy. A feedback linearization tool is first applied to transform the nonlinear vehicle dynamics into a linear heterogeneous state-space model and then a distributed adaptive control protocol has been designed to keep equal inter-vehicular spacing between any consecutive vehicles while maintaining a desired longitudinal velocity of the entire platoon. The proposed scheme utilizes only the neighbouring state information. Simulation results demonstrated the effectiveness of the proposed platoon control scheme. Moreover, the practical feasibility of the scheme was validated by hardware experiments with real robots.

Declaration

No portion of the work referred to in this thesis has been submitted in support of an application for another degree or qualification of this or any other university or other institute of learning.

Copyright Statement

Publications

Journal Papers:

1). **J.Hu**, P.Bhowmick, I.Jang, F.Arvin and A.Lanzon. 'A decentralized cluser formation containment framework for multi-robot systems.' *Manuscript submitted for review to* **IEEE Transactions on Robotics**.

2). **J.Hu**, P.Bhowmick and A.Lanzon. 'Two-layer distributed formation-containment control strategy for linear swarm systems: Algorithm and experiments.' *Manuscript submitted for review to* **International Journal of Robust and Nonlinear Control**.

3). **J.Hu**, P.Bhowmick, F.Arvin, A.Lanzon and B.Lennox. 'Cooperative control of heterogeneous connected vehicle platoons: An adaptive leader-following approach.' **IEEE Robotics and Automation Letters**, 5(2):977-984, 2020.

4). **J.Hu**, P.Bhowmick and A.Lanzon. 'Distributed adaptive time-varying group formation tracking for multiagent systems with multiple leaders on directed graphs.' **IEEE Transactions on Control of Network Systems**, 7(1):140-150, 2020.

5). **J.Hu** and A.Lanzon. 'Distributed finite-time consensus control for heterogeneous battery energy storage systems in droop-controlled microgrids.' **IEEE Transactions on Smart Grid**, 10(5):4751-4761, 2019.

6). **J.Hu** and A.Lanzon. 'An innovative tri-rotor drone and associated distributed aerial drone swarm control.' **Robotics and Autonomous Systems**, 103:162-174, 2018.

Conference Papers:

1). **J.Hu** and A.Lanzon. 'Cooperative adaptive time-varying formation tracking for multi-agent systems with LQR performance index and switching directed topologies.' **57th IEEE Conference on Decision and Control (CDC)**, Miami, USA, 2018.

2). **J.Hu** and A.Lanzon. 'Cooperative control of innovative tri-rotor drones using robust feedback linearization.' **12th UKACC International Conference on Control (CONTROL)**, Sheffield, UK, 2018.

3). O.Skeik, **J.Hu**, F.Arvin, and A.Lanzon. 'Cooperative control of integrator negative imaginary systems with application to rendezvous multiple mobile robots.' **12th International Workshop on Robot Motion and Control (RoMoCo)**, Poznan, Poland, 2019.

Acknowledgements

First and foremost, I would like to thank my supervisor Prof.Alexander Lanzon for his guidance and fruitful research discussions during the past three years. In my mind, Alexander is a true master of control engineering, who reaches a very high level in both theory and applications. It is my honor to be a PhD student under his supervision and I'm grateful for his trust in my abilities.

I would also like to thank Dr.Farshad Arvin and Prof.Barry Lennox for leading me into the area of robotics and offering me the Postdoctoral Research Associate position in UoM. I will treasure this precious opportunity and prove my research capacity in swarm intelligence and multi-robot systems during the following contract time.

I want to say thank you to my partner Dr.Parijat Bhowmick, we spent a lot of time discussing the strategies together and now all of our effort have paid off. Besides, I also thank all my friends and colleagues in Control Systems Group and Robotics Group for helping me and bringing me happiness.

Last but not the least, I owe my deepest gratitude to my wife Hong Zhu and my parents, who have provided me with unconditional love, support, and understanding throughout my life. In my eyes, Hong is the most kind and beautiful woman in this world.

To My Wife Hong

Chapter 1

Introduction

1.1 Background and Motivation

Cooperative control of multi-agent systems (MASs) is the study by which a large number of mostly homogeneous robots are coordinated to accomplish a desired mission in a collaborative manner [3–5]. MASs are usually distinguished by the following features: the robots in a swarm are operated via distributed control techniques; communication is limited in the sense that only neighbouring agents communicate among themselves; all robots in a swarm follow the same set of rules and work in unison to achieve a common goal [6, 7]; stability of a swarm system does not collapse even if some of the agents leave the network, or if some new agents join the network. Control strategies in MASs are primarily inspired from the behaviour of natural swarms, for example, swarms of ants, bees, birds and fishes [6, 7].

MASs have gained immense popularity in both theory and practice due to its adaptability to environmental changes, scalability, reliability, robustness to hardware and communication faults, high degree of parallelism and overall cost effectiveness compared to a single sophisticated robot [8, 9]. MASs are being applied in variety of real-world problems, for instance, in military applications (such as entrapment/escorting mission [6], target localization and mapping [10, 11], security surveillance [12–15], etc.); search, rescue and retrieval operations especially in hazardous environments (e.g., in nuclear power plants, in

earthquake-devastated areas, in extreme weather conditions, etc.) [16, 17]; in precision agriculture, smart farming and large-scale food production applications [18–21]; in space and planetary exploration [22, 23]; in cooperative transportation [24, 25]; in flocking and target localization [26]; etc. MASs have experienced rapid growth over the past two decades due to in part the emergence of consensus-based MAS theory and advancements in the cooperative control techniques [27–29].

Here, we present a precise and effective survey of the significant research work related to theory and applications of MASs, different types of control frameworks used in MASs and also, some popular cooperative control strategies such as formation tracking and containment. In [30], an image-based, partially distributed formation control framework has been proposed for multi-robot systems involving additional UAVs equipped with multiple on-board cameras used as control units. In [6], null-space based behavioural control techniques are proposed to achieve entrapment/escorting mission involving multiple mobile robots. In [31], constrained optimization method for multi-robot formation control in dynamic environments is presented where the robots adjust the parameters of the formation to avoid collisions with static and moving obstacles. The paper [31] also demonstrates two practical applications of the developed control technique in navigating a team of aerial vehicles in formation and in cooperative transportation by a small team of mobile manipulators. However, the robot swarm in the previous works is controlled via centralized control protocols, which largely increases the communication costs during the real-time implementation.

In order to reduce the network bandwidth and the cost involved due to huge communication infrastructure required for centralized control strategy, decentralized control schemes are now being widely used which depend only on the local information, that is, information from the neighbours. In [32], a distributed observer based formation control framework is developed to track the centroid of relative formations of a multi-robot system described with first-order dynamics. Moreover, in this paper, the theory has been validated on a real set-up with five mobile Khepera III robots. In [33], to tackle the issues like inconsistent range measurement or mismatches in inter-robot distances, these factors are considered as parameters in a gradient-based formation control law to achieve constant collective translation, rotation, or their combinations. The article [34] presents a distributed formation control technique for a team of aerial or ground robots to be operated in a dynamic environment.

The proposed methodology applies constrained optimization and multi-robot consensus to obtain the required parameters of the desired formation avoiding static and dynamic obstacles. In [35], a new type of leader-to-formation stability is introduced which addresses the safety, robustness and performance issues related to variety of formation interconnection structures. This notion has also found important applications in obstacle avoidance of leader-follower vehicle formations. In [36], a decentralized formation tracking control law is developed to ensure global exponential and concurrent synchronization of Lagrangian systems (e.g., robots, drones) in presence of dynamic networks having nonlinear and time-varying elements. The proposed theory has also been extended to multi-robot systems with non-identical dynamics and high degree of coupling. In [9], the authors have introduced a distributed, robust and scalable control protocol for large-scale swarm systems to attain complex formation shapes. The methodology [9] also invokes a probabilistic swarm guidance developed using in-homogeneous Markov chain algorithm. The articles [37–39] have explored modelling and formation control strategies for nonholonomic mobile robots including obstacle avoidance.

So far, we have discussed mostly the research contributions laid in the area of formation control of small-scale and large-scale swarm robotic systems. Similar to formation control, containment control is also an active research area where the followers are required to converge into the convex hull formed by the leaders. We highlight an example to explain the importance of containment control: Consider a group of mobile robots comprised of leaders and followers engaged in a rescue and navigation mission, where the leader robots have sensors to detect the obstacles but the followers does not. The leaders can navigate the followers safely towards the destination by detecting the obstacles in the path while the followers always stay inside a 'moving' safe zone generated by the leaders. In [40], a distributed containment control protocol is proposed for agents having double integrator dynamics in the presence of both static and dynamic leaders. In [41], the authors designed a discontinuous and a continuous distributed containment control laws for MASs with general linear dynamics and multiple leaders where the leaders may have separate control inputs. Moreover, the results are extended to output-feedback case and also, applied for MASs with matching uncertainties. The article [42] has addressed the problem of finite-time attitude containment control for multiple rigid bodies, for example, robot manipulators, space craft,

etc. In this work, the attitudes of the followers are constrained to stay within a limit decided by the attitudes of the leaders (in the form of a convex hull).

Most of aforementioned works have dealt with homogeneous robot swarms. However, it is investigated that many real-world tasks need heterogeneous robots to accomplish the task. In the recent years, heterogeneous MAS [7] is gaining prominence compared to the homogeneous swarm since the former provides more powerful and versatile framework for solving complex real-world problems which cannot be done by homogeneous robot agents. For instance, in a cooperative search and target localization problem, a synergistic integration of both aerial and ground vehicles is necessary to facilitate complementary capabilities and features [12]. Heterogeneity in a swarm can be structural or behavioural. For example, in a precision agriculture application, a proper coordination of both Unmanned Aerial Vehicles (UAVs) and Unmanned Ground Vehicles (UGVs) are required. Whereas, in some other application, a swarm of structurally homogeneous robots can be divided into different layers according to the assigned tasks. For instance, in the formation containment problem, the robots are categorized as leaders, followers and targets. In [43], a Lyapunov theory based decentralized formation control strategy is given for heterogeneous MASs and a rescue and surveillance operation involving a set of UAV and UGV agents is considered to show a prospective application. A decentralized navigation method is proposed in [44] for a heterogeneous swarm in which a single leader navigates other robots that have different translational and rotational velocity and acceleration, sensing distance and angle while maintaining global connectivity. In some applications, the robots in the swarm may also have different behaviors, for example, the robot swarm may split into different clusters and all the clusters can work together to achieve the collective goal. Variety of formation and containment control methodologies have been discussed in the research articles [45–48] from a theoretical perspective, but the papers did not include experimental results to validate their theory.

Motivated by the aforementioned progress and challenge of MASs and especially by the increasing need to develop state-of-art control techniques, in this thesis, we aim to develop advanced formation control theory and apply them into real applications.

1.2 Thesis Organization

This thesis is organized as follows:

Chapter 2: Preliminaries: Some related preliminaries including matrix theory, linear system theory, Lyapunov stability theory and basic algebraic graph theory are introduced.

Chapter 3: Distributed Adaptive Group Formation Tracking for Multi-Agent Systems: This chapter proposes a fully distributed control protocol that achieves time-varying group formation tracking for linear multi-agent systems connected via directed graph. The group formation tracking often leads to sub-formations especially when the leaders are placed far apart or they have separate control inputs. In the proposed approach, the followers are distributed into several subgroups and each subgroup attains the predefined sub-formation along with encompassing the leaders. Each subgroup can be assigned multiple leaders, contrary to the single-leader case considered in most of the existing literature, which makes the current problem non-trivial. When multiple leaders exist in a subgroup, the sub-formation attained by that subgroup keeps tracking a convex combination of the states of the leaders. A distributed adaptive control protocol has been introduced in this paper which uses only relative state information and thus avoids direct computation of the graph Laplacian matrix. Due to virtue of this, the proposed scheme remains effective even when some of the agents get disconnected from the network due to sudden communication failure. An algorithm is provided to outline the steps to design the control law to attain time-varying group formation tracking with multiple leaders. Towards the end, a case study on multi-target surveillance operation is taken up to show an important application of the proposed adaptive control technique. The results in this chapter have been published in [15].

Chapter 4: Two-Layer Fully Distributed Formation-Containment Control Scheme for Multi-Agent Systems: This chapter addresses the problem of designing a two-layer fully distributed formation-containment control scheme for linear time-invariant multi-agent systems with directed communication topology, where the states of the leaders attain a pre-specified time-varying/stationary formation and the states of the followers converge into the convex hull spanned by the states of the leaders. To achieve formation-containment,

a set of fully distributed control protocols is developed utilizing the neighbouring state information, which enables the proposed scheme operate without using global information about the entire interaction topology. The conditions to achieve formation-containment are suggested and a theoretical proof of the proposed scheme is also derived exploiting the Lyapunov stability approach. An algorithm is written to provide systematic guidelines on how to implement the control protocols in practice. It is argued that the consensus problem, formation tracking problem, and containment control problem can all be viewed as special cases of formation-containment. At the end, two case studies including simulations and real hardware experiments have been explored in detail to demonstrate the usefulness and effectiveness of the proposed scheme.

Chapter 5: Observer-Based Optimal Formation Control of Innovative Tri-Rotor UAVs Using Robust Feedback Linearization: This chapter presents a novel unmanned aerial vehicle platform based on a three rotor configuration, which can achieve the highest level of manoeuvrability in all 6 dimensions (i.e. 3D position and 3D attitude). The three propellers can be tilted independently to obtain full force and torque vectoring authority, such that this new aerial robotic platform can overcome the limitations of a classic quadrotor UAV that can not change its attitude while hovering at a stationary position. A robust feedback linearization controller is developed to deal with this highly coupled and nonlinear dynamics of the proposed tri-rotor UAV, which linearises the dynamics globally using geometric transformations to produce a linear model that matches the Jacobi linearization of the nonlinear dynamics at the operating point of interest. A distributed formation control tracking protocol is then proposed to control a swarm of tri-rotor UAVs. The 3D position and 3D attitude of each vehicle can be controlled independently to follow a desired time-varying formation. The effectiveness of the designed control strategy is illustrated in a realistic virtual reality simulation environment based on real hardware parameters from a physical construction. The results in this chapter have been published in [13].

Chapter 6: Cooperative Control of Heterogeneous Connected Vehicle Platoons: Automatic cruise control of a platoon of multiple connected vehicles in an automated highway system has drawn significant attention of the control practitioners over the past two decades due to its ability to reduce traffic congestion problems, improve traffic throughput and enhance safety of highway traffic. This chapter proposes a two-layer distributed control

scheme to maintain the string stability of a heterogeneous and connected vehicle platoon moving in one dimension with constant spacing policy assuming constant velocity of the lead vehicle. A feedback linearization tool is applied first to transform the nonlinear vehicle dynamics into a linear heterogeneous state-space model and then a distributed adaptive control protocol has been designed to keep equal inter-vehicular spacing between any consecutive vehicles while maintaining a desired longitudinal velocity of the entire platoon. The proposed scheme utilizes only the neighbouring state information (i.e. relative distance, velocity and acceleration) and the leader is not required to communicate with each and every one of the following vehicles directly since the interaction topology of the vehicle platoon is designed to have a spanning tree rooted at the leader. Simulation results demonstrated the effectiveness of the proposed platoon control scheme. Moreover, the practical feasibility of the scheme was validated by hardware experiments with real robots. The results in this chapter have been published in [49].

Chapter 7: Conclusions and Future Works: In the final chapter the contributions of this thesis are summarised and possible directions of future research are discussed.

Chapter 2

Preliminaries

This chapter is intended to be used as a quick reference for the understanding and derivation of the main results in the subsequent chapters. Some mathematical results needed to develop the main ideas of this thesis including matrix theory, linear system theory and graph theory are presented.

2.1 Matrix Theory

Definition 2.1.1 ([50]). The Kronecker product of $A \in \mathbb{R}^{m\times n}$ and $B \in \mathbb{R}^{p\times q}$ is defined as

$$A \otimes B = \begin{bmatrix} a_{11}B & \cdots & a_{1n}B \\ \vdots & \ddots & \vdots \\ a_{m1}B & \cdots & a_{mn}B \end{bmatrix},$$

and it has following properties:

1). $A \otimes (B+C) = A \otimes B + A \otimes C$,

2). $(kA) \otimes B = A \otimes (kB) = k(A \otimes B)$,

3). $(A \otimes B)(C \otimes D) = (AC) \otimes (BD)$,

4). $(A \otimes B)^{-1} = A^{-1} \otimes B^{-1}$,

5). $(A \otimes B)^{\mathrm{T}} = A^{\mathrm{T}} \otimes B^{\mathrm{T}}$,

6). if A and B are both positive definite (positive semi-definite), so is $A \otimes B$.

Note that A, B, C and D are the matrices with compatible dimensions for multiplication.

Definition 2.1.2 ([50]). A square matrix $A \in \mathbb{R}^{n\times n}$ is called a nonsingular M-matrix if all its off-diagonal elements are non-positive and all eigenvalues of A have positive real parts.

Lemma 2.1.1 ([51]). Let $L \in \mathbb{R}^{n\times n}$ be an M-matrix with $\det[L] \neq 0$. Then, there exists a positive definite matrix $G = \mathrm{diag}\{g_1, \ldots, g_N\}$ such that $GL + L^T G > 0$.

Lemma 2.1.2 ([52]). Suppose $a \in \mathbb{R}_{\geq 0}$, $b \in \mathbb{R}_{\geq 0}$, $p \in \mathbb{R}_{>0}$ and $q \in \mathbb{R}_{>0}$ such that $\frac{1}{p} + \frac{1}{q} = 1$, then $ab \leq \frac{a^p}{p} + \frac{b^q}{q}$. Moreover, $ab = \frac{a^p}{p} + \frac{b^q}{q}$ if and only if $a^p = b^q$.

2.2 Linear System Theory

Consider the following linear time-invariant system

$$\begin{cases} \dot{x}(t) = Ax(t) + Bu(t) \\ y(t) = Cx(t) + Du(t) \end{cases} \tag{2.1}$$

where $A \in \mathbb{R}^{n\times n}$, $B \in \mathbb{R}^{n\times m}$, $C \in \mathbb{R}^{q\times n}$, $D \in \mathbb{R}^{q\times m}$ and $x(t) \in \mathbb{R}^n$, $u(t) \in \mathbb{R}^m$ and $y(t) \in \mathbb{R}^q$ is the state, control input and control output, respectively.

Definition 2.2.1 ([53]). For any initial state $x(0)$, if there exists control input $u(t)$ such that the state $x(t)$ of system (2.1) can converge to the origin in a finite time, then system (2.1) is called controllable or (A,B) is controllable.

Lemma 2.2.1 ([53]). If rank $\left[B, AB, \ldots, A^{n-1}B\right] = n$, then $(A,B)$is controllable.

Lemma 2.2.2 ([53]). (PBH test for controllability) (A,B) is controllable if and only if rank $[sI - A, B] = n$ for all $s \in \mathbb{C}$.

Definition 2.2.2 ([53]). If for any $t_1 > 0$, the initial state $x(0)$ can be determined from the time history of the input $u(t)$ and the output $y(t)$ in the interval of $[0, t_1]$. Then the pair (C,A) is said to be observable.

Lemma 2.2.3 ([53]). If rank $\left[C^T, A^T C^T, \ldots, (A^{n-1})^T C^T\right] = n$, then $(C, A)$is observable.

Lemma 2.2.4 ([53]). (PBH test for observability) (C, A) is observable if and only if rank $\left[(sI - A)^T, C^T\right]^T = n$ for all $s \in \mathbb{C}$.

Definition 2.2.3 ([53]). If matrix A is Hurwitz, then system (2.1) is asymptotically stable.

Definition 2.2.4 ([53]). If there exists a matrix $K \in \mathbb{R}^{m \times n}$ such that $A + BK$ is Hurwitz, then system (2.1) is stabilizable or (A,B) is stabilizable.

Lemma 2.2.5 ([53]). System (2.1) is stabilizable if and only if rank $[sI - A, B] = n$ for all $s \in \mathbb{C}^+$, where $\mathbb{C}^+ = \{s | s \in \mathbb{C}, Re(s) \geq 0\}$ represents the closed right complex space.

Definition 2.2.5 ([53]). If there exists a matrix $K \in \mathbb{R}^{n \times q}$ such that $A + KC$ is Hurwitz, then system (2.1) is detectable or (A,B) is detectable.

Lemma 2.2.6 ([53]). System (2.1) is stabilizable if and only if rank $\left[(sI - A)^T, C^T\right]^T = n$ for all $s \in \mathbb{C}^+$.

2.3 Lyapunov Stability Theory

In this section, some basic stability analysis theorems are introduced.

Consider a nonlinear system

$$\dot{x} = f(x, t), \tag{2.2}$$

where $x \in \mathcal{U} \subset \mathbb{R}^n$ is the state of the system, $\mathcal{U} \subset \mathbb{R}^n$ is a domain with $x = 0$ as an interior point, and $f : \mathcal{U} \subset \mathbb{R}^n \times [0, +\infty) \to \mathbb{R}^n$ is a continuous function with $f(0, t) = 0$.

Definition 2.3.1 (Lyapunov stability, [54]). For the system (2.2), the equilibrium point $x = 0$ is said to be Lyapunov stable if for any given constant $R \in \mathbb{R}_{>0}$, there exists a constant r to ensure that $\|x(t)\| < R$, $\forall t > 0$ if $\|x(0)\| < r$. Otherwise, the equilibrium point is unstable.

Definition 2.3.2 (Asymptotic stability, [54]). For the system (2.2), the equilibrium point $x = 0$ is asymptotically stable if it is Lyapunov stable and furthermore $\lim_{t \to \infty} x(t) = 0$.

Definition 2.3.3 (Global asymptotic stability, [54])**.** If the asymptotic stability defined in Definition 2.3.2 holds for any initial state in $\mathbb{R}^n$, the equilibrium point is said to be globally asymptotically stable.

Definition 2.3.4 (Positive definite function, [54])**.** A function $V(x) \in \mathcal{U} \subset \mathbb{R}^n$ is said to be locally positive definite if $V(x) > 0$ for $x \in \mathcal{U}$ except at $x = 0$ where $V(x) = 0$. If $\mathcal{U} = \mathbb{R}^n$, i.e., the above property holds for the entire state space, $V(x)$ is said to be globally positive definite.

Definition 2.3.5 (Lyapunov function, [54])**.** If in $\mathcal{U} \in \mathbb{R}^n$ containing the equilibrium point $x = 0$, the function $V(x)$ is positive definite and has continuous partial derivatives, and if its time derivative along any state trajectory of system (2.2) is non-positive, i.e.,

$$\dot{V}(x) \leq 0,$$

then $V(x)$ is a Lyapunov function.

Definition 2.3.6 (Radially unbounded function, [54])**.** A positive definite function $V(x) : \mathbb{R}^n \longrightarrow \mathbb{R}$ is said to be radially unbounded if $V(x) \longrightarrow \infty$ as $\|x\| \longrightarrow \infty$.

Theorem 2.3.1 (Lyapunov theorem for global stability, [54])**.** For the system (2.2) with $\mathcal{U} \in \mathbb{R}^n$, if there exists a function $V(x) : \mathbb{R}^n \longrightarrow \mathbb{R}$ with first order derivatives such that

- $V(x)$ is positive definite
- $\dot{V}(x)$ is negative definite
- $V(x)$ is radially unbounded

then the equilibrium point $x = 0$ is globally asymptotically stable.

Definition 2.3.7 (Positively invariant set, [55])**.** A set M is a positively invariant set with respect to (2.2) if

$$x(0) \in M \Rightarrow x(t) \in M, \ \forall\, t \geq 0.$$

Theorem 2.3.2 (LaSalle's invariance principle, [55])**.** Let $\omega \subset \mathcal{U}$ be a compact set that is positively invariant with respect to (2.2). Let $V : \mathcal{U} \to \mathbb{R}$ be a continuously differentiable function such that $\dot{V}(x) \leq 0$ in $\mathcal{U}$. Let O be the set of all points in $\mathcal{U}$ where $\dot{V} = 0$. Let M be the largest invariant set in O. Then every solution starting in O approaches M as $t \to \infty$.

2.4 Graph Theory

Let $\mathcal{G} = (\mathcal{V}, \mathcal{E}, \mathcal{A})$ be a weighted and directed graph for which $\mathcal{V} = \{1, 2, \ldots, N\}$ is a nonempty set of nodes, $\mathcal{E} \subset \mathcal{V} \times \mathcal{V}$ is the set of edges and $\mathcal{A} = \left[a_{ij}\right] \in \mathbb{R}^{N \times N}$ is the adjacency matrix corresponding to the graph. An edge denoted by (i, j) indicates that information flows from node i to node j and, in this case, node i is considered as a neighbour of node j. a_{ij} is the weight of edge (j, i) and $a_{ij} \neq 0$ if $(j, i) \in \mathcal{E}$. In-degree matrix associated with $\mathcal{G}$ is defined as $\mathcal{D} = \text{diag}\{d_i\} \in \mathbb{R}^{N \times N}$ with $d_i = \sum_{j=1}^{N} a_{ij}$ and the Laplacian matrix $L \in \mathbb{R}^{N \times N}$ of $\mathcal{G}$ is given by $L = \mathcal{D} - \mathcal{A}$. If node i observes the leader, an edge $(0, i)$ is said to exist with weighting gain $g_i > 0$ as a pinned node. We denote the pinning matrix as $G = \text{diag}\left\{g_i\right\} \in \mathbb{R}^{N \times N}$. Within a directed graph, a spanning tree exists if the graph has a 'root' node having directed path to each of the remaining nodes. A directed graph without any cycle is termed as 'directed acyclic graph'.

Lemma 2.4.1 ([56]). If $\mathcal{G}$ contains a spanning tree, then zero is a simple eigenvalue of L with associated right eigenvector $\mathbf{1}_N$, and all the other $N - 1$ eigenvalues have nonnegative real parts.

Chapter 3

Distributed Adaptive Group Formation Tracking for Multi-Agent Systems

3.1 Introduction

Over the past two decades, cooperative as well as distributed control of MASs have drawn significant attention of the researchers from multiple disciplines of engineering and mathematics because of its wide applications in multi-robot cooperation [57–59], distributed sensor networks [60, 61], renewable energy storage systems [28], etc. This research domain primarily includes three topics – consensus control [27, 29, 62], containment control [41] and formation control [63]. Among them, formation control of MASs is a potential field of research that has witnessed an immense growth in the last fifteen years [64]. Time-invariant formation control of a swarm of quad-rotors has been reported in [65], while formation control of MASs on a time-varying trajectory is still an important issue which requires further attention.

Time-varying formation control of MASs involves rate of change of the formation states, which causes major challenges to design distributed control schemes. A 'bearing-based formation control' of a swarm of single integrator agents was introduced in [66] using the leader-first follower structure. Fixed-time formation control of an assembly of moving

robots considering the time-delay constraint was analyzed in [67]. Dynamic formation control for second-order MASs using graph Laplacian approach was studied in [68]. In [69], an affine formation maneuver control technique was proposed to configure a particular geometric pattern by the agents while achieving the desired maneuvers. Subsequently, time-varying formation control with application to unmanned aerial vehicles is investigated in [13,70,71]. However, in [13, 70, 71], the proposed control protocols utilize the smallest nonzero eigenvalue of the graph Laplacian matrix which indicates that the control schemes are not fully distributed [72]. To circumvent direct computation of the eigenvalues of the graph Laplacian matrix, distributed control protocols are now being widely used which depend only on the local information, that is, information from the neighbours. In this context, the work of [73] should be highlighted which proposes a fully distributed control protocol for MASs with an undirected graph. However, it has been found that MASs on undirected graphs suffer from lack of robustness and reliability especially when communication failure occurs and some of the agents get disconnected resulting in a change in the graph topology [72]. On the contrary, MASs connected via directed graphs are more reliable and offer some robustness to topology changes. In [74], a fully distributed control scheme was introduced to solve the output regulation problem for linear and heterogeneous MASs on a directed communication graph.

Formation control of MASs with a single leader has been studied extensively in [13,66–71], while a formation tracking problem with multiple leaders is a relatively unexplored area which needs more effort. Formation and tracking control of MASs having multiple targets (considered as leaders) are non-trivial and relatively more complex than single-leader operations [72]. Very often, in order to accomplish distributed tasks, a MAS may need to be decomposed into several subgroups, where each subgroup may contain multiple leaders. In the literature, the topic 'group formation tracking' deals with formation tracking of MASs containing multiple subgroups. In contrast to 'complete formation' which deals with only a single group, 'group formation' is more complicated and challenging since the latter involves interactions within each subgroup as well as among the subgroups and also, multiple 'sub-formations'. However, in many recent chapters, for instance in [13, 66–71], only formation tracking control problems are considered which urges more attention towards

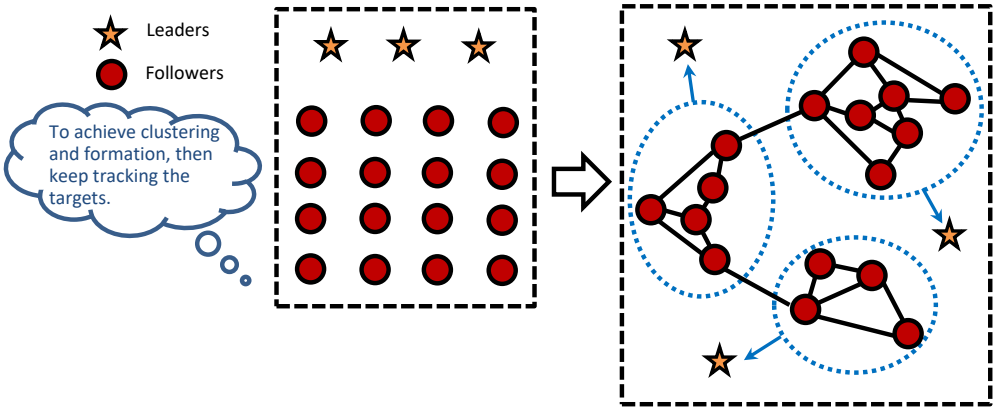

Figure 3.1: Group formation tracking control scheme proposed for multi-agent systems.

solving the group formation tracking problems. Applications like search and rescue operations, multi-target surveillances, etc., extensively rely on group formation tracking concepts involving multiple leaders where the leaders may also have some exogenous inputs. In [47,75–77], group consensus control problems specialized to first-order and second-order MASs have been addressed, but the techniques in general cannot be applied directly to solve time-varying group formation tracking (TGFT) problems for higher-order MASs. Thus the problem of distributed TGFT where each subgroup may have multiple leaders (or targets) deserves further research.

The aforementioned issues motivate us to investigate the TGFT problems for linear MASs on directed graph containing multiple leaders. The primary objective is to spread the agents into several subgroups and to achieve sub-formation for each individual subgroups along with reference tracking (as illustrated in Fig. 3.1). It is shown that consensus control, formation control and cluster control can all be viewed as particular scenarios of the TGFT problem addressed in this chapter. The contributions of this chapter can be summarized as follow:

1) The TGFT problem for MASs with directed communication graph is explored, where each subgroup is able to reach a desired sub-formation surrounding the respective leaders. In contrast with the existing literature, in this chapter, each subgroup can be assigned multiple leaders and the leaders may be subjected to bounded exogenous (either reference or disturbance) input independent of the other agents and their interactions;

2) The TGFT control protocol proposed in this chapter does not require the information

about the entire graph, unlike most of the existing formation control strategies. The proposed control law uses only the relative state information and thereby avoids explicit computation of the eigenvalues of the graph Laplacian matrix. Due to this, the control architecture becomes fully distributed, re-configurable and scalable for large-scale networked systems.

The rest of the chapter proceeds as follows. Section 3.2 discusses the problem statement. In Section 3.3, TGFT problem is solved via a Lyapunov approach using a nonlinear, adaptive and distributed control law. A case study on multi-target surveillance problem is given in Section 3.4 to highlight a potential application of the proposed scheme. Section 3.5 concludes the chapter mentioning several future research directions.

3.2 Problem Formulation

Consider that a MAS is comprised of N agents including M followers and $N-M$ leaders. Let $F = \{1,2,\ldots,M\}$ and $E = \{M+1, M+2,\ldots,N\}$ be the sets of the followers and leaders respectively. For any $i, j \in \{1,2,\ldots,N\}$, the weight of an interaction edge w_{ij} is defined as

$$w_{ij} = \begin{cases} 0 \text{ when } i = j \text{ or } (j,i) \notin \mathcal{E}, \\ b_j \text{ when } j \in E \text{ and } (j,i) \in \mathcal{E}, \\ a_{ij} \text{ when both } i, j \in F \text{ and } (j,i) \in \mathcal{E} \end{cases} \tag{3.1}$$

where $b_j \in \mathbb{R}_{>0}$ and $a_{ij} \in \mathbb{R}$ are known constants for all i and j, and $\mathcal{E}$ is the set of edges defined in Section 2.4.

The homogeneous leader and follower agents are described by the state-space equations

$$\dot{x}_i(t) = Ax_i(t) + Bu_i(t) \ \forall i \in \{1,2,\ldots,N\}, \tag{3.2}$$

where $x_i(t) \in \mathbb{R}^n$ and $u_i(t) \in \mathbb{R}^m$ are respectively the state and control input vectors of the ith agent $\forall t \geq 0$. $A \in \mathbb{R}^{n\times n}$ and $B \in \mathbb{R}^{n\times m}$ are constant matrices where $\text{rank}(B) = m$, $m \leq n$ and (A,B) is stabilizable.

Assumption 3.2.1. Let $u_k(t)$ $\forall k \in E$ represent the exogenous input for the kth leader which is independent of all the other agents and the network topology. We assume $\|u_k(t)\| \leq \sigma$ for all $t \geq 0$ for a given $\sigma \in \mathbb{R}_{\geq 0}$.

Then the Laplacian matrix L corresponding to the graph $\mathcal{G}$ can be partitioned as $L = \begin{bmatrix} L_1 & L_2 \\ 0_{(N-M)\times M} & 0_{(N-M)\times(N-M)} \end{bmatrix}$ where $L_1 \in \mathbb{R}^{M\times M}$ and $L_2 \in \mathbb{R}^{M\times(N-M)}$.

Let $h_F(t) = \left[h_1^T(t), h_2^T(t), \ldots, h_M^T(t)\right]^T$ generate the desired continuous differential formation where $h_i(t) \in \mathbb{R}^n$ for all $t \geq 0$ and all $i \in \{1, \ldots, M\}$ is a preset vector known to the ith follower.

Suppose the MAS (3.2) is decomposed into p subgroups $(p \geq 1)$ and accordingly, the node set $\mathcal{V}$ consists of $\mathcal{V}_1, \ldots, \mathcal{V}_p$ satisfying $\mathcal{V}_k \neq \emptyset$, $\mathcal{V} = \bigcup_{k=1}^{p} \mathcal{V}_k$ and $\mathcal{V}_k \bigcap \mathcal{V}_l = \emptyset$ for any $k, l \in \{1, 2, \ldots, p\}$ and $k \neq l$. Let $\bar{i} \in \{1, 2, \ldots, p\}$ denote the subscript of a subgroup and $\mathcal{G}_{\bar{i}}$ represents the part of the entire graph $\mathcal{G}$ which corresponds to the subgroup $V_{\bar{i}}$. $n_{\bar{i}}$ and $\hat{n}_{\bar{i}}$ denote respectively the numbers of followers and leaders in the subgroup $\mathcal{V}_{\bar{i}}$. Note, in a MAS, a leader agent must not have any neighbour, while a follower agent should have at least one neighbour. A follower is said to be 'well-informed' if it is connected to all the leaders and 'uninformed' if it is not connected to any of the leaders.

For any subgroup $\bar{i} \in \{1, 2, \ldots, p\}$, the desired time-varying sub-formation is characterized by the vector $\bar{h}_{\bar{i}}(t) = \left[h_{\varsigma_{\bar{i}}+1}^T(t), h_{\varsigma_{\bar{i}}+2}^T(t), \ldots, h_{\varsigma_{\bar{i}}+n_{\bar{i}}}^T(t)\right]^T$ where $\varsigma_{\bar{i}} = \sum_{k=0}^{\bar{i}-1} n_k$ with $n_0 = 0$ and each element in $\bar{h}_{\bar{i}}(t)$ is piece-wise continuously differentiable. It can be readily verified that $h_F(t) = \left[\bar{h}_1^T(t), \bar{h}_2^T(t), \ldots, \bar{h}_p^T(t)\right]^T$ reflects the formation vector for the entire MAS (3.2). $\bar{x}_{\bar{i}} = \left[x_{\varsigma_{\bar{i}}+1}^T(t), x_{\varsigma_{\bar{i}}+2}^T(t), \ldots, x_{\varsigma_{\bar{i}}+n_{\bar{i}}}^T(t)\right]^T$ and $\hat{x}_{\bar{i}} = \left[x_{\hat{\varsigma}_{\bar{i}}+1}^T(t), x_{\hat{\varsigma}_{\bar{i}}+2}^T(t), \ldots, x_{\hat{\varsigma}_{\bar{i}}+\hat{n}_{\bar{i}}}^T(t)\right]^T$ represent the state vector of the followers and the leaders respectively of the $\bar{i}^{th}$ subgroup, where $\hat{\varsigma}_{\bar{i}} = M + \sum_{k=0}^{\bar{i}-1} \hat{n}_k$ with $\hat{n}_0 = 0$.

A MAS is said to achieve time-varying group formation tracking (TGFT) with multiple leaders if for any given bounded initial states

$$\lim_{t\to\infty} \left(\bar{x}_{\bar{i}}(t) - \bar{h}_{\bar{i}}(t) - \mathbf{1}_{n_{\bar{i}}} \sum_{k=\hat{\varsigma}_{\bar{i}}+1}^{\hat{\varsigma}_{\bar{i}+\hat{n}_{\bar{i}}}} \alpha_k x_k(t) \right) = 0 \tag{3.3}$$

for all $\bar{i} \in \{1, 2, \ldots, p\}$, where α_k is a positive constant that satisfies $\sum_{k=\hat{\varsigma}_{\bar{i}}+1}^{\hat{\varsigma}_{\bar{i}+\hat{n}_{\bar{i}}}} \alpha_k = 1$.

The problem statement considered here is to develop a fully distributed control technique for a MAS given in (3.2) to achieve sub-formations when the followers are divided into several subgroups and each subgroup is assigned one or multiple leaders to track.

3.3 Group Formation Controller Design

Motivated by [78], a TGFT control protocol is constructed below

$$\begin{cases} u_i = (c_i + \rho_i)K\xi_i + \gamma_i - \mu f(\xi_i) \\ \dot{c}_i = \xi_i^T \Gamma \xi_i \end{cases} \forall i \in F \tag{3.4}$$

where $\xi_i = \sum_{j=1}^{M} w_{ij}\big[(x_i - h_i) - (x_j - h_j)\big] + \sum_{k=M+1}^{N} w_{ik}\big[(x_i - h_i) - x_k\big]$ denotes the group formation tracking error; $c_i(t)$ with $c_i(0) > 0$ represents the coupling weight assigned to the ith agent; $\mu > 0$, $K \in \mathbb{R}^{m\times n}$ and $\Gamma \in \mathbb{R}^{n\times n}$ are all constant controller parameters to be selected appropriately; ρ_i and γ_i are continuously differentiable functions of ξ_i and h_i respectively; and $f(\cdot)$ is a nonlinear function to be determined later.

Let $x_F = \big[x_1^T, \ldots, x_M^T\big]^T$, $x_E = \big[x_{M+1}^T, \ldots, x_N^T\big]^T$, $u_E = \big[u_{M+1}^T, \ldots, u_N^T\big]^T$, $\gamma = \big[\gamma_1^T, \gamma_2^T, \ldots, \gamma_M^T\big]^T$ and $F(\xi) = \big[f^T(\xi_1), f^T(\xi_2), \ldots, f^T(\xi_M)\big]^T$ denote a few shorthand. The closed-loop system dynamics of the MAS (3.2) embedded with the TGFT control protocol (3.4) can be expressed in a structured form as

$$\begin{cases} \dot{x}_F = \big[I_M \otimes A + (C+\rho)L_1 \otimes BK\big]x_F + \big[(C+\rho)L_2 \otimes BK\big]x_E + (I_M \otimes B)\gamma \\ \qquad - \big[(C+\rho)L_1 \otimes BK\big]h_F - \mu(I_M \otimes B)F(\xi), \\ \dot{x}_E = (I_{N-M} \otimes A)x_E + (I_{N-M} \otimes B)u_E, \end{cases} \tag{3.5}$$

where $C = \mathrm{diag}\{c_1, \ldots, c_M\}$ and $\rho = \mathrm{diag}\{\rho_1, \ldots, \rho_M\}$.

Assumption 3.3.1. For each subgroup, at least one leader should exist which provides a reference trajectory to the followers. Any follower in a given subgroup is assumed to be either well-informed or uninformed. If a follower belongs to the uninformed category, then it is connected to at least one well-informed follower via a directed path to it.

Assumption 3.3.2. The subsets $\mathcal{V}_1, \mathcal{V}_2, \ldots, \mathcal{V}_p$ of the node set $\mathcal{V}$ do not form any cycle among them.

Based on Assumption 3.3.2, L_1 has a particular structure as shown below [47]

$$L_1 = \begin{bmatrix} L_{11} & 0 & \cdots & 0 \\ L_{21} & L_{22} & \cdots & 0 \\ \vdots & \vdots & \ddots & \vdots \\ L_{p1} & L_{p2} & \cdots & L_{pp} \end{bmatrix}, \tag{3.6}$$

where $L_{\bar{i}\bar{i}}$ is the Laplacian matrix corresponding to $\mathcal{G}_{\bar{i}}$, and $L_{\bar{i}\bar{j}}$ and $L_{\bar{j}\bar{i}}$ together express the mutual interaction between the $\bar{i}^{th}$ and $\bar{j}^{th}$ subgroups where $\bar{i},\bar{j} \in \{1,\dots,p\}$ and $\bar{i} \neq \bar{j}$.

Assumption 3.3.3. Every row-sum of $L_{\bar{i}\bar{j}}$ is zero when $\bar{j} < \bar{i}$ for $\bar{i},\bar{j} \in \{1,\dots,p\}$.

Remark 3.3.1. If two subgroups are connected via positive edges (i.e., edges having positive weights), then the subgroups interact in a 'cooperative' relation. On the contrary, if they are connected via negative edges, then the subgroups respond to each other in a 'competitive' relation. Both these modes exist together in a MAS and ensure that all the subgroups work in unison to achieve individual sub-formations along with tracking the respective leaders.

Lemma 3.3.1. If Assumptions 3.3.1-3.3.3 are satisfied, then $-L_1^{-1}L_2$ has the following form

$$-L_1^{-1}L_2 = \begin{bmatrix} e_1 & 0 & \cdots & 0 \\ 0 & e_2 & \cdots & 0 \\ \vdots & \vdots & \ddots & \vdots \\ 0 & 0 & \cdots & e_p \end{bmatrix}, \tag{3.7}$$

where $e_{\bar{i}} = \mathbf{1}_{n_{\bar{i}}}[b_{\hat{\varsigma}_{\bar{i}}+1}, b_{\hat{\varsigma}_{\bar{i}}+2}, \dots, b_{\hat{\varsigma}_{\bar{i}+\hat{n}_{\bar{i}}}}]/\sum_{k=\hat{\varsigma}_{\bar{i}}+1}^{\hat{\varsigma}_{\bar{i}+\hat{n}_{\bar{i}}}} b_k$.

Proof. We start with only one leader associated with each subgroup. For the $\bar{i}^{th}$ subgroup, let the vector $\hat{e}_{\bar{i}} \in \mathbb{R}^{n_{\bar{i}}}$ have $\sum_{j=\hat{\varsigma}_{\bar{i}}+1}^{\hat{\varsigma}_{\bar{i}}+\hat{n}_{\bar{i}}} w_{(\varsigma_{\bar{i}}+i),j}$ as its ith element if the ith agent of this subgroup observes the leader, and all the other entries are 0. If Assumptions 3.3.1-3.3.3 hold, then $L_{\bar{i}\bar{i}}$ is non-singular $\forall \bar{i} \in \{1,\dots,p\}$ and we can express $\hat{e}_{\bar{i}} = L_{\bar{i}\bar{i}}\mathbf{1}_{n_{\bar{i}}}$, which readily implies

$$L_{\bar{i}\bar{i}}^{-1}\hat{e}_{\bar{i}} = \mathbf{1}_{n_{\bar{i}}}. \tag{3.8}$$

Let $\bar{e}_j \in \mathbb{R}^{\hat{n}_{\bar{i}}}$ $(j \in \{\hat{\varsigma}_{\bar{i}}+1,\dots,\hat{\varsigma}_{\bar{i}}+\hat{n}_{\bar{i}}\})$ with 1 as its $(j-\hat{\varsigma}_{\bar{i}})$th component and 0 elsewhere. Post-multiplying both the sides of (3.8) by $\bar{e}_j^T b_j/\sum_{k=\hat{\varsigma}_{\bar{i}}+1}^{\hat{\varsigma}_{\bar{i}+\hat{n}_{\bar{i}}}} b_k$, we get

$$L_{\bar{i}\bar{i}}^{-1}\hat{e}_{\bar{i}}\bar{e}_j^T(b_j/\sum_{k=\hat{\varsigma}_{\bar{i}}+1}^{\hat{\varsigma}_{\bar{i}+\hat{n}_{\bar{i}}}} b_k) = \mathbf{1}_{n_{\bar{i}}}\bar{e}_j^T(b_j/\sum_{k=\hat{\varsigma}_{\bar{i}}+1}^{\hat{\varsigma}_{\bar{i}+\hat{n}_{\bar{i}}}} b_k). \tag{3.9}$$

It can be found that

$$\begin{aligned} &\sum_{j=\hat{\varsigma}_{\bar{i}}+1}^{\hat{\varsigma}_{\bar{i}+\hat{n}_{\bar{i}}}} \left(\mathbf{1}_{n_{\bar{i}}}\bar{e}_j^T(b_j/\sum_{k=\hat{\varsigma}_{\bar{i}}+1}^{\hat{\varsigma}_{\bar{i}+\hat{n}_{\bar{i}}}} b_k) \right) \\ &= (1/\sum_{k=\hat{\varsigma}_{\bar{i}}+1}^{\hat{\varsigma}_{\bar{i}+\hat{n}_{\bar{i}}}} b_k)(\mathbf{1}_{n_{\bar{i}}} \otimes [b_{\hat{\varsigma}_{\bar{i}}+1}, b_{\hat{\varsigma}_{\bar{i}}+2}, \dots, b_{\hat{\varsigma}_{\bar{i}+\hat{n}_{\bar{i}}}}]) \\ &= e_{\bar{i}}. \end{aligned} \tag{3.10}$$

From (3.9) and (3.10), we have

$$L_{\bar{i}\bar{i}}e_{\bar{i}} = \sum_{j=\hat{\varsigma}_{\bar{i}}+1}^{\hat{\varsigma}_{\bar{i}+\hat{n}_{\bar{i}}}} \hat{e}_{\bar{i}}\bar{e}_j^T (b_j / \sum_{k=\hat{\varsigma}_{\bar{i}}+1}^{\hat{\varsigma}_{\bar{i}+\hat{n}_{\bar{i}}}} b_k). \tag{3.11}$$

Then we have

$$\begin{aligned} L_1 \begin{bmatrix} e_1 & 0 & \cdots & 0 \\ 0 & e_2 & \cdots & 0 \\ \vdots & \vdots & \ddots & \vdots \\ 0 & 0 & \cdots & e_p \end{bmatrix} \\ = \begin{bmatrix} L_{11}e_1 & 0 & \cdots & 0 \\ 0 & L_{22}e_2 & \cdots & 0 \\ \vdots & \vdots & \ddots & \vdots \\ 0 & 0 & \cdots & L_{pp}e_p \end{bmatrix} \\ = -L_2. \end{aligned} \tag{3.12}$$

Since L_1 is non-singular, the conclusion is straightforward from (3.12). □

Since B is assumed to have full rank m, there exists the pseudo inverse $\tilde{B} \in \mathbb{R}^{m\times n}$ such that $\tilde{B}B = I_m$. We can also choose another matrix $\bar{B} \in \mathbb{R}^{(n-m)\times n}$ depending on the left null space of B such that $\bar{B}B = 0$ and $\left[\tilde{B}^T, \bar{B}^T\right]^T$ is non-singular.

Theorem 3.3.1 is the main contribution of this chapter which establishes the conditions to be satisfied by the MAS (3.2) to achieve TGFT applying the fully distributed and nonlinear control protocol proposed in (3.4), provided the agents and the network hold certain properties. Moreover, the leaders are subjected to exogenous (either reference or disturbance) inputs independent of the dynamics of the agents and the network topology.

Theorem 3.3.1. Suppose Assumptions 3.2.1-3.3.3 hold and for a given $\sigma \geq 0$, the positive constant μ satisfies

$$\mu > \sigma. \tag{3.13}$$

If the following formation feasibility condition

$$\bar{B}Ah_i - \bar{B}\dot{h}_i = 0 \tag{3.14}$$

is satisfied for a given set of $h_i(t) \in \mathbb{R}^n$ for all $t \geq 0$ and for all $i \in F$, then TGFT is achieved by the MAS (3.2) on applying the fully distributed and nonlinear control protocol given in

(3.4) with $K = -R^{-1}B^TP$, $\Gamma = PBR^{-1}B^TP$, $\gamma_i = \tilde{B}\dot{h}_i - \tilde{B}Ah_i$ and $\rho_i = \xi_i^T P\xi_i$, where $P > 0$ is the solution of the algebraic Riccati equation (ARE)

$$A^TP + PA + Q - PBR^{-1}B^TP = 0 \tag{3.15}$$

for given $Q > 0$ and $R > 0$. The nonlinear function $f(\cdot)$ used in (3.4) is specified as

$$f(\xi_i(t)) = \begin{cases} \frac{B^TP\xi_i(t)}{\|B^TP\xi_i(t)\|} & \text{when } \left\|B^TP\xi_i(t)\right\| \neq 0; \\ 0 & \text{when } \left\|B^TP\xi_i(t)\right\| = 0; \end{cases} \tag{3.16}$$

for all $i \in F$.

Proof. Since via Assumption 3.3.1, each subgroup contains a directed spanning tree, it can be proved that all the eigenvalues of $L_{\bar{i}\bar{i}}$ have positive real part for all $\bar{i} \in \{1,\ldots,p\}$ [72]. Applying Lemma 2.1.1, there exists a real diagonal matrix $\Xi_{\bar{i}} > 0$ such that

$$\Xi_{\bar{i}}L_{\bar{i}\bar{i}} + L_{\bar{i}\bar{i}}^T\Xi_{\bar{i}} > 0 \; \forall \bar{i} \in \{1,2,\ldots,p\}. \tag{3.17}$$

Define block diagonal matrices $\Xi = \text{diag}\{\Xi_1,\ldots,\Xi_p\}$ and $\Delta = \text{diag}\{\delta_1 I_{n_1},\ldots,\delta_p I_{n_p}\}$ where $\delta_{\bar{i}} > 0$ are required to be chosen such that $\Delta\Xi L_1 + L_1^T\Delta\Xi > 0$ holds. Now, we will show that there always exists a set of $\delta = \{\delta_1,\ldots,\delta_p\}$ such that the relation $\Delta\Xi L_1 + L_1^T\Delta\Xi > 0$ holds.

Let $\Theta_{\bar{i}} = \Xi_{\bar{i}}L_{\bar{i}\bar{i}} + L_{\bar{i}\bar{i}}^T\Xi_{\bar{i}}$ and

$$\Phi_{\bar{i}} = \begin{bmatrix} \delta_1\Theta_1 & \delta_2 L_{21}^T\Xi_2 & \cdots & \delta_{\bar{i}}L_{\bar{i}1}^T\Xi_{\bar{i}} \\ \delta_2\Xi_2L_{21} & \delta_2\Theta_2 & \cdots & \delta_{\bar{i}}L_{\bar{i}2}^T\Xi_{\bar{i}} \\ \vdots & \vdots & \ddots & \vdots \\ \delta_{\bar{i}}\Xi_{\bar{i}}L_{\bar{i}1} & \delta_{\bar{i}}\Xi_{\bar{i}}L_{\bar{i}2} & \cdots & \delta_{\bar{i}}\Theta_{\bar{i}} \end{bmatrix} \; \forall \bar{i} \in \{1,\ldots,p\}.$$

For $\bar{i} = 2$, applying Schur Complement Lemma [79], we obtain $\Phi_2 > 0$ if and only if there exist $\delta_1 > 0$ and $\delta_2 > 0$ such that $\delta_1\Theta_1 > 0$ and

$$\delta_1\Theta_1 - \delta_2 L_{21}^T\Xi_2\Theta_2^{-1}\Xi_2L_{21} > 0. \tag{3.18}$$

Since $\Theta_1 > 0$ and $\Theta_2 > 0$ via (3.17), we can always find a δ_2 sufficiently smaller that δ_1 such that (3.18) holds. The same arguments can be pursued to prove [47] that there always exist $\delta_1 > \delta_2 > \cdots > \delta_p$ such that $\Phi_p = \Delta\Xi L_1 + L_1^T\Delta\Xi > 0$ invoking (3.17).

Let the global formation tracking error be $\xi_F = [\xi_1^T,\ldots,\xi_M^T]^T$. Define $z_i = x_i - h_i \; \forall i \in F$ and $z_F = [z_1^T,\ldots,z_M^T]^T$. Now ξ_F can be written in a compact form as

$$\xi_F = (L_1 \otimes I_n)z_F + (L_2 \otimes I_n)x_E. \tag{3.19}$$

Substituting (3.5) into the derivative of (3.19), the expressions for $\dot{\xi}_F$ and $\dot{c}_i$ are obtained as

$$\begin{cases} \dot{\xi}_F = \big[I_M \otimes A + L_1(C+\rho)\otimes BK\big]\xi_F + (L_1\otimes A)h_F - (L_1\otimes I_n)\dot{h}_F \\ \qquad + (L_1\otimes B)\gamma + (L_2\otimes B)u_E - \mu(L_1\otimes B)F(\xi), \\ \dot{c}_i = \xi_i^T\Gamma\xi_i. \end{cases} \tag{3.20}$$

Consider the following Lyapunov function candidate

$$V_1 = \sum_{i=1}^{M}\frac{1}{2}\varphi_i(2c_i+\rho_i)\rho_i + \frac{1}{2}\sum_{i=1}^{M}\varphi_i(c_i-\beta)^2 \tag{3.21}$$

where $\Delta\Xi = \mathrm{diag}\{\varphi_1,\ldots,\varphi_M\}$ is a positive definite matrix with $\varphi_i \in \mathbb{R}_{>0}\ \forall i \in F$ such that $\Delta\Xi L_1 + L_1^T\Delta\Xi > 0$, and β is a positive constant to be determined later. As $c_i(0) > 0$ for all $i \in F$, it follows from $\dot{c}_i(t) \geq 0$ that $c_i(t) > 0$ for all $t > 0$. Therefore, V_1 is positive definite and $V_1 = 0$ when $\xi_i = 0\ \forall i \in F$.

Now, the time derivative of V_1 along any trajectory of (3.20) is given by

$$\begin{aligned} \dot{V}_1 &= \sum_{i=1}^{M}[\varphi_i(c_i+\rho_i)\dot{\rho}_i + \varphi_i\rho_i\dot{c}_i] + \sum_{i=1}^{M}\varphi_i(c_i-\beta)\dot{c}_i \\ &= \sum_{i=1}^{M}2\varphi_i(c_i+\rho_i)\xi_i^T P\dot{\xi}_i + \sum_{i=1}^{M}\varphi_i(\rho_i+c_i-\beta)\dot{c}_i. \end{aligned} \tag{3.22}$$

Note that

$$\sum_{i=1}^{M}\varphi_i(\rho_i+c_i-\beta)\dot{c}_i = {\xi_F}^T[(C+\rho-\beta I)\Delta\Xi\otimes\Gamma]\xi_F \tag{3.23}$$

and

$$\begin{aligned} &\sum_{i=1}^{M}2\varphi_i(c_i+\rho_i)\xi_i^T P\dot{\xi}_i = 2{\xi_F}^T[(C+\rho)\Delta\Xi\otimes P]\dot{\xi_F} \\ &= {\xi_F}^T[(C+\rho)\Delta\Xi\otimes(PA+A^TP) - (C+\rho)(\Delta\Xi L_1 + L_1^T\Delta\Xi)(C+\rho)\otimes\Gamma]\xi_F \\ &\quad + 2\xi_F^T[(C+\rho)\Delta\Xi L_1\otimes PA]h_F - 2\xi_F^T[(C+\rho)\Delta\Xi L_1\otimes P]\dot{h}_F \\ &\quad + 2\xi_F^T[(C+\rho)\Delta\Xi L_1\otimes PB]\gamma + 2\xi_F^T[(C+\rho)\Delta\Xi L_2\otimes PB]u_E \\ &\quad - 2\mu\xi_F^T[(C+\rho)\Delta\Xi L_1\otimes PB]F(\xi) \\ &\leq {\xi_F}^T[(C+\rho)\Delta\Xi\otimes(PA+A^TP) - \lambda_1^{min}(C+\rho)^2\otimes\Gamma]\xi_F \\ &\quad + 2\xi_F^T[(C+\rho)\Delta\Xi L_1\otimes PA]h_F - 2\xi_F^T[(C+\rho)\Delta\Xi L_1\otimes P]\dot{h}_F \\ &\quad + 2\xi_F^T[(C+\rho)\Delta\Xi L_1\otimes PB]\gamma + 2\xi_F^T[(C+\rho)\Delta\Xi L_2\otimes PB]u_E \\ &\quad - 2\mu\xi_F^T[(C+\rho)\Delta\Xi L_1\otimes PB]F(\xi), \end{aligned} \tag{3.24}$$

where λ_1^{min} represents the smallest positive eigenvalue of $\Delta\Xi L_1 + L_1^T \Delta\Xi$.

If condition (3.14) holds, then we have

$$\bar{B}Ah_i - \bar{B}\dot{h}_i + \bar{B}B\gamma_i = 0, \tag{3.25}$$

since $\bar{B}B = 0$. On letting $\gamma_i = \tilde{B}\dot{h}_i - \tilde{B}Ah_i \; \forall i \in F$, it follows that

$$\tilde{B}Ah_i - \tilde{B}\dot{h}_i + \tilde{B}B\gamma_i = 0. \tag{3.26}$$

From (3.25) and (3.26) and using the fact that $\left[\tilde{B}^T, \bar{B}^T\right]^T$ is non-singular, it implies

$$Ah_i - \dot{h}_i + B\gamma_i = 0 \; \forall i \in F, \tag{3.27}$$

which can be rewritten in a compact form

$$[I_M \otimes A]\, h_F - (I_M \otimes I_n)\dot{h}_F + (I_M \otimes B)\,\gamma = 0. \tag{3.28}$$

Pre-multiplying both sides of (3.28) by $(C+\rho)\Delta\Xi L_1 \otimes P$, we obtain

$$\left[(C+\rho)\Delta\Xi L_1 \otimes PA\right] h_F - \left[(C+\rho)\Delta\Xi L_1 \otimes P\right]\dot{h}_F + \left[(C+\rho)\Delta\Xi L_1 \otimes PB\right]\gamma = 0. \tag{3.29}$$

Substituting (3.23) and (3.24) into (3.22), we get

$$\begin{aligned} \dot{V}_1 \leq\; & \xi_F^T[(C+\rho)\Delta\Xi \otimes [PA + A^T P + \Gamma] - (\lambda_1^{min}(C+\rho)^2 + \beta\Delta\Xi) \otimes \Gamma]\xi_F \\ & + 2\xi_F^T[(C+\rho)\Delta\Xi L_2 \otimes PB]u_E - 2\mu\xi_F^T[(C+\rho)\Delta\Xi L_1 \otimes PB]F(\xi). \end{aligned} \tag{3.30}$$

From (3.16), it is straightforward to show that

$$\xi_i^T PBf(\xi_i) = \left\|B^T P\xi_i\right\| \forall i \in F \tag{3.31}$$

and

$$\begin{aligned} \xi_i^T PBf(\xi_j) &\leq \left\|B^T P\xi_i\right\| \left\|f(\xi_j)\right\| \;\; \forall i \neq j \\ &\leq \left\|B^T P\xi_i\right\| \end{aligned} \tag{3.32}$$

by applying the Cauchy-Schwarz inequality [55]. Subsequently, we have the following relation

$$\begin{aligned} & -2\mu\xi_F[(C+\rho)\Delta\Xi L_1 \otimes PB]F(\xi) \\ & = -2\mu\sum_{i=1}^{M}(c_i+\rho_i)\varphi_i\xi_i^T PB\sum_{j=1}^{M} w_{ij}[f(\xi_i) - f(\xi_j)] \\ & \quad -2\mu\sum_{i=1}^{M}(c_i+\rho_i)\varphi_i\sum_{k=M+1}^{N} w_{ik}\xi_i^T PBf(\xi_i) \\ & \leq -2\mu\sum_{i=1}^{M}(c_i+\rho_i)\varphi_i\sum_{k=M+1}^{N} w_{ik}\left\|B^T P\xi_i\right\|. \end{aligned} \tag{3.33}$$

Since Assumption 3.2.1 holds, it follows that

$$\begin{aligned}
&2\xi_F[(C+\rho)\Delta\Xi L_2 \otimes PB]u_E \\
&= 2\sum_{i=1}^{M}(c_i+\rho_i)\varphi_i \sum_{k=M+1}^{N} w_{ik}\xi_i^T PBu_k \\
&\leq 2\sum_{i=1}^{M}(c_i+\rho_i)\varphi_i \sum_{k=M+1}^{N} w_{ik}\|B^T P\xi_i\|\|u_k\| \\
&\leq 2\sigma\sum_{i=1}^{M}(c_i+\rho_i)\varphi_i \sum_{k=M+1}^{N} w_{ik}\|B^T P\xi_i\|. \qquad (3.34)
\end{aligned}$$

From Lemma 2.1.2, we have

$$-\xi_F^T\left[[\lambda_1^{min}(C+\rho)^2+\beta\Delta\Xi]\otimes\Gamma\right]\xi_F \leq -2{\xi_F}^T[\sqrt{\lambda_1^{min}\beta\Delta\Xi}(C+\rho)\otimes\Gamma]\xi_F. \qquad (3.35)$$

Selecting $\beta \geq \frac{\max_{i\in F}\varphi_i}{\lambda_1^{min}}$ and $\mu > \sigma$, the inequality given in (3.30) implies

$$\dot{V}_1 \leq {\xi_F}^T\left[(C+\rho)\Delta\Xi\otimes[PA+A^TP-\Gamma]\right]\xi_F \qquad (3.36)$$

invoking (3.33), (3.34) and (3.35). Now, (3.36) can be simplified to

$$\dot{V}_1 \leq {\zeta_F}^T\left[I_M\otimes(PA+A^TP-PBR^{-1}B^TP)\right]\zeta_F \qquad (3.37)$$

by applying the change of variable $\zeta_F = (\sqrt{(C+\rho)\Delta\Xi}\otimes I)\xi_F$. This implies $\dot{V}_1 \leq 0$, since from (3.15), $PA+A^TP-PBR^{-1}B^TP = -Q < 0$ for given $Q > 0$ and $R > 0$. Also, from (3.37), $\dot{V}_1 = 0$ only when $\zeta_F = 0$. This implies asymptotic stability of (3.20) in closed-loop invoking LaSalle's invariance principle [55]. Therefore, $\lim_{t\to\infty}\zeta_F(t) = 0$ and hence

$$\lim_{t\to\infty}\xi_F(t) = 0, \qquad (3.38)$$

since ζ_F and ξ_F are related via non-singular transformation.

From (3.19) and (3.38), one gets

$$\lim_{t\to\infty}\left[x_F(t)-h_F(t)-(-L_1^{-1}L_2\otimes I_n)x_E(t)\right] = 0. \qquad (3.39)$$

Applying Lemma 3.3.1, (3.39) can be rewritten as

$$\lim_{t\to\infty}\left[x_F(t)-h_F(t)-\left(\begin{bmatrix} e_1 & 0 & \cdots & 0 \\ 0 & e_2 & \cdots & 0 \\ \vdots & \vdots & \ddots & \vdots \\ 0 & 0 & \cdots & e_p \end{bmatrix}\otimes I_n\right)x_E(t)\right] = 0. \qquad (3.40)$$

Rearranging (3.40) we have

$$\lim_{t\to\infty}\left(\begin{bmatrix}\bar{x}_1(t)-\bar{h}_1(t)-(e_1\otimes I_n)\hat{x}_1\\ \vdots \\ \bar{x}_p(t)-\bar{h}_p(t)-(e_p\otimes I_n)\hat{x}_p\end{bmatrix}\right)=0, \tag{3.41}$$

that is, for any $\bar{i}\in\{1,2,\ldots,p\}$,

$$\lim_{t\to\infty}\left[\bar{x}_{\bar{i}}(t)-\bar{h}_{\bar{i}}(t)-\mathbf{1}_{n_{\bar{i}}}\sum_{k=\hat{\varsigma}_{\bar{i}}+1}^{\hat{\varsigma}_{\bar{i}+\hat{n}_{\bar{i}}}}\left(\frac{b_k}{\sum_{j=\hat{\varsigma}_{\bar{i}}+1}^{\hat{\varsigma}_{\bar{i}+\hat{n}_{\bar{i}}}}b_j}x_k(t)\right)\right]=0. \tag{3.42}$$

Hence, it can be concluded that the predefined time-varying sub-formation $\bar{h}_{\bar{i}}$ is achieved by all the subgroups and the followers in each subgroup track a convex combination of the states of the respective leaders. This completes the proof. □

Remark 3.3.2. As the formation feasibility condition given in (3.14) imposes some constraints on the dynamics of the agents and the communication topology, not all types of time-varying formations may be achieved by the followers. In order to design the TGFT protocol, the formation feasibility condition needs to be satisfied a priori, which signifies that a desired formation must be compatible with the dynamics of the agents. Note that the function $f(\xi_i)$ in (3.4) is nonsmooth, implying that the formation tracking controller (3.4) is discontinuous. Since the right hand of (3.4) is measurable and locally essentially bounded, the well-posedness and the existence of the solution to (3.20) can be understood in the Filippov sense [80].

Remark 3.3.3. In contrast to the results reported in [77], where only 'group formation stabilization' problems are addressed, the nonlinear, adaptive control protocol designed in this chapter can be used to deal with 'group formation tracking' problems as well. Also, direct computation of the smallest positive eigenvalue of the Laplacian matrix is avoided in the proposed scheme, which uses only relative state information with respect to the neighbours. In virtue of this, the proposed control scheme becomes scalable and re-configurable for large-scale networked systems.

Remark 3.3.4. When $\hat{n}_{\bar{i}}=1\ \forall\bar{i}\in\{1,2,\ldots,p\}$, Theorem 1 specializes to cluster control problems as discussed in [47, 75, 76]. If $p=1$, it is straightforward to assert that the TGFT problem reduces to the formation tracking problem with multiple leaders as done in [81]. In

the case where $p = 1$ and $M = N - 1$, Theorem 1 can be applied to deal with the standard formation tracking problem [13]. It can further be noted that the TGFT problem solved in this chapter reduces to the consensus problem, as discussed in [74] and [78], when $h_i = 0$ $\forall i \in \{1, \ldots, M\}$, $p = 1$ and $M = N - 1$. Therefore, consensus problem, formation problem, and cluster problem can all be viewed as special cases of the TGFT problem addressed in this chapter.

Following Theorem 3.3.1, a systematic procedure to construct the control law u_i is given in Algorithm 1.

Algorithm 1 Procedure to design the control law for TGFT problem involving multiple leaders

1: **for** each agent $i \in \{1, \ldots, M\}$ **do**
2: suppose the MAS (3.2) satisfies Assumptions 3.2.1-3.3.3;
3: select the desired formation reference $h_i(t) \in \mathbb{R}^n$ $\forall t \geq 0$;
4: **if** formation feasibility condition (3.14) is satisfied **then**
5: choose a positive constant $\mu > \sigma$ for a given $\sigma \geq 0$;
6: find $P > 0$ by solving the ARE (3.15) for given $Q > 0$ and $R > 0$;
7: compute the controller gain matrices K and Γ, and the smooth function ρ_i using $P > 0$;
8: choose the matrices $\tilde{B}$ and $\bar{B}$ such that $\tilde{B}B = I_m$ and $\bar{B}B = 0$. Then find γ_i using $\dot{h}_i$, h_i and the matrices $\tilde{B}$ and $\bar{B}$;
9: design the nonlinear function $f(\cdot)$ based on (3.16);
10: construct the adaptive and nonlinear control protocol u_i given in (3.4);
11: **else**
12: back to Step 3;
13: **end if**
14: **end for**

3.4 Application: Multi-Target Surveillance of Nonholonomic Mobile Robots

In this section, the proposed TGFT control protocol has been utilized to solve a multi-target surveillance problem for a group of nonholonomic mobile robots.

3.4.1 Robot Dynamics

Let us consider a scenario where twelve nonholonomic mobile robots are engaged in a multi-target surveillance operation in a 2D plane. Each of the robots is assumed to possess the same dynamics and structure, and they are described by the following first-order differential equations in terms of the global coordinates as

$$\begin{aligned}\dot{x}_{xi} &= v_i \cos\theta_i,\\ \dot{x}_{yi} &= v_i \sin\theta_i,\\ \dot{\theta}_i &= \omega_i \quad \forall i \in \{1,\ldots,12\},\end{aligned}$$

where x_{xi} and x_{yi} together represent the position of the ith robot in the $X-Y$ plane (i.e., in Cartesian coordinates); v_i and ω_i denote respectively the linear and angular velocities; and θ_i represents the heading angle measured in an anticlockwise sense from the positive X axis.

To avoid saturation of the electric motors, the linear velocity of each mobile robot is constrained to

$$v_i \leq v_{max},$$

where $v_{max} = 10$m/s is the velocity limit.

For each mobile robot, we introduce a new control input q_i such that

$$\dot{v}_i = q_i.$$

Define $v_{xi} = v_i \cos\theta_i$ and $v_{yi} = v_i \sin\theta_i$ as the components of the linear velocity along the X and Y directions respectively. Then, we have $\dot{x}_{xi} = v_{xi}$ and $\dot{x}_{yi} = v_{yi}$. The dynamics can be expressed in terms of q_i and ω_i as

$$\begin{bmatrix}\dot{v}_{xi}\\ \dot{v}_{yi}\end{bmatrix} = \begin{bmatrix}\cos\theta_i & -v_i\sin\theta_i\\ \sin\theta_i & v_i\cos\theta_i\end{bmatrix}\begin{bmatrix}q_i\\ \omega_i\end{bmatrix}.$$

Assuming $v_i \neq 0$, the control input is designed as

$$\begin{bmatrix}q_i\\ \omega_i\end{bmatrix} = \begin{bmatrix}\cos\theta_i & \sin\theta_i\\ -\frac{\sin\theta_i}{v_i} & -\frac{\cos\theta_i}{v_i}\end{bmatrix}\begin{bmatrix}u_{xi}\\ u_{yi}\end{bmatrix}.$$

Now, applying feedback linearization, we obtain the linearized state-space model for each mobile robot (including the followers and leaders) which conforms to (3.2) with $u_i = [u_{xi}^T, u_{yi}^T]^T$

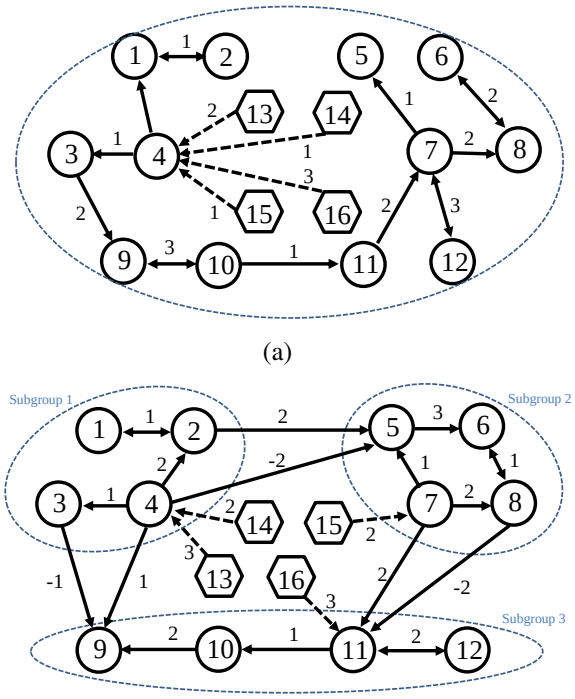

Figure 3.2: Interaction topology (a) before 60s and (b) after 60s.

and $x_i = [x_{xi}^T, v_{xi}^T, x_{yi}^T, v_{yi}^T]^T$ and the matrices A and B are given by

$$A = \begin{bmatrix} 0 & 1 & 0 & 0 \\ 0 & 0 & 0 & 0 \\ 0 & 0 & 0 & 1 \\ 0 & 0 & 0 & 0 \end{bmatrix}, \quad B = \begin{bmatrix} 0 & 0 \\ 1 & 0 \\ 0 & 0 \\ 0 & 1 \end{bmatrix}.$$

3.4.2 Group Formation and Tracking

In this case study, it is assumed that there are four targets (labelled as 13,14,15,16) moving in the same direction during first 60 seconds. After that, due to bounded external disturbances the targets start moving away from each other. In order to achieve this operation, $u_{13} = [-0.5, 2]^T$, $u_{14} = [-0.5, 2]^T$, $u_{15} = [1, 1]^T$ and $u_{16} = [2, -0.5]^T$ are applied to the targets during 60 - 61.5 seconds. Note that these external disturbances are unknown to the followers. In the first stage $(0 - 60\text{s})$, the follower robots are expected to build a circular formation surrounding all four targets (considered as leaders). After 60s, the followers are divided into three subgroups to form individual sub-formations around each target for better monitoring as the targets start moving away in arbitrary directions due to the effect of

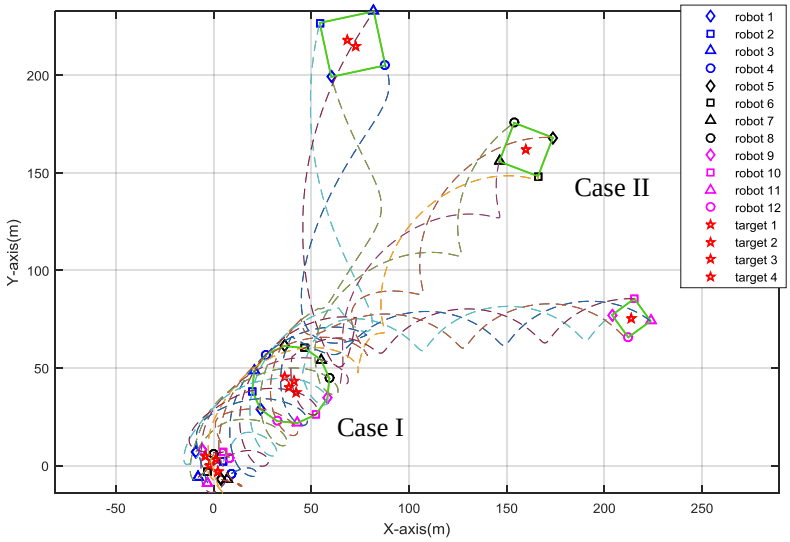

Figure 3.3: Formation and sub-formation diagrams for the multi-robot system in $X-Y$ plane.

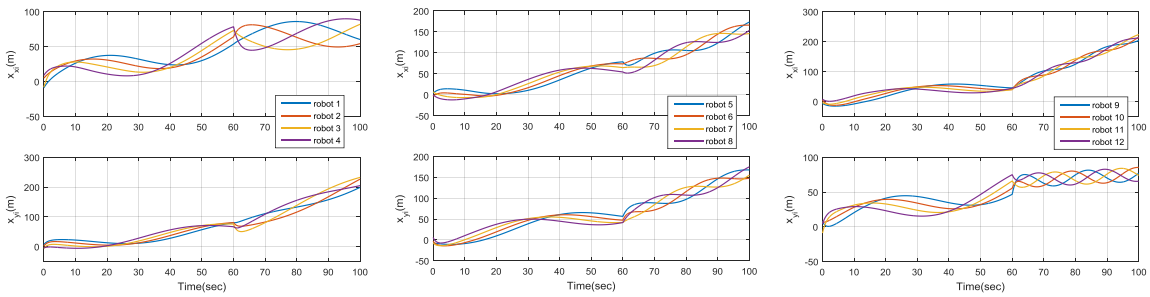

(a) (b) (c)

Figure 3.4: Time evolvement of the positions of the follower robots belonging to (a) Subgroup 1, (b) Subgroup 2, and (c) Subgroup 3.

external disturbance.

Case I (Complete formation, 0-60s): The graph shown in Fig. 3.2(a) illustrates the interconnection of the robots engaged in the surveillance operation. The time-varying circular formation for the follower robots is specified by

$$h_i(t) = \begin{bmatrix} r\sin\left(wt + \frac{2(i-1)\pi}{12}\right) \\ wr\cos\left(wt + \frac{2(i-1)\pi}{12}\right) \\ r\cos\left(wt + \frac{2(i-1)\pi}{12}\right) \\ -wr\sin\left(wt + \frac{2(i-1)\pi}{12}\right) \end{bmatrix} \quad \forall i \in \{1,2,\ldots,12\},$$

where $r = 20$m and $w = 0.1$rad/s.

Let us choose $\tilde{B} = \begin{bmatrix} 0 & 1 & 0 & 0 \\ 0 & 0 & 0 & 1 \end{bmatrix}$ and $\bar{B} = \begin{bmatrix} 1 & 0 & 0 & 0 \\ 0 & 0 & 1 & 0 \end{bmatrix}$, such that $\tilde{B}B = I_2$ and $\bar{B}B = 0$.

Note that this choice of $\bar{B}$ and $h_i(t)$ satisfies the formation feasibility condition (3.14) given in Theorem 3.3.1.

We choose $Q = \begin{bmatrix} 0.05 & 0 & 0 & 0 \\ 0 & 0.01 & 0 & 0 \\ 0 & 0 & 0.2 & 0 \\ 0 & 0 & 0 & 0.01 \end{bmatrix}$ and $R = \begin{bmatrix} 1 & 0 \\ 0 & 1 \end{bmatrix}$, and on solving the ARE (3.15), we get

$$P = \begin{bmatrix} 0.1512 & 0.2236 & 0 & 0 \\ 0.2236 & 0.6762 & 0 & 0 \\ 0 & 0 & 0.4253 & 0.4472 \\ 0 & 0 & 0.4472 & 0.9510 \end{bmatrix} > 0.$$

The controller gain matrices are then calculated as

$$K = \begin{bmatrix} -0.2236 & -0.6762 & 0 & 0 \\ 0 & 0 & -0.4472 & -0.9510 \end{bmatrix}$$

and

$$\Gamma = \begin{bmatrix} 0.0500 & 0.1512 & 0 & 0 \\ 0.1512 & 0.4572 & 0 & 0 \\ 0 & 0 & 0.2000 & 0.4253 \\ 0 & 0 & 0.4253 & 0.9044 \end{bmatrix}.$$

$\mu = 1$ is selected for a given $\sigma = 0.5$ and the nonlinear functions $f(\xi_i)$ are also constructed according to (3.10) to form the TGFT control protocol (3.4). The function ρ_i is computed as

$$\rho_i = \xi_i^T \begin{bmatrix} 0.1512 & 0.2236 & 0 & 0 \\ 0.2236 & 0.6762 & 0 & 0 \\ 0 & 0 & 0.4253 & 0.4472 \\ 0 & 0 & 0.4472 & 0.9510 \end{bmatrix} \xi_i,$$

and γ_i is obtained as

$$\gamma_i = \begin{bmatrix} -0.2\sin(0.1t + \frac{2(i-1)\pi}{12}) \\ -0.2\cos(0.1t + \frac{2(i-1)\pi}{12}) \end{bmatrix} \quad \forall i \in \{1, 2, \ldots, 12\}.$$

Fig. 3.3 shows that the follower robots $\forall i \in \{1, 2, \ldots, 12\}$ gradually attain the circular formation specified by $h_i(t)$ starting from arbitrary initial positions. Moreover, the formation continues to revolve around the targets.

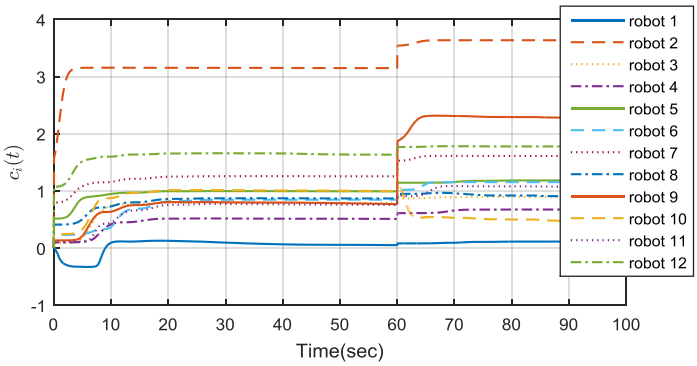

Figure 3.5: Variation of the coupling gains c_i with respect to time.

Case II (Sub-formations, 60-100s): These twelve mobile robots are divided into three subgroups, namely, $\mathcal{V}_1 = \{1,2,3,4\}$, $\mathcal{V}_2 = \{5,6,7,8\}$ and $\mathcal{V}_3 = \{9,10,11,12\}$ depending on the relative positions of the targets. $\mathcal{V}_1$ has been assigned two targets (13 and 14), while each of $\mathcal{V}_2$ and $\mathcal{V}_3$ has one target. Fig. 3.2(b) shows the modified interaction topology corresponding to Case II. The desired time-varying sub-formations for all three subgroups are specified by

$$h_i(t) = \begin{cases} \begin{bmatrix} 20\sin(0.1t+2(i-1)\pi/4) \\ 2\cos(0.1t+2(i-1)\pi/4) \\ 20\cos(0.1t+2(i-1)\pi/4) \\ -2\sin(0.1t+2(i-1)\pi/4) \end{bmatrix} & i \in \mathcal{V}_1, \\ \begin{bmatrix} 15\sin(0.2t+2(i-1)\pi/4) \\ 3\cos(0.2t+2(i-1)\pi/4) \\ 15\cos(0.2t+2(i-1)\pi/4) \\ -3\sin(0.2t+2(i-1)\pi/4) \end{bmatrix} & i \in \mathcal{V}_2, \\ \begin{bmatrix} 10\sin(0.3t+2(i-1)\pi/4) \\ 3\cos(0.3t+2(i-1)\pi/4) \\ 10\cos(0.3t+2(i-1)\pi/4) \\ -3\sin(0.3t+2(i-1)\pi/4) \end{bmatrix} & i \in \mathcal{V}_3. \end{cases}$$

For the same $\tilde{B}$, $\bar{B}$ and other controller parameters as taken in Case I, it can be readily verified that the sub-formations specified by $h_i(t)$ above, for all $i \in \mathcal{V}_1$, $\mathcal{V}_2$ and $\mathcal{V}_3$, satisfy the group formation feasibility constraint (3.14) and hence, each subgroup will achieve the individual sub-formations according to Theorem 3.3.1. The functions γ_i for all $i \in \{1,\ldots,12\}$ are

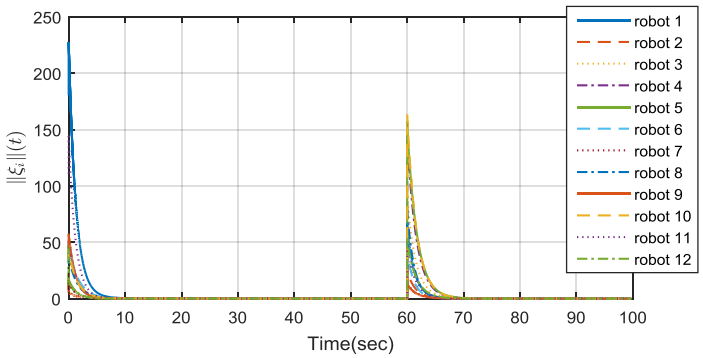

Figure 3.6: Time-variation of 2-norms of the group formation tracking errors ξ_i.

mentioned below as

$$\gamma_i = \begin{cases} \begin{bmatrix} -0.2\sin\left(0.1t + \frac{2(i-1)\pi}{4}\right) \\ -0.2\cos\left(0.1t + \frac{2(i-1)\pi}{4}\right) \end{bmatrix} & i \in \mathcal{V}_1, \\ \begin{bmatrix} -0.6\sin\left(0.2t + \frac{2(i-1)\pi}{4}\right) \\ -0.6\cos\left(0.2t + \frac{2(i-1)\pi}{4}\right) \end{bmatrix} & i \in \mathcal{V}_2, \\ \begin{bmatrix} -0.9\sin\left(0.3t + \frac{2(i-1)\pi}{4}\right) \\ -0.9\cos\left(0.3t + \frac{2(i-1)\pi}{4}\right) \end{bmatrix} & i \in \mathcal{V}_3. \end{cases}$$

The time evolution of the spatial positions of the robots (both the followers and the targets) are plotted in Fig. 3.3 which reveals that for $t \leq 60$s, the follower robots $(1, 2, \ldots, 12)$ together give rise to a dodecagon-shaped formation and keep rotating around the four targets. Fig. 3.5 depicts the time-variations of the coupling weights $c_i(t)$ $\forall i \in \{1, 2, \ldots, 12\}$ which shows that the coupling weights remain bounded $\forall t \geq 0$ and they converge to finite positive values. Fig. 3.6 illustrates that the 2-norm of the group formation tracking error $\xi_i(t)$ for each follower decays sharply to zero which confirms the followers are able to track a convex combination of the positions of the targets. After $t > 60$s, we observe that three subgroups are formed and they eventually attain the predefined time-varying circular sub-formations surrounding the respective targets. Fig 3.5 shows that for $t > 60$s, the coupling weights adapt to a new set of finite values to counteract the changeover from complete formation to sub-formation. Thus, TGFT involving multiple targets is achieved by the TGFT control protocol introduced in this chapter. Henceforth, it can be concluded that the multi-target surveillance operation is accomplished by the designed control law.

3.5 Conclusion

A distributed, adaptive and nonlinear control protocol has been introduced in this chapter to achieve TGFT for linear MASs having directed communication topology. The control objectives also include sub-formation and tracking, that is, the followers are divided into several subgroups depending on the positions of the leaders and each subgroup reaches individual sub-formations while tracking the positions of the respective leaders attached to that subgroup. In contrast to existing literature, the present chapter addresses the group formation tracking problem where each subgroup can have multiple leaders and the leaders may have separate control inputs. The proposed scheme finds a lot of applications in swarm robotics especially in multi-target surveillance operations where the targets (considered as leaders) may be placed far apart and sometimes, the targets may keep on changing their positions due to external disturbance. In order to tackle such constraints, in this chapter, each target considers a bounded exogenous input (reference or disturbance) in its dynamic model instead of being characterized as an autonomous system. The proposed control technique is fully distributed as it requires only the relative state information and does not need to calculate the eigenvalues of the graph Laplacian. The advantage of using an appropriate blending of adaptive and nonlinear control techniques is to render the proposed control scheme robust to network topology changes because in the future, this work may be extended to deal with parameter variations and model uncertainties of the agents. Moreover, the TGFT problem should be also extended tor heterogeneous MASs.

Chapter 4

Two-Layer Fully Distributed Formation-Containment Control Scheme for Multi-Agent Systems

4.1 Introduction

Recently, with the development of algebraic graph theory, many consensus-based control strategies have been applied to solve formation control problems [82]. Formation tracking control of first-order MASs is analyzed in [83]. In [84], a distributed formation control strategy is applied to a group of second-order MASs based on local neighbour-to-neighbour information exchange. A finite-time formation control protocol for second-order MASs is proposed in [85], where a time-invariant formation tracking is achieved within finite time. It is worth emphasizing that in some practical applications the dynamics of the agents can only be described by high-order models. [86] discusses the formation stability problems for general high-order swarm systems, and the result is extended to deal with formation tracking for multiple high-order autonomous agents by using a two-level consensus approach given in [87]. Experimental results on static formation of quadrotor swarm systems based on consensus approach are reported in [65], while time-varying formation control of MASs is still an active area of research which requires further attentions.

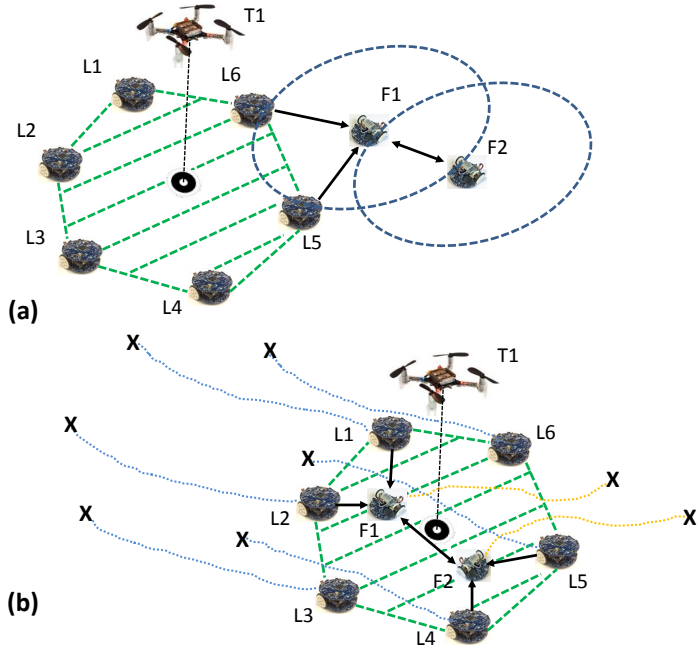

Figure 4.1: A visual illustration of the formation containment activity involving six leader robots, two follower robots and a target (the quadrotor): (a) The leader robots have already achieved a hexagonal formation and keep tracking the target while the followers have entered into the sensing range of two right-most leaders; (b) The leaders detect the followers, start communicating with them and finally, make them converged into the convex hull (indicated by Green dotted lines) spanned by the positions of the leaders.

Another significant research topic in the cooperative control of MASs is the containment control, which deals with multiple leaders and where the states of the followers are required to converge into a convex hull spanned by those of the leaders. In [88], containment control problems for both continuous-time and discrete-time MASs with general linear dynamics under directed communication topologies are investigated. Containment control is applied to a group of mobile autonomous agents with single-integrator kinematics under both fixed and switching communication networks in [89]. Besides, theoretical results for containment control of autonomous vehicles with double-integrator dynamics are validated through experiments in [40]. Mei *et al.* [90] have studied the distributed containment control problem for networked Lagrangian systems with multiple dynamic leaders in presence of parametric uncertainties. However, it is assumed in [90] that the leaders do not communicate among themselves , which is not usual in real-time applications.

Based on the formation control and containment control, the notion of formation-containment is proposed in the recent years, which requires the states of leaders to develop certain formation while the states of followers converge into the convex hull spanned by the states of the

leaders. One of the potential applications of formation-containment control is 'search and rescue problem' of mobile robots in hazardous and extreme environments, where the leader robots with detection devices are able to achieve a predefined formation depending on the surrounding environment and the follower robots then move into a safe region formed by the leaders. An example is shown in Fig. 4.1. The articles [91–93] have laid major contribution in the area of formation-containment control of Euler-Lagrange systems: in [91], a cooperative and adaptive formation-containment control framework has been introduced for networked Euler-Lagrange systems without using relative velocity information; in [92], the development of [91] has been extended to consider the effect of input saturation; while in [93], the formation-containment control problem of Euler-Lagrange systems is solved in an event-triggered framework. Formation-containment control of first-order and second-order MASs are investigated in [94] and [95], respectively. LQR-based formation-containment of high-order MASs is developed in [96]. The output formation-containment problem of coupled heterogeneous linear systems with undirected graph and directed graph are addressed in [97] and [63] respectively. In [78], the authors have proposed fully distributed consensus protocols to achieve leader-follower consensus in directed graphs under external disturbances. In practice, bidirectional communication is not robust and reliable when unexpected communication failure occurs. To counteract sudden communication channel disruptions during real-time implementation, it is required to study formation-containment control with directed interaction topology. In some of the applications, a MAS should not only accomplish the given formation-containment task, but also track the desired trajectories provided by a virtual leader, which may have nonzero control input. A virtual leader may be considered as a pseudo agent which generates the formation reference signal for the leader agents. To the best of authors' knowledge, fully distributed formation-containment control problem for linear MASs with a virtual leader having its own control input independent of the agents and the network topology are not yet explored much.

Motivated by the issues stated above, the distributed formation-containment problem for LTI MASs with directed communication topologies is investigated in this chapter. First, the entire MAS is decomposed into the leaders' layer and the followers' layer, and fully distributed protocols are designed based on neighbouring state information, which make the

proposed control design fully distributed and independent of global information about communication topologies. Then, conditions to achieve formation-containment are presented, where a feasible formation set is also given. An algorithm to design the adaptive control law is proposed which involves a particular algebraic Riccati equation (ARE). It is shown that the consensus problem, formation tracking problem, and containment control problem can all be viewed as special cases of formation-containment problem solved in this chapter. Finally, numerical examples are provided to demonstrate the effectiveness of the proposed theory.

Compared to the existing results on formation-containment control of MASs, the proposed results of this chapter offer several advantages as mentioned below:

- In the present approach, we have considered a separate control input for the virtual leader (i.e. the formation reference) independent of the other agents and their interactions, in contrast to the existing results which consider the virtual agent to be an autonomous system only. Due to this improvisation, the time-varying formation of the leaders can also track any given bounded reference signal;
- Another advantage of the proposed scheme is that it does not need to compute the Laplacian matrix of the communication topology, unlike most of the existing cooperative control strategies. The proposed method uses only the relative state information and thereby avoids explicit computation of the Laplacian matrix and hence, the scheme is scalable for large-scale networked systems;
- The dynamics of the leaders and followers are not restricted to first/second-order models often considered in the literature for simplicity. Therefore, the actual system dynamics of the agents can be handled in the present approach. Furthermore, the communication topology of the MASs can be both directed as well as undirected which enables the proposed scheme to be flexible, reconfigurable and robust to network topology changes.

Rest of the chapter is organized as follows. Section 4.2 discusses the problem formulation. Section 4.3 contains the main contribution of the chapter, which derives a two-layer

fully distributed formation-containment control protocol for networked MASs with time-varying formation reference. Two detailed case studies are considered in Section 4.4 to show the effectiveness of the proposed methodology. One of them deals with the formation-containment of a team of networked satellites, and the other one shows experimental validation using nonholonomic mobile robots. Section 4.5 concludes the chapter mentioning the future research directions.

4.2 Problem Formulation

Consider a MAS of N agents, which consists of M followers and rest $N-M$ leaders. Let $F = \{1,2,\ldots,M\}$ and $E = \{M+1,M+2,\ldots,N\}$ be the sets of the followers and leaders respectively. The dynamics of each agent is described by

$$\dot{x}_i = Ax_i + Bu_i \qquad \forall i \in \{1,2,\ldots,N\}, \tag{4.1}$$

where $x_i = x_i(t) \in \mathbb{R}^n$ is the state of the ith agent and $u_i = u_i(t) \in \mathbb{R}^m$ is the associated control input for all $t \in \mathbb{R}_{\geq 0}$. $A \in \mathbb{R}^{n\times n}$ and $B \in \mathbb{R}^{n\times m}$ are constant matrices with $\text{rank}(B) = m$ and (A,B) being stabilizable. The desired trajectory of a formation (i.e., the formation reference) is generated by a separate agent, called the *virtual leader*. It is also considered as the $(N+1)^{th}$ leader with the dynamics

$$\dot{x}_{N+1} = (A+BK_1)x_{N+1} + Bu_{N+1}, \tag{4.2}$$

where $x_{N+1} = x_{N+1}(t) \in \mathbb{R}^n$ and $u_{N+1} = u_{N+1}(t) \in \mathbb{R}^m$ are its state and control input, respectively, for all $t \in \mathbb{R}_{\geq 0}$ and $K_1 \in \mathbb{R}^{m\times n}$ is a constant matrix to be chosen by the designer to meet the requirement of the task.

Assumption 4.2.1. The bounded control input $u_{N+1}(t)$ is unknown to all leaders and followers, and there exists a positive constant σ such that $\|u_{N+1}(t)\| \leq \sigma \; \forall t$.

Being inspired from the developments of [96] and [97], a two-layer framework is adopted to handle the distributed formation-containment problem, which consists of the leaders' formation layer and the followers' containment layer. In the first layer, the leaders are supposed to achieve a predetermined time-varying formation and move together following

a desired reference. In the second layer, all the followers are expected to converge into a convex hull spanned by the leaders. The *two-layer formation-containment* is said to be met if and only if the control objectives in both the layers are achieved. The communication topology among each agent is denoted by $\mathcal{G}$ which satisfies the following assumption.

Assumption 4.2.2. Suppose the neighbours of a leader are only leaders or the virtual leader, and the neighbours of a follower are either leaders or followers.

Under Assumption 4.2.2, the Laplacian matrix L associated with the graph $\mathcal{G}$ can be partitioned as

$$L = \begin{bmatrix} L_1 & L_2 & 0_{M\times 1} \\ 0_{(N-M)\times M} & L_3 & L_4 \\ 0_{1\times M} & 0_{1\times(N-M)} & 0_{1\times 1} \end{bmatrix} \tag{4.3}$$

where $L_1 \in \mathbb{R}^{M\times M}$, $L_2 \in \mathbb{R}^{M\times(N-M)}$, $L_3 \in \mathbb{R}^{(N-M)\times(N-M)}$ and $L_4 \in \mathbb{R}^{(N-M)\times 1}$. Desired formation of the leaders is specified by the vector $h_E = \left[h_{M+1}^T, h_{M+2}^T, \ldots, h_N^T\right]^T$ where $h_i \in \mathbb{R}^n$ for all $i \in E$. h_i can be time-varying as well and in that case, $h_i(t) \in \mathbb{R}^n$ for all $t \in \mathbb{R}_{\geq 0}$. Desired formation h_i is pre-specified to the ith leader. For simplicity of presentation, explicit dependence of h_i on time $t \in \mathbb{R}_{\geq 0}$ is omitted.

Definition 4.2.1. The leaders are said to achieve time-varying formation tracking with the virtual leader if for any given bounded initial states and any $j \in E$,

$$\lim_{t\to\infty} \left(x_j(t) - h_j(t) - x_{N+1}(t)\right) = 0. \tag{4.4}$$

Definition 4.2.2. The followers are said to achieve containment if for any given bounded initial states and any $k \in F$, there exist nonnegative constants α_{kj} satisfying $\sum_{j=M+1}^{N} \alpha_{kj} = 1$ such that

$$\lim_{t\to\infty} \left(x_k(t) - \sum_{j=M+1}^{N} \alpha_{kj} x_j(t) \right) = 0. \tag{4.5}$$

Definition 4.2.3. The MAS (4.1) is said to achieve formation-containment if for any given bounded initial states, any $k \in F$ and $j \in E$, there exist nonnegative constants α_{kj} satisfying $\sum_{j=M+1}^{N} \alpha_{kj} = 1$ such that (4.4) and (4.5) hold simultaneously.

Remark 4.2.1. According to Definitions 4.2.1–4.2.3, it can be argued that if $M = 0$, the two-layer formation-containment problem reduces to 'formation tracking' problem. If $M = 0$

and $h_E \equiv 0$, the formation-containment problem specializes to 'consensus seeking' problem. Moreover, if $h_E \equiv 0$ and leaders have no neighbours, then we can conclude that the formation-containment problem specializes to 'containment' problem. Therefore, the consensus seeking, formation tracking and containment control can all be viewed as special cases of formation-containment control problem.

In this chapter, we introduce a fully distributed time-varying formation-containment control (FCC) protocol given below:

$$\begin{cases} u_i = K_1 x_i + (c_i + \rho_i) K_2 \xi_i - \mu f(\xi_i), \\ \dot{c}_i = \xi_i^T \Gamma \xi_i, \end{cases} \quad \forall i \in E; \tag{4.6}$$

$$\begin{cases} u_i = K_1 x_i + (\hat{c}_i + \hat{\rho}_i) K_2 \varsigma_i - \eta f(\varsigma_i), \\ \dot{\hat{c}}_i = \varsigma_i^T \Gamma \varsigma_i, \end{cases} \quad \forall i \in F; \tag{4.7}$$

where

$$\xi_i = \sum_{j=M+1}^{N} a_{ij}\big[(x_i - h_i) - (x_j - h_j)\big] + a_{i,N+1}\big[(x_i - h_i) - x_{N+1}\big] \quad \text{and} \quad \varsigma_i = \sum_{j=1}^{N} a_{ij}(x_i - x_j). \tag{4.8}$$

Above, $c_i(t)$ and $\hat{c}_i(t)$ denote the time-varying coupling weights associated with the ith agent with $c_i(0) \geq 0$ and $\hat{c}_i(0) \geq 0$; $K_1 \in \mathbb{R}^{m\times n}$, $K_2 \in \mathbb{R}^{m\times n}$ and $\Gamma \in \mathbb{R}^{n\times n}$ are constant matrices to be chosen; η and μ are positive constants to be selected; $\hat{\rho}_i$ and ρ_i are smooth functions of ς_i and ξ_i respectively; and $f(.)$ represents a nonlinear function to be determined later.

If two-layer formation-containment is achieved, the leaders will first attain the desired formation (time-varying/stationary) and keep tracking the reference trajectory generated by the virtual leader, and after that, the followers will converge into the convex hull spanned by the leaders. This chapter primarily focuses on the following issues: (i) under which conditions the formation-containment can be achieved, and (ii) the steps to design a fully distributed (i.e., distributed and adaptive) control protocol to achieve two-layer formation-containment.

4.3 Formation-Containment Control Protocol Design

In this section, the problem of designing a fully distributed formation-containment control (FCC) protocol for LTI MASs, represented by (4.1), is investigated.

Assumption 4.3.1. The interaction topology among the leaders has a spanning tree with the virtual leader being the root node.

Assumption 4.3.2. For each follower, there exists at least one leader that has a directed path to it.

The following lemma taken from [42] can be proved under Assumptions 4.3.1 and 4.3.2.

Lemma 4.3.1. [42] If the directed interaction topology $\mathcal{G}$ satisfies Assumptions 4.3.1 and 4.3.2, then all the eigenvalues of L_1 and L_3 have positive real parts, each entry of $-L_1^{-1}L_2$ is nonnegative, and each row of $-L_1^{-1}L_2$ has a sum equal to one.

Let $x_F = \left[x_1^T, x_2^T, \ldots, x_M^T\right]^T$, $x_E = \left[x_{M+1}^T, x_{M+2}^T, \ldots, x_N^T\right]^T$, $F(\varsigma) = \left[f^T(\varsigma_1), f^T(\varsigma_2), \ldots, f^T(\varsigma_M)\right]^T$ and $F(\xi) = \left[f^T(\xi_{M+1}), f^T(\xi_{M+2}), \ldots, f^T(\xi_N)\right]^T$. Note that x_F and x_E are variables of time $t \in \mathbb{R}_{\geq 0}$. With the fully distributed formation-containment control (FCC) protocol given by (4.7) and (4.6), the closed-loop dynamics of the MAS (4.1) can be written in a compact form as

$$\begin{cases} \dot{x}_E = \left[I_{N-M} \otimes (A + BK_1) + (C+\rho)L_3 \otimes BK_2\right]x_E + \left[(C+\rho)L_4 \otimes BK_2\right]x_{N+1} \\ \qquad - \left[(C+\rho)L_3 \otimes BK_2\right]h_E - \mu(I_{N-M} \otimes B)F(\xi) \\ \dot{c}_i = \xi_i^T \Gamma \xi_i; \end{cases} \tag{4.9}$$

$$\begin{cases} \dot{x}_F = \left[I_M \otimes (A + BK_1) + (\hat{C}+\hat{\rho})L_1 \otimes BK_2\right]x_F + \left[(\hat{C}+\hat{\rho})L_2 \otimes BK_2\right]x_E - \eta(I_M \otimes B)F(\varsigma) \\ \dot{\hat{c}}_i = \varsigma_i^T \Gamma \varsigma_i; \end{cases} \tag{4.10}$$

where $\rho = \text{diag}\{\rho_{M+1}, \ldots, \rho_N\}$, $C = \text{diag}\{c_{M+1}, \ldots, c_N\}$, $\hat{C} = \text{diag}\{\hat{c}_1, \ldots, \hat{c}_M\}$, and $\hat{\rho} = \text{diag}\{\hat{\rho}_1, \ldots, \hat{\rho}_M\}$,.

Let the global formation tracking error vector of the leaders be $\xi = [\xi_{M+1}^T, \ldots, \xi_N^T]^T$ where ξ_i for all $i \in \{M+1, \ldots, N\}$ are as defined in (4.8). Let $z_i = x_i - h_i$ for all $i \in E$ and $z_E = \left[z_{M+1}^T, \ldots, z_N^T\right]^T$. Now, ξ can be written in the Kronecker product form as

$$\xi = (L_3 \otimes I_n)z_E + (L_4 \otimes I_n)x_{N+1}. \tag{4.11}$$

Note that z_E, x_{N+1} and ξ are all time-dependent vectors for all $t \in \mathbb{R}_{\geq 0}$. If formation tracking is achieved asymptotically by the leaders, then we have $\lim_{t\to\infty} \xi(t) = 0$ which implies from

(4.11)

$$\lim_{t\to\infty}\left[x_E(t)-h_E(t)+L_3^{-1}L_4\otimes x_{N+1}(t)\right]=0. \tag{4.12}$$

From Assumption 4.3.1 it follows that $L_3^{-1}L_4=-\mathbf{1}_{N-M}$ [42], then (4.12) reduces to

$$\lim_{t\to\infty}\left[x_E(t)-h_E(t)-\mathbf{1}_{N-M}\otimes x_{N+1}(t)\right]=0. \tag{4.13}$$

Subsequently, the global containment error of the followers is denoted by $\varsigma=[\varsigma_1^T,\ldots,\varsigma_M^T]^T$ which can be expressed in a compact form as:

$$\varsigma=(L_2\otimes I_n)x_E+(L_1\otimes I_n)x_F. \tag{4.14}$$

Note that x_E, x_F and ς are all time-dependent vectors. If the containment phase is reached asymptotically by the followers, then we can write $\lim_{t\to\infty}\varsigma(t)=0$. This implies from (4.14)

$$\lim_{t\to\infty}\left[x_F(t)-(-L_1^{-1}L_2\otimes I_n)x_E(t)\right]=0. \tag{4.15}$$

Therefore, the MAS (4.1) achieves the formation-containment by applying the fully distributed FCC protocol (4.7) and (4.6), if for any given bounded initial states,

$$\begin{cases}\lim_{t\to\infty}\varsigma(t)=0 \quad \text{and}\\ \lim_{t\to\infty}\xi(t)=0.\end{cases} \tag{4.16}$$

The following theorem is the main contribution of this chapter which establishes the conditions to be satisfied by the MASs (4.1) to achieve formation-containment applying the fully distributed FCC protocol proposed in (4.7) and (4.6), provided the agents and the network hold certain properties. Moreover, the virtual leader has its own control input u_{N+1} independent of the dynamics of the agents and the network topology.

Theorem 4.3.1. Suppose, Assumptions 4.2.1-4.3.2 hold and for a given $\sigma\geq 0$, the constants η and μ satisfy the relation

$$\eta\geq\mu\geq\sigma. \tag{4.17}$$

If the following formation feasibility condition

$$(A+BK_1)(h_i-h_j)-(\dot{h}_i-\dot{h}_j)=0 \qquad \forall i,j\in E, \tag{4.18}$$

is satisfied for a given choice of $K_1\in\mathbb{R}^{m\times n}$ and $h_i\in\mathbb{R}^n$, then the two-layer formation-containment is achieved with the fully distributed FCC protocol given in (4.7) and (4.6)

with $K_2 = -R^{-1}B^TP$, $\Gamma = PBR^{-1}B^TP$, $\hat{\rho}_i = \varsigma_i^T P\varsigma_i$ and $\rho_i = \xi_i^T P\xi_i$, where $P > 0$ is the solution of the algebraic Riccati equation:

$$(A+BK_1)^T P + P(A+BK_1) + Q - PBR^{-1}B^TP = 0 \tag{4.19}$$

for given $Q > 0$ and $R > 0$. The nonlinear function $f(.)$ used in (4.7) and (4.6) is designed as:

$$f(\chi) = \begin{cases} \dfrac{B^TP\chi}{\|B^TP\chi\|} & \text{when } \|B^TP\chi\| \neq 0, \\ 0 & \text{when } \|B^TP\chi\| = 0; \end{cases} \tag{4.20}$$

where $\chi \in \mathbb{R}^n$ represents either ς_i or ξ_i for all $i \in \{1,2,\ldots,N\}$.

Proof. The proof has been divided into two parts: Part I establishes the formation tracking by the leaders; while Part II deals with containment of the followers.

(**Part I:** *Formation tracking*) We first derive the closed-loop dynamics of the leaders approaching formation tracking with the help of the proposed distributed and adaptive control law (4.6). Substituting (4.6) into (4.1) and then, substituting further the resulting expression into the derivative of (4.11), we obtain

$$\begin{cases} \dot{\xi} = \big[I_{N-M} \otimes (A+BK_1) + (C+\rho)L_3 \otimes BK_2\big]\xi + [L_3 \otimes (A+BK_1)]h_E - (L_3 \otimes I_n)\dot{h}_E \\ \qquad -\mu(L_3 \otimes B)F(\xi) - (L_3\mathbf{1}_{N-M} \otimes B)u_{N+1} \qquad \text{and} \\ \dot{c}_i = \xi_i^T \Gamma \xi_i. \end{cases} \tag{4.21}$$

Achieving formation tracking by the leaders is posed as an asymptotic stability problem of the closed-loop dynamics (4.21) involving $\dot{\xi}$ and $\dot{c}_i$. In order to prove asymptotic stability of (4.21) using Lyapunov stability approach, we consider the following Lyapunov function candidate

$$V_1 = \frac{1}{2}\sum_{i=M+1}^{N} g_i(2c_i + \rho_i)\rho_i + \frac{1}{2}\sum_{i=M+1}^{N} g_i(c_i - \alpha)^2 \tag{4.22}$$

where $g_i > 0$ for all i, $c_i(t) > 0$ for all $t \geq 0$ and for all i since $\Gamma > 0$, $\rho_i > 0$ for all i since $P > 0$, and $\alpha > 0$. Therefore, $V_1 > 0$. Since the sub-Laplacian matrix L_3 corresponding to the interaction topology of the leaders is a non-singular M-matrix (exploiting the property given in Lemma 4.3.1), there exists a diagonal positive definite matrix $G \in \mathbb{R}^{(N-M)\times(N-M)}$ such that

$$GL_3 + L_3^T G > 0 \tag{4.23}$$

holds via Lemma 2.1.1. As the scalar parameters g_i can take any positive values as decided by the designer, we may choose $G = \text{diag}\{g_{M+1}, g_{M+2}, \ldots, g_N\}$ such that (4.23) is satisfied. The time derivative of V_1 along any trajectories of (4.21) is obtained as:

$$\begin{aligned}\dot{V}_1 &= \sum_{i=M+1}^{N} [g_i(c_i+\rho_i)\dot{\rho}_i + g_i\rho_i\dot{c}_i] + \sum_{i=M+1}^{N} g_i(c_i-\alpha)\dot{c}_i \\ &= \sum_{i=M+1}^{N} 2g_i(c_i+\rho_i)\xi_i^T P\dot{\xi}_i + \sum_{i=M+1}^{N} g_i(\rho_i+c_i-\alpha)\dot{c}_i. \end{aligned} \tag{4.24}$$

We will first convert the summation terms present in (4.24) into the Kronecker product form aiming to finally express $\dot{V}_1$ in a quadratic form with respect to ξ. Note that

$$\sum_{i=M+1}^{N} g_i(\rho_i+c_i-\alpha)\dot{c}_i = \xi^T\left[(C+\rho-\alpha I)\,G\otimes\Gamma\right]\xi, \tag{4.25}$$

and

$$\begin{aligned}&\sum_{i=M+1}^{N} 2g_i(c_i+\rho_i)\xi_i^T P\dot{\xi}_i \\ &= 2\xi^T\left[(C+\rho)G\otimes P\right]\dot{\xi} \\ &= \xi^T\left[(C+\rho)G\otimes\left[P(A+BK_1)+(A+BK_1)^T P\right] - (C+\rho)(GL_3+L_3^T G)(C+\rho)\otimes\Gamma\right]\xi \\ &\quad + 2\xi^T\left[(C+\rho)GL_3\otimes P(A+BK_1)\right]h_E - 2\xi^T\left[(C+\rho)GL_3\otimes P\right]\dot{h}_E \\ &\quad - 2\mu\xi\left[(C+\rho)GL_3\otimes PB\right]F(\xi) - 2\xi\left[(C+\rho)GL_3\otimes PB\right](\mathbf{1}_{N-M}\otimes u_{N+1}) \\ &\le \xi^T\left[(C+\rho)G\otimes\left[P(A+BK_1)+(A+BK_1)^T P\right] - \lambda_0^{\min}(C+\rho)^2\otimes\Gamma\right]\xi \\ &\quad + 2\xi^T\left[(C+\rho)GL_3\otimes P(A+BK_1)\right]h_E - 2\xi^T\left[(C+\rho)GL_3\otimes P\right]\dot{h}_E \\ &\quad - 2\mu\xi^T\left[(C+\rho)GL_3\otimes PB\right]F(\xi) - 2\xi\left[(C+\rho)GL_3\otimes PB\right](\mathbf{1}_{N-M}\otimes u_{N+1})\end{aligned} \tag{4.26}$$

where $\lambda_0^{\min}$ represents the smallest positive eigenvalue of $\left[GL_3+L_3^T G\right]$. We will now simplify each of the terms appearing in expressions (4.25) and (4.26). From (4.20), it is straightforward to show that

$$\xi_i^T PBf(\xi_i) = \left\|B^T P\xi_i\right\| \qquad \forall i\in\{M+1, M+2, \ldots, N\}. \tag{4.27}$$

Applying Cauchy-Schwarz inequality [55] on (4.27), we obtain

$$\begin{aligned}\xi_i^T PBf(\xi_j) &\le \left\|B^T P\xi_i\right\|\left\|f(\xi_j)\right\| \\ &= \left\|B^T P\xi_i\right\| \qquad \forall i\neq j.\end{aligned} \tag{4.28}$$

We now simplify the following term containing $F(\xi)$

$$
\begin{aligned}
&-2\mu\xi^T\left[(C+\rho)GL_3\otimes PB\right]F(\xi)\\
=&-2\mu\sum_{i=M+1}^{N}(c_i+\rho_i)g_i\xi_i^T PB\sum_{j=M+1}^{N}a_{ij}[f(\xi_i)-f(\xi_j)]-2\mu\sum_{i=M+1}^{N}(c_i+\rho_i)g_ia_{i,N+1}\xi_i^T PBf(\xi_i)\\
=&-2\mu\sum_{i=M+1}^{N}(c_i+\rho_i)g_i\sum_{j=M+1}^{N}a_{ij}\left[\xi_i^T PBf(\xi_i)-\xi_i^T PBf(\xi_j)\right]\\
&-2\mu\sum_{i=M+1}^{N}(c_i+\rho_i)g_ia_{i,N+1}\xi_i^T PBf(\xi_i)\\
\leq&-2\mu\sum_{i=M+1}^{N}(c_i+\rho_i)g_ia_{i,N+1}\left\|B^T P\xi_i\right\|
\end{aligned}
\tag{4.29}
$$

since $\left[\xi_i^T PBf(\xi_i)-\xi_i^T PBf(\xi_j)\right]\leq 0\ \forall i$ from (4.27) and (4.28), and rest of the parameters c_i, ρ_i, g_i, μ are all positive. Subsequently, we simplify another component, as shown below, involving the virtual leader's input u_{N+1}

$$
\begin{aligned}
&-2\xi\left[(C+\rho)GL_3\otimes PB\right](\mathbf{1}_{N-M}\otimes u_{N+1})\\
=&-2\sum_{i=M+1}^{N}(c_i+\rho_i)g_ia_{i,N+1}\xi_i^T PBu_{N+1}\\
\leq&\ 2\sum_{i=M+1}^{N}(c_i+\rho_i)g_ia_{i,N+1}\left\|B^T P\xi_i\right\|\|u_{N+1}\|\\
\leq&\ 2\sigma\sum_{i=M+1}^{N}(c_i+\rho_i)g_ia_{i,N+1}\left\|B^T P\xi_i\right\|\quad\text{[due to Assumption 4.2.2].}
\end{aligned}
\tag{4.30}
$$

Applying the simplified conditions (4.29) and (4.30) into (4.26) and selecting $\mu\geq\sigma$, the expression for $\dot{V}_1$ reduces to

$$
\begin{aligned}
\dot{V}_1\leq&\ \xi^T\left[(C+\rho)G\otimes\left[P(A+BK_1)+(A+BK_1)^T P+\Gamma\right]-(\lambda_0^{\min}(C+\rho)^2+\alpha G)\otimes\Gamma\right]\xi\\
&+2\xi^T\left[(C+\rho)GL_3\otimes P(A+BK_1)\right]h_E-2\xi^T\left[(C+\rho)GL_3\otimes P\right]\dot{h}_E\\
&-2(\mu-\sigma)\sum_{i=M+1}^{N}(c_i+\rho_i)g_ia_{i,N+1}\left\|B^T P\xi_i\right\|\\
\leq&\ \xi^T\left[(C+\rho)G\otimes\left[P(A+BK_1)+(A+BK_1)^T P+\Gamma\right]-(\lambda_0^{\min}(C+\rho)^2+\alpha G)\otimes\Gamma\right]\xi\\
&+2\xi^T\left[(C+\rho)GL_3\otimes P(A+BK_1)\right]h_E-2\xi^T\left[(C+\rho)GL_3\otimes P\right]\dot{h}_E.
\end{aligned}
\tag{4.31}
$$

Now, the formation feasibility condition (4.18) can be expressed in a compact form

$$
[L_3\otimes(A+BK_1)]h_E-(L_3\otimes I_n)\dot{h}_E=0,
\tag{4.32}
$$

and upon pre-multiplying both sides of (4.32) by $(C+\rho)G\otimes P$, we get

$$[(C+\rho)GL_3\otimes P(A+BK_1)]h_E-[(C+\rho)GL_3\otimes P]\dot{h}_E=0. \tag{4.33}$$

Plugging (4.33) into (4.31), the expression for $\dot{V}_1$ gets further reduced to

$$\dot{V}_1 \leq \xi^T[(C+\rho)G\otimes[P(A+BK_1)+(A+BK_1)^TP+\Gamma]-(\lambda_0^{\min}(C+\rho)^2+\alpha G)\otimes\Gamma]\xi. \tag{4.34}$$

Now, using a common matrix property $X^2+Y^2\geq 2XY$ where $X>0$ and $Y>0$ [52], we find

$$-\xi^T\left[(\lambda_0^{\min}(C+\rho)^2+\alpha G)\otimes\Gamma\right]\xi\leq -2\xi^T\left[\sqrt{\lambda_0^{\min}\alpha G}(C+\rho)\otimes\Gamma\right]\xi \tag{4.35}$$

assuming $X=\sqrt{\lambda_0^{\min}}(C+\rho)>0$ and $Y=\sqrt{\alpha G}>0$. Selecting $\alpha\geq\frac{\max_{i\in E}g_i}{\lambda_0^{\min}}$, $\mu\geq\sigma$ and substituting (4.35) into (4.34), the expression of $\dot{V}_1$ becomes

$$\dot{V}_1\leq\xi^T\left[(C+\rho)G\otimes\left(P(A+BK_1)+(A+BK_1)^TP-\Gamma\right)\right]\xi. \tag{4.36}$$

Let us introduce a change of variable $\zeta=\left(\sqrt{(C+\rho)G}\otimes I\right)\xi$ in (4.36) and it yields

$$\dot{V}_1\leq\zeta^T\left[I_{N-M}\otimes\left(P(A+BK_1)+(A+BK_1)^TP-PBR^{-1}B^TP\right)\right]\zeta. \tag{4.37}$$

This implies $\dot{V}_1\leq 0$ using the ARE given in (4.19), and $V_1=0$ only when $\zeta=0$. Therefore, by applying the LaSalle's invariance principle [55], the closed-loop dynamics (4.21) can be guaranteed to be asymptotically stable. It implies

$$\lim_{t\to\infty}\zeta(t)=0 \tag{4.38}$$

which in turn implies

$$\lim_{t\to\infty}\xi(t)=0, \tag{4.39}$$

since ζ and ξ are related via non-singular transformation. (4.39) confirms that the leaders achieve the pre-specified formation given by h_E at $t\to\infty$ under the influence of the proposed formation tracking control law (4.6) while keep tracking the reference (x_{N+1}) provided by the virtual leader.

(**Part II:** *Containment*) Once the leaders achieve formation tracking under the application of the proposed formation tracking protocol (4.6), it is now the turn of the followers to

undergo the containment phase. We will start with deriving the closed-loop containment error dynamics ($\dot{\varsigma}$) of the followers. Inserting the containment control law (4.7) into (4.10) and invoking (4.11)-(4.14), we obtain the dynamics of $\dot{\varsigma}$ and $\dot{\hat{c}}_i$ as mentioned below:

$$\begin{cases} \dot{\varsigma} = [(C+\rho)L_2L_3 \otimes BK_2]\,[x_E(t) - h_E(t) - \mathbf{1}_{N-M} \otimes x_{N+1}(t)] \\ \qquad + \left[I_M \otimes (A+BK_1) + (\hat{C}+\hat{\rho})L_1 \otimes BK_2\right]\varsigma - \eta(L_1 \otimes B)F(\varsigma) - \mu(L_2 \otimes B)F(\xi) \qquad \text{and} \\ \dot{\hat{c}}_i = \varsigma_i^T \Gamma \varsigma_i. \end{cases} \tag{4.40}$$

Similar to Part I, achieving containment by the followers has been cast as an asymptotic stability problem of the containment error dynamics (4.40). Following the Lyapunov approach adopted in Part I to establish asymptotic stability, in Part II also, we consider a similar Lyapunov function candidate

$$V_2 = \frac{1}{2}\sum_{i=1}^{M} \varphi_i(2\hat{c}_i + \hat{\rho}_i)\hat{\rho}_i + \frac{1}{2}\sum_{i=1}^{M} \varphi_i(\hat{c}_i - \beta)^2 \tag{4.41}$$

which consists of $\varphi_i > 0$ for all $i \in \{1,\ldots,M\}$, $\hat{c}_i(t) > 0$ for all $t \geq 0$ and for all i since $\Gamma > 0$, $\hat{\rho}_i > 0$ for all i since $P > 0$, and $\beta > 0$. Thus, $V_2 > 0$. Since the sub-Laplacian matrix L_1 corresponding to the leaders' interaction graph is a non-singular M-matrix according to Lemma 4.3.1, there exists a diagonal positive definite matrix $\Xi \in \mathbb{R}^{M\times M}$ such that

$$\Xi L_1 + L_1^T \Xi > 0 \tag{4.42}$$

holds via Lemma 2.1.1. As the scalar parameters φ_i can take any positive values, we may propose $\Xi = \text{diag}\{\varphi_1, \varphi_2, \ldots, \varphi_M\} > 0$ such that (4.42) is satisfied. The next step is to find $\dot{V}_2$ along the trajectory of (4.40) as shown below:

$$\begin{aligned} \dot{V}_2 &= \sum_{i=1}^{M} \left[\varphi_i(\hat{c}_i + \hat{\rho}_i)\dot{\hat{\rho}}_i + \varphi_i\hat{\rho}_i\dot{\hat{c}}_i\right] + \sum_{i=1}^{M} \varphi_i(\hat{c}_i - \beta)\dot{\hat{c}}_i \\ &= \sum_{i=1}^{M} 2\varphi_i(\hat{c}_i + \hat{\rho}_i)\varsigma_i^T P\dot{\varsigma}_i + \sum_{i=1}^{M} \varphi_i(\hat{\rho}_i + \hat{c}_i - \beta)\dot{\hat{c}}_i. \end{aligned} \tag{4.43}$$

Similar to Part I, $\dot{V}_2$ needs to be expressed in a quadratic form with respect to ς. In order to do so, we expand the summation-terms present in (4.43) and rearrange them in the Kronecker product form:

$$\sum_{i=1}^{M} \varphi_i(\hat{\rho}_i + \hat{c}_i - \beta)\dot{\hat{c}}_i = \varsigma^T \left[(\hat{C} + \hat{\rho} - \beta I)\Xi \otimes \Gamma\right]\varsigma \tag{4.44}$$

and

$$
\begin{aligned}
&\sum_{i=1}^{M} 2\varphi_i(\hat{c}_i+\hat{\rho}_i)\varsigma_i^T P\dot{\varsigma}_i \\
&= 2\varsigma^T\left[(\hat{C}+\hat{\rho})\Xi\otimes P\right]\dot{\varsigma} \\
&= \varsigma^T\left[(\hat{C}+\hat{\rho})\Xi\otimes\left(P(A+BK_1)+(A+BK_1)^T P\right)-(\hat{C}+\hat{\rho})(\Xi L_1+L_1^T\Xi)(\hat{C}+\hat{\rho})\otimes\Gamma\right]\varsigma \\
&\quad +2\varsigma^T\left((C+\rho)\Xi L_2L_3\otimes PBK_2\right)(x_E-h_E-\mathbf{1}_{N-M}\otimes x_{N+1})-2\eta\varsigma^T\left[(\hat{C}+\hat{\rho})\Xi L_1\otimes PB\right]F(\varsigma) \\
&\quad -2\mu\varsigma^T\left[(\hat{C}+\hat{\rho})\Xi L_2\otimes PB\right]F(\xi) \\
&\le \varsigma^T\left[(\hat{C}+\hat{\rho})\Xi\otimes\left(P(A+BK_1)+(A+BK_1)^T P\right)-\lambda_1^{\min}(\hat{C}+\hat{\rho})^2\otimes\Gamma\right]\varsigma \\
&\quad +2\,\varsigma^T\left((C+\rho)\Xi L_2L_3\otimes PBK_2\right)(x_E-h_E-\mathbf{1}_{N-M}\otimes x_{N+1})-2\eta\varsigma^T\left[(\hat{C}+\hat{\rho})\Xi L_1\otimes PB\right]F(\varsigma) \\
&\quad -2\mu\varsigma^T\left[(\hat{C}+\hat{\rho})\Xi L_2\otimes PB\right]F(\xi),
\end{aligned}
\tag{4.45}
$$

where $\lambda_1^{\min}$ represents the smallest positive eigenvalue of $\left[\Xi L_1+L_1^T\Xi\right]$. We will now simplify the components of (4.45) which are not in the quadratic form with respect to ς. The terms involving the nonlinear function $F(\varsigma)$ can be linked with an upper bound using (4.28)

$$-2\eta\varsigma^T[(\hat{C}+\hat{\rho})\Xi L_1\otimes PB]F(\varsigma)\le -2\eta\sum_{i=1}^{M}(\hat{c}_i+\hat{\rho}_i)\varphi_i\left\|B^T P\varsigma_i\right\|\sum_{k=M+1}^{N}a_{ik} \quad \text{and} \tag{4.46}$$

$$-2\mu\varsigma^T[(\hat{C}+\hat{\rho})\Xi L_2\otimes PB]F(\xi)\le 2\mu\sum_{i=1}^{M}(\hat{c}_i+\hat{\rho}_i)\varphi_i\left\|B^T P\varsigma_i\right\|\sum_{k=M+1}^{N}a_{ik}. \tag{4.47}$$

Since the leaders have already achieved the formation specified by h_E (in Part I), the following relation holds:

$$x_E-h_E-\mathbf{1}_{N-M}\otimes x_{N+1}=0 \tag{4.48}$$

which is equivalent to

$$(I_{N-M}\otimes I_n)(x_E-h_E-\mathbf{1}_{N-M}\otimes x_{N+1})=0. \tag{4.49}$$

Pre-multiplying both sides of (4.49) by $(C+\rho)\,\Xi L_2L_3\otimes PBK_2$, we get

$$\left[(C+\rho)\,\Xi L_2L_3\otimes PBK_2\right](x_E-h_E-\mathbf{1}_{N-M}\otimes x_{N+1})=0. \tag{4.50}$$

Substituting (4.46), (4.47) and (4.50) into (4.45), we derive a simplified expression of $\dot{V}_2$ as noted below:

$$\dot{V}_2 \leq \varsigma^T \left[(\hat{C}+\hat{\rho})\Xi \otimes \Big(P(A+BK_1) + (A+BK_1)^T P + \Gamma \Big) - \Big(\lambda_1^{\min} (\hat{C}+\hat{\rho})^2 + \beta\Xi \Big) \otimes \Gamma \right] \varsigma$$
$$- 2(\eta - \mu) \sum_{i=1}^{M} (\hat{c}_i + \hat{\rho}_i)\varphi_i \left\| B^T P \varsigma_i \right\| \sum_{k=M+1}^{N} a_{ik}. \tag{4.51}$$

Now, applying the property $X^2 + Y^2 \geq 2XY$ of positive definite matrices [52], we have the following relation

$$-\varsigma^T \left[(\lambda_1^{\min} (\hat{C}+\hat{\rho})^2 + \beta\Xi) \otimes \Gamma \right] \varsigma \leq -2\varsigma^T \left[\sqrt{\lambda_1^{\min} \beta\Xi} (\hat{C}+\hat{\rho}) \otimes \Gamma \right] \varsigma. \tag{4.52}$$

(4.51) can now be simplified by using (4.52) and selecting $\beta \geq \frac{\max_{i \in F} \varphi_i}{\lambda_1^{\min}}$ and $\eta \geq \mu$

$$\dot{V}_2 \leq \varsigma^T \left[(\hat{C}+\hat{\rho})\Xi \otimes \Big(P(A+BK_1) + (A+BK_1)^T P - \Gamma \Big) \right] \varsigma. \tag{4.53}$$

Define a change of variable $\Upsilon = \left(\sqrt{(\hat{C}+\hat{\rho})\Xi} \otimes I \right) \varsigma$ and plugging it into (4.53), we have

$$\dot{V}_2 \leq \Upsilon^T \left[I_M \otimes \Big(P(A+BK_1) + (A+BK_1)^T P - PBR^{-1}B^T P \Big) \right] \Upsilon \tag{4.54}$$

which implies $\dot{V}_2 \leq 0$ using the ARE given in (4.19) and $\dot{V}_2 = 0$ only when $\Upsilon = 0$. Now, invoking LaSalle's invariance principle [55], it can ensured that the containment error dynamics (4.40) is asymptotically stable which ultimately implies

$$\lim_{t \to \infty} \varsigma(t) = 0. \tag{4.55}$$

The above analysis proves that the containment error goes to zero as $t \to \infty$, which ensures that the followers will asymptotically converge into the convex hull spanned by the leaders. Combining Parts I and II it can be concluded that the MAS (4.1) satisfying Assumptions 4.2.1-4.3.2 accomplishes two-layer formation-containment tracking applying the proposed fully-distributed FCC protocol (4.6) and (4.7). This completes the proof. □

Below, we provide a set of guidelines for the control practitioners to implement the proposed fully distributed two-layer formation-containment control (FCC) scheme in practical applications.

While analysing the two-layer formation-containment problem and deriving the FCC protocol in Theorem 4.3.1, we observe a number of significant aspects which we will describe in the following remarks.

Algorithm 2 Procedure to design a fully distributed control scheme for two-layer formation-containment problem

1: **for** each agent $i \in \{1, \ldots, N\}$ **do**
2: design a two-layer communication graph that satisfies Assumptions 4.2.1-4.3.2;
3: fix the desired formation reference h_E for leaders;
4: choose an appropriate feedback gain K_1 to widen the set of feasible formation;
5: **if** formation feasibility condition (4.18) is satisfied **then**
6: compute controller parameters $K_2 = -R^{-1}B^T P$ and $\Gamma = PBR^{-1}B^T P$ by solving ARE (4.19) for given $Q > 0$ and $R > 0$;
7: design the smooth functions $\hat{\rho}_i$ and ρ_i as described in Theorem 4.3.1;
8: choose positive constants η and μ according to (4.17) for a given $\sigma > 0$;
9: construct the nonlinear function $f(.)$ according to (4.20);
10: construct the fully-distributed formation-containment control (FCC) protocol given in (4.6) and (4.7);
11: **else**
12: back to Step 4;
13: **end if**
14: **end for**

Remark 4.3.1. The formation feasibility condition (4.18) imposed in Theorem 4.3.1 is a common restriction in the consensus-based formation control literature [13, 46, 96]. This criteria needs to be checked *a priori* to confirm whether a desired formation shape, specified by h_E, is possible to be achieved by the leaders. In this regard, the gain matrix K_1 plays a major role in selecting the formation reference h_E as K_1 is the only parameter in the formation feasibility criteria (4.18) that can be freely adjusted. If it fails then the formation shape needs to be changed. In case of static formation, it is easier to find K_1 for given (A, B) of the leaders, but it may not be straightforward in case of a time-varying formation to find an appropriate K_1 matrix to satisfy (4.18). In particular, it depends on the experience of a designer. However, in many practical applications, for example, in robotic applications employing nonholonomic mobile robots, the nonlinear dynamics of a robot can be feedback linearized into single or double integrator dynamics and then, it becomes much easier to find an appropriate K_1 matrix that can satisfy the formation feasibility criteria (4.18) for a particular choice of h_E. In this paper, we have considered two case studies to address the issue of finding K_1 for a given leader's dynamics and a desired formation shape.

Remark 4.3.2. The nonlinear function $f(\cdot)$, defined in (4.20), is included in the proposed FCC protocols (4.6) and (4.7) to handle the time-varying dynamics of the virtual leader. In contrast to most of the existing results in the formation-containment literature, the present

work does not presume the virtual leader to be an autonomous system; it may have a separate control (either reference or disturbance) input (u_{N+1}). But, the nonlinear function $f(\cdot)$ makes the FCC action *discontinuous*, which may produce 'chattering effect' due to frequent 'zero-crossing' and causes severe performance degradation. In order to avoid the chattering phenomenon in practical applications, the *boundary layer technique* proposed in [41] can be exploited which redefines the nonlinear function $f(\cdot)$ to make the control action *continuous* by removing the zero-crossing criteria. Although in this method, the formation tracking or containment errors cannot be made exactly zero but can be made infinitesimally small, which is sufficient to achieve satisfactory performance and most importantly, this technique minimizes the chattering effect.

Remark 4.3.3. In contrast to the developments reported in [96], where only formation-containment stabilization problem is addressed, the proposed distributed and adaptive control protocol can be used to deal with formation tracking and containment problems. Moreover, explicit computation of the smallest positive eigenvalue of the graph Laplacian matrix is avoided by using the distributed adaptive control scheme, where the the agents use only relative state information of the neighbours and hence, global information about the entire graph is not required. This feature renders the proposed FCC scheme *reconfigurable* in case of communication topology changes and *scalable* for large-scale networked systems. Note further that the proposed two-layer formation-containment problem reduces to the standard 'consensus problem' when $h_i = 0\ \forall i \in \{M+1,\ldots,N\}$, $u_{N+1}(t) = 0$, and $M = 0$, such that the results discussed in [78] can be viewed as a special case of the result of this chapter.

In the proposed formation-containment control scheme as derived in Theorem 4.3.1, the states of the followers converge into the convex hull spanned by the states of the leaders. However, it doesn't explicitly mention that whether the positions of the followers in a convex hull can also be controlled. In this context, the following theorem expands Theorem 4.3.1 to show an explicit relationship among the states of followers $x_i(t)$, $i \in F$, the time-varying formation of the leaders $h_i(t)$, $i \in E$, and the trajectory of the virtual leader $x_{N+1}(t)$.

Theorem 4.3.2. Suppose the assumptions of Theorem 1 hold and the MAS (4.1) achieves formation-containment by applying the fully distributed FCC protocol (4.6) and (4.7). The

states of followers satisfy the following relationship

$$\lim_{t\to\infty}\left(x_i(t)-\sum_{j=M+1}^{N} l_{ij}h_j(t)-x_{N+1}(t)\right)=0 \qquad \forall i\in F \tag{4.56}$$

where l_{ij} denotes the entries of $-L_1^{-1}L_2$.

Proof. If the assumptions of Theorem 1 are satisfied, the formation-containment of MAS given in (4.1) is accomplished by applying the adaptive control laws (4.7) and (4.6). From the proof of Theorem 1, it can be readily observed that if (4.39) and (4.55) hold simultaneously, then from (4.13) and (4.15) we have

$$\lim_{t\to\infty}\left[x_F(t)-(-L_1^{-1}L_2\otimes I_n)(h_E(t)+\mathbf{1}_{N-M}\otimes x_{N+1}(t))\right]=0. \tag{4.57}$$

It follows from Lemma 4.3.1 that

$$-L_1^{-1}L_2\mathbf{1}_{N-M}=\mathbf{1}_M. \tag{4.58}$$

Substituting (4.58) into (4.57), we obtain

$$\lim_{t\to\infty}\left[x_F(t)-(-L_1^{-1}L_2\otimes I_n)h_E(t)-\mathbf{1}_M\otimes x_{N+1}(t))\right]=0, \tag{4.59}$$

which is equivalent to (4.56) $\forall i\in F$. This completes the proof. □

Theorem 4.3.2 reveals that the states of the followers are jointly determined by the communication graph, the time-varying formation of the leaders, and the formation reference. According to (4.56), it can be shown that the states of the followers will also give rise to a time-varying formation determined by the convex combination of the formation h_E of the leaders with respect to the formation reference x_{N+1}. Therefore, the states of the followers not only converge into the convex hull spanned by the leaders, but also maintain a time-varying formation inside the convex hull.

4.4 Case Studies

4.4.1 Formation-Containment of Networked Satellites

In this section, a numerical example is given to illustrate the effectiveness of the proposed formation-containment control (FCC) scheme developed in the previous section. Consider

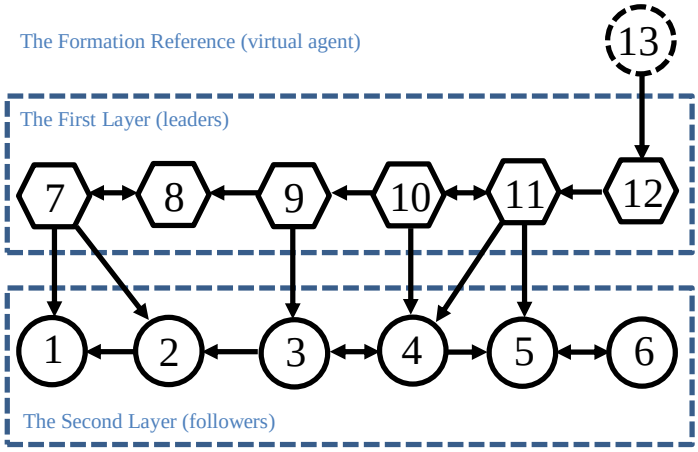

Figure 4.2: A two-layer multi-agent systems with directed communication topology.

a group of twelve networked satellites and the two-layer communication topology among twelve satellites is shown in Fig. 4.2, where it is assumed that the interaction has 0-1 weights and there are six leaders in the first layer and six followers in the second layer. The dynamics of each satellite is described by (4.1) with

$$A = \begin{bmatrix} 0 & 1 & 0 \\ 0 & 0 & 1 \\ -4 & -1 & -4 \end{bmatrix} \text{ and } B = \begin{bmatrix} 0 & 1 \\ 0 & -1 \\ 1 & 0 \end{bmatrix},$$

and the desired formation reference is described by (4.2) with $K_1 = \begin{bmatrix} 0 & 0 & 0 & 0 \\ 0 & 0 & 0 & 0 \end{bmatrix}$ and the control input u_{N+1} has been made zero.

The control objective of this theoretical case study is to let the assembly of six leader satellites maintain a circular time-varying parallel hexagon formation and keep rotating around the predefined formation reference (also called the virtual leader). Then the positions of the six followers are required to converge into the convex hull spanned by those six leaders. The time-varying circular formation of the leaders is specified by

$$h_i(t) = \begin{bmatrix} 15\sin\left(t + \frac{(i-7)\pi}{3}\right) \\ 15\cos\left(t + \frac{(i-7)\pi}{3}\right) \\ -15\sin\left(t + \frac{(i-7)\pi}{3}\right) \end{bmatrix}, \ \forall i \in \{7, 8, \ldots, 12\}.$$

It can be verified that the formation tracking feasibility condition (4.19) in Theorem 4.1 is satisfied with this $h_i(t)$. Thus, if the predefined time-varying formation $h_i(t)$ is achieved, the

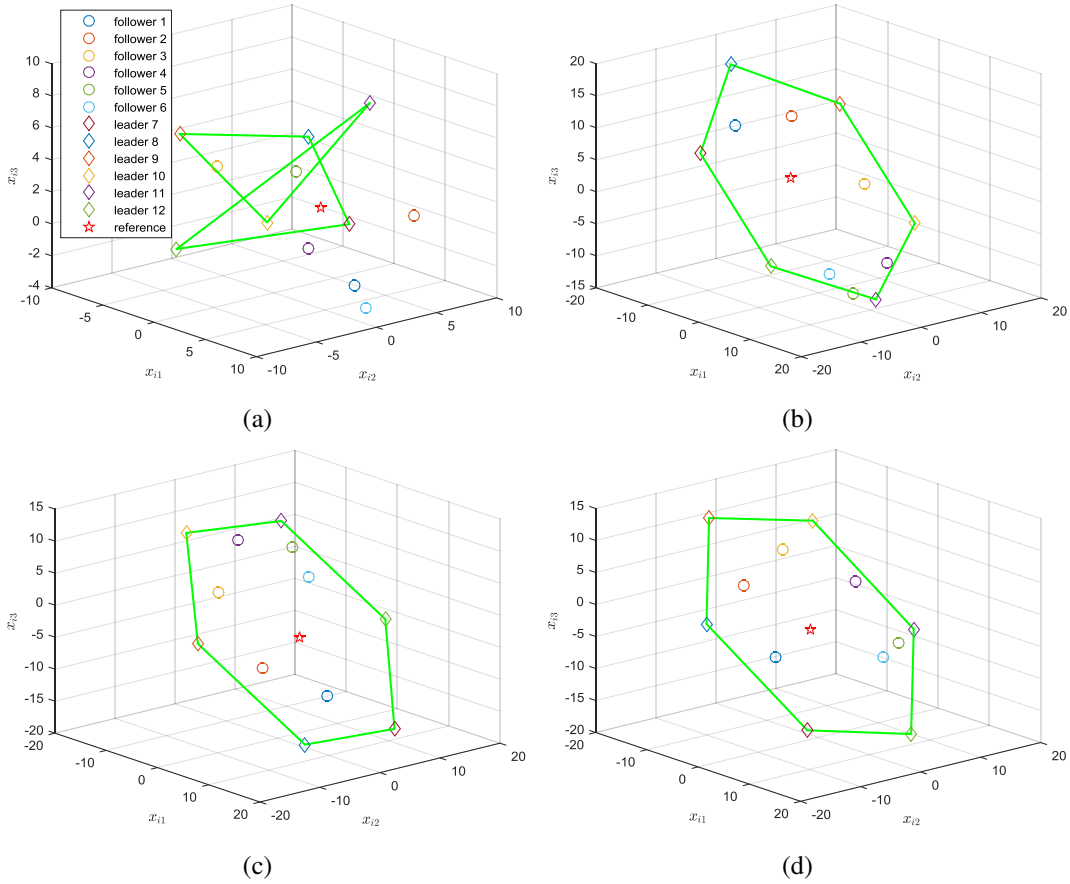

Figure 4.3: Position of the agents at time instants: (a) $t = 0$s; (b) $t = 10$s; (c) $t = 20$s; (d) $t = 40$s.

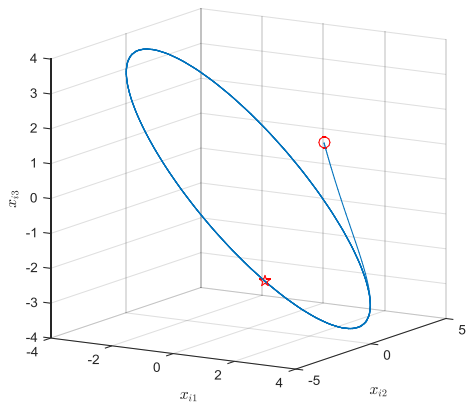

Figure 4.4: Trajectory of the formation reference signal.

six leaders will be placed at the six vertices of a parallel hexagon and keep rotating around the reference signal with an angular velocity of 1 rad/s. The followers will also converge into the parallel hexagon formed by the leaders.

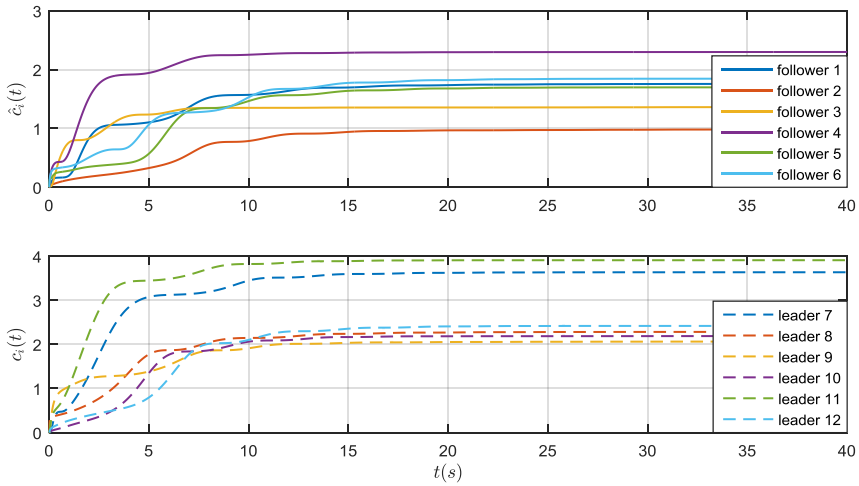

Figure 4.5: Variation of the coupling weights with respect to time.

According to Algorithm 2, the controller gains can be obtained as

$$K_2 = \begin{bmatrix} -0.0022 & -0.0812 & -0.0257 \\ -0.1804 & 0.2749 & 0.0790 \end{bmatrix},$$

$$\Gamma = \begin{bmatrix} -0.0325 & 0.0494 & 0.0142 \\ 0.0494 & -0.0822 & -0.0238 \\ 0.0142 & -0.0238 & -0.0069 \end{bmatrix},$$

by choosing $Q = \begin{bmatrix} 0.05 & 0 & 0 \\ 0 & 0.05 & 0 \\ 0 & 0 & 0.05 \end{bmatrix}$, $R = \begin{bmatrix} 1 & 0 \\ 0 & 1 \end{bmatrix}$, and the constants $\eta = \mu = 0.2$ for a given $\sigma = 0$.

Let the initial values of the coupling weights $\hat{c}_i(0) = 0$ and $c_i(0) = 0$ for all the satellites and the initial states of each of the satellites be chosen pseudorandomly with a uniform distribution in the interval $(-10, 10)$.

The spatial positions of the satellites at different time instants are depicted in Fig. 4.2 while Fig. 4.3 shows the state trajectory of the predefined formation reference within 40s. The variation of the coupling weights $\hat{c}_i$ and c_i are shown in Fig. 4.4. The 2-norms of the formation tracking error of the leaders and the containment error of the followers are depicted in Fig. 4.5. From these figures, it is observed that the six leaders form a parallel hexagon which keeps rotating around the desired formation reference, and the followers eventually converge into this hexagonal region formed by the leaders while maintaining the same velocity as that of the leaders. Also, the coupling weights are bounded and converge to some finite positive

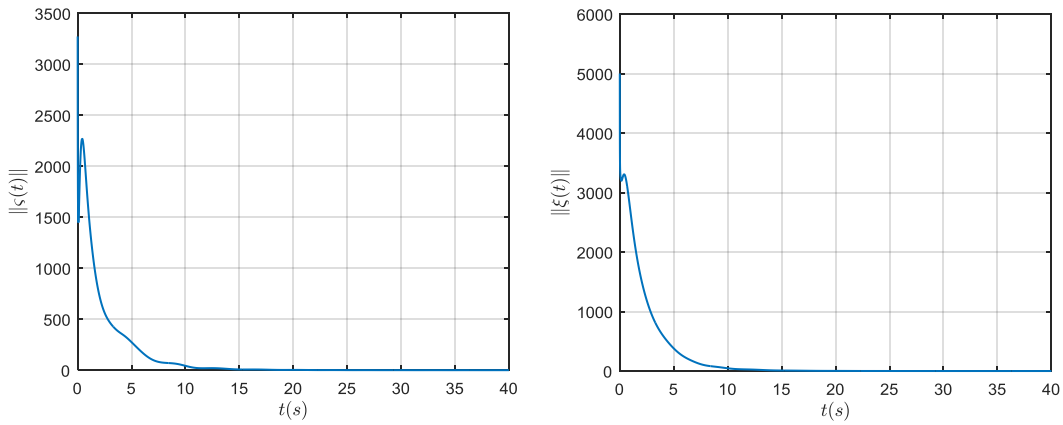

(a) (b)

Figure 4.6: Variations of the 2-norms of the (a) containment error (ς), and (b) formation error (ξ) with respect to time.

constants. It is now concluded that the desired formation-containment is achieved applying the fully distributed FCC protocol given in (4.7) and (4.6).

4.4.2 Experimental Validation Results with Mobile Robots

In the hardware experiment, we used small-scale, autonomous mobile robots, Mona [1], to test the feasibility of the proposed FCC scheme. Mona is a low-cost, open-source, miniature robot which has been developed for swarm robotic applications. As shown in Fig. 4.7, Mona has two 6V low power DC geared-motors connected directly to its wheels having 32mm diameter and the robot has a circular chassis having 80mm diameter. The main processor embedded in this robot is an AVR microcontroller equipped with an external clock having 16MHz frequency. Each robot is equipped with NRF24101 wireless transceiver module for inter-robot communication. The robots are operated and controlled by Arduino Mini/Pro microcontroller boards which are programmed by using the existing open-source software modules. The experimental platform includes a 1.2m $\times$ 1.2m blue arena and a digital camera connected to a host PC which operates the entire tracking system. The position tracking system used in this experiment is an open-source multi-robot localization platform [98]. The tracking system is not only capable of following a robot's position but also capable of measuring its velocity and detecting its orientations by identifying the unique circular tags attached on top of the robots. The state information is transmitted to the computer via the ROS communication framework and then the relative state information is sent to the

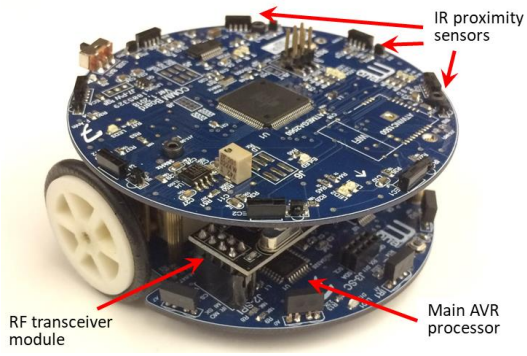

Figure 4.7: The autonomous mobile robot, Mona [1], used in the hardware experiment.

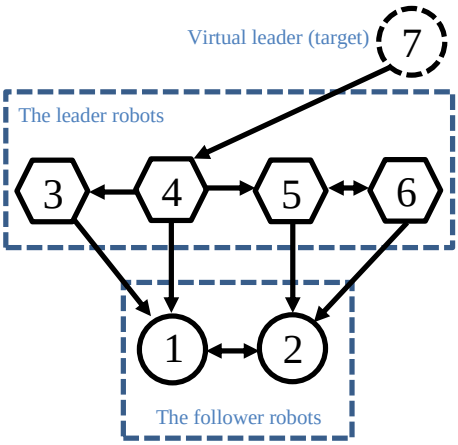

Figure 4.8: The directed communication topology among the robots considered in the hardware experiment.

corresponding robot using RF transceiver module.

In the experiment, six nonholonomic mobile robots (Mona) were considered to perform a formation-containment activity. Each mobile robot can be feedback linearized into a double integrator system as shown in Section 3.4.

In this experimental demonstration, the four leader robots will form a square-shaped region (i.e., the convex hull) in the experimental arena and the two follower robots is expected to converge into this safe region. Fig. 4.8 depicts the directed interaction topology among the six mobile robots. The state of the virtual leader (labelled with no. 7) is arbitrarily chosen as $[0.7, 0, 0.7, 0]^T$. The control objective of this experiment is to let the four leader robots to achieve a planar square formation, tracking the virtual target and keep surrounding the followers. The time-varying circular formation for the leader robots is specified by

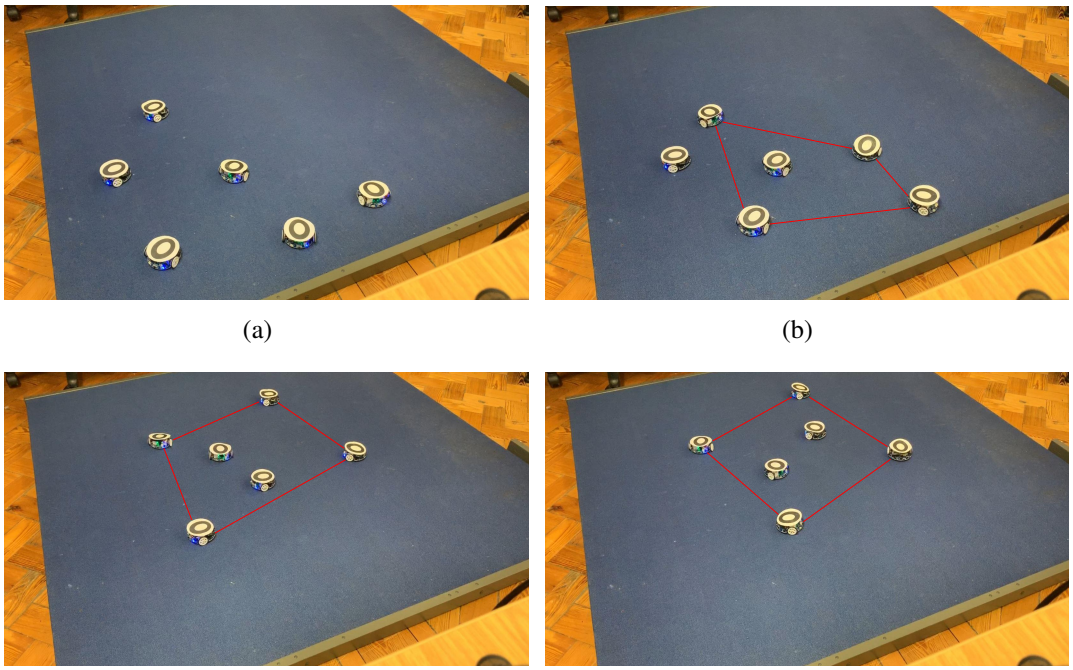

(a) (b)

(c) (d)

Figure 4.9: Progress of the formation-containment mission being achieved by a team of six mobile robots in real-time hardware experiment. (a) Initial orientation of the robots at $t = 0$s; (b) At $t = 20$s: leader robots are about to attain the desired square formation; (c) At $t = 40$s: leaders have already achieved the formation and two follower robots have also converged into the area spanned by the leaders; (d) At $t = 80$s: the whole assembly of the leaders has moved towards the centre of the arena following the location of the given target along with the followers being surrounded by them – mission accomplished.

$$h_i(t) = \begin{bmatrix} r\sin\left(\omega t + \frac{2(i-1)\pi}{4}\right) \\ \omega r\cos\left(\omega t + \frac{2(i-1)\pi}{4}\right) \\ r\cos\left(\omega t + \frac{2(i-1)\pi}{4}\right) \\ -\omega r\sin\left(\omega t + \frac{2(i-1)\pi}{4}\right) \end{bmatrix} \qquad \forall i \in \{3,4,5,6\}$$

where $r = 0.3$m and $\omega = 0.1$rad/s denote respectively the radius and angular velocity of the desired time-varying formation. It can be verified that the formation tracking feasibility condition (4.18) of Theorem 4.3.1 is satisfied in the present scenario and hence, when the predefined time-varying formation $h_i(t)$ is achieved, the leaders will automatically be placed at the four vertices of a square. After attaining the desired formation, the assembly of the leader robots keeps on rotating around the tracking reference with a constant angular velocity of 0.1rad/s and two follower robots will eventually converge into this area.

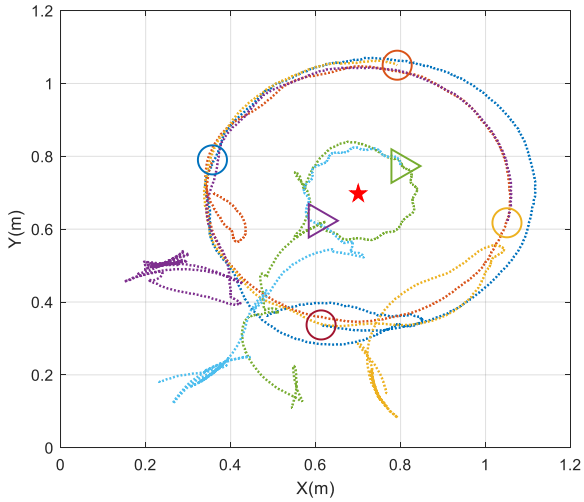

Figure 4.10: Position trajectories of the robots in the XY plane during the course of achieving formation tracking and containment in the hardware experiment under the application of the proposed FCC protocol. In this figure, the circles represent the leaders, the triangles denote the followers and the star indicates the target to be tracked.

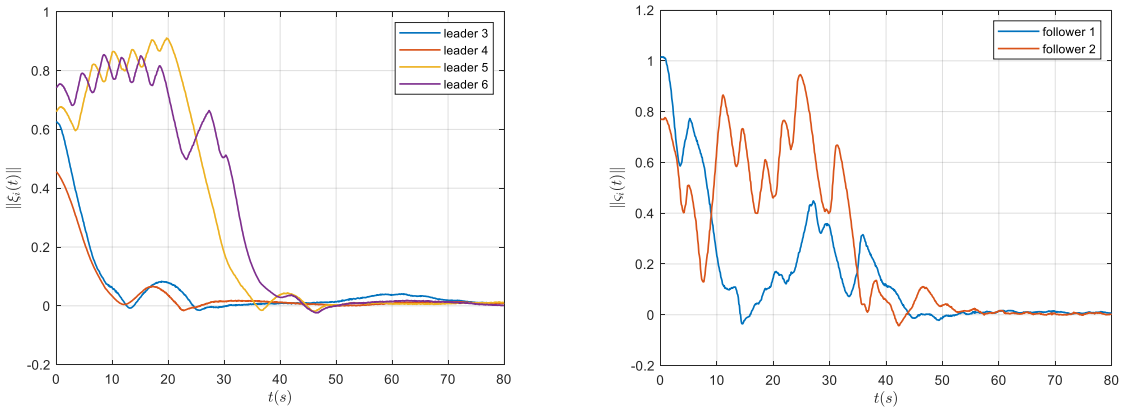

(a) (b)

Figure 4.11: Time variation of the 2-norms of (a) formation tracking error $\xi_i(t)$ of the leaders and (b) containment error $\varsigma_i(t)$ of the followers.

Fig. 4.9(a)–4.9(d) presents the hardware experiment results on achieving the formation-containment by a team of six nonholonomic mobile robots (Mona) on a planar surface. Fig. 4.9(a) shows the initial orientation (at $t = 0$s) of the robots on the arena. Fig. 4.9(b) depicts the progress of the mission at $t = 20$s from which it is apparent that the four leader robots are moving in the right track to attain the expected square formation and subsequently, Fig. 4.9(c) reveals that the leader robots have truly achieved the desired square formation (at $t = 40$s) and the two follower robots have also converged into the area spanned by the leaders. Finally, Fig. 4.9(d) portrays that the assembly of the leaders has moved towards the centre of the arena in order to track the position of the given target without disturbing the

formation and the followers have also moved accordingly being surrounded by the leaders. This then concludes that the formation-containment mission has been achieved successfully under the application of the proposed distributed FCC scheme. Fig. 4.10 complements the hardware experiment result presented in Fig. 4.9(a)–4.9(d) by plotting the position trajectories of all six robots in the XY plane during the course of achieving the formation tracking and containment in the hardware experiment. Fig. 4.10 traces the movement of the robots staring from the initial positions until they converge at the desired locations to attain the leaders' formation around the given target (marked by the Red star) and the followers' containment within the area spanned by the positions of the leader robots. Finally, time evolvement of the 2-norms of the formation tracking error $\xi_i(t)$ of four leaders and the containment error $\varsigma_i(t)$ of two followers are shown in Fig. 4.11(a) and 4.11(b). The figures reveal that both the formation tracking and containment errors die down to zero within 80s which is in agreement with the fact that the experiment also took 80s to accomplish the mission as reflected in Fig. 4.9(d). It can hence be ascertained that both formation tracking and containment have been achieved by the team of six mobile robots under the influence of the proposed distributed FCC scheme.

Even though we have used lab-based experimental set-up, small-scale robots and open source software modules, but the experimental results reflect usefulness of the proposed scheme in finding potential applications in robotics. High precision performance is also possible to be achieved by the proposed scheme with improvised camera tracking system, high-end embedded micro-controllers and advanced robots.

4.5 Conclusions

In this chapter, a fully distributed formation-containment problem for linear MASs with directed graphs is investigated. A two-layer control architecture is proposed to solve the formation-containment problem, which consists of the leaders' formation layer and the followers' containment layer. To achieve formation-containment, distributed adaptive protocols are constructed based on relative state information, which made the proposed control design fully distributed without using global information about the interaction topology.

Then, algorithms are presented to construct the control laws by testing formation feasibility condition and solving algebraic Riccati equation. The stability of the proposed scheme is proved by Lyapunov theory. Moreover, it is proved that the states of followers not only converge into the convex hull spanned by those of leaders but also maintain certain formation determined by the leaders and the virtual agent. Finally, the effectiveness of the proposed strategy is verified by numerical simulations and experiments with formation-containment tasks of networked satellites and mobile robots.

Future works may consider time delays and nonlinear dynamics of the MASs, and robust methods such as [99, 100] can be applied to design a robust FCC protocol.

Chapter 5

Observer-Based Optimal Formation Control of Innovative Tri-Rotor UAVs Using Robust Feedback Linearization

5.1 Introduction

In recent years, cooperative control of multi-rotor Unmanned Aerial Vehicles (UAVs) have received significant attention from both the practical engineering and academic communities due to their broad prospect in applications [101]. When working together, they are able to perform complex tasks with excellent efficiency and reliability, such as search and rescue [102], crop and weed management in agriculture [103], oil pipeline surveillance [104], etc. Aiming at more efficient configurations in terms of size, autonomy, flight range, payload capacity and other factors, some innovative vehicle platforms are developed by researchers [105]. One of such aerial robotic platforms that holds new and significant properties is the tri-rotor UAV, which is cost effective with more flexibility and agility [2], [106].

The proposed tri-rotor UAV has three rotors arranged in an equilateral triangular configuation and each rotor is attached to a servo motor that can independently change the rotating direction of the propeller. Thus, complete 3D thrust and 3D torque vectoring authority is achieved, which means that the vehicle does not have a nominally upright flying orientation:

it can fly in any orientation chosen by the user. Any time-dependent 3D position trajectory can be tracked at the same time as tracking any time-dependent 3D attitude trajectory. This configuration guarantees the UAV a high level of flexibility and maneuverability for attitude control and position movement. Compared to the quadrotor, this innovative configuration also requires less hover power and hence provides longer flight time [107], which makes it ideal for deployment in various missions.

To the best of the author's knowledge, no prior literature has studied a tri-rotor UAV configuration with completely independent tilted-rotor capability on all three rotors. The tri-rotor UAV introduced in [108] only has one servo motor that is installed on the arm, which cannot hold different attitudes while hovering. A triangular quadrotor is proposed in [107], which contains a single large rotor fixed on the main body. This configuration requires more power to hover and causes uncompensated gyroscopic drift.

In contrast to a quadrotor UAV, which has zero angular momentum in hover, a tri-rotor UAV has persistent angular moment, and hence also gyroscopic dynamics due to the asymmetric configuration of the system which poses significant control systems complexities. Furthermore, independent attitude and trajectory tracking can and should be considered simultaneously. However, the control algorithm in [109] only considers attitude stabilization (as opposed to simultaneous independent attitude and trajectory tracking) and the control design proposed in [110] only focus on the static hovering. In this chapter, both these two objectives (i.e. simultaneous independent 3D attitude and 3D trajectory tracking) are considered for the tri-rotor UAV in order to overcome the limitation of quadrotors and thus create more possibilities when performing special tasks through aerial robotic platforms.

Furthermore, swarm robotics is a field of multi-robotics where a group of robots are controlled in a distributed way to perform complex tasks in a more efficient way than using a single robot [111]. As a key control technique in swarm robotics, distributed cooperative control of multi-agent systems has also experienced a rapid growth in the research efforts from the international robotics community, which includes consensus control [27], [112], rendezvous control [113], obstacle avoidance [114], formation control [115], [116], etc. Formation control of multi-agent systems is hence a key active area of research which shows broad applications [117]. In applications where the goal cannot be accomplished by a single

robot or a single aerial robotic vehicle due to physical limitations in its capability, formation control has been flagged as an important underpinning methodology. It can be applied to a variety of areas, such as cooperative surveillance [118], target enclosing [119], load transport [120], etc. Based on a consensus strategy, [84] proved that leader-follower, virtual structure and behavior-based formation control approaches can be unified in the framework of consensus problems. [86] discussed the formation stability problems for general high-order swarm systems, but the question how to achieve desired formation was not considered. Static formation experiments on quadrotor swarm systems based on consensus approaches is achieved in [65], while time-varying formation control of aerial swarm systems is still a vigorously active research topic with much progress still needed.

Motivated by the challenges stated above, the combination of time-varying formation control and the proposed innovative tri-rotor drone is developed and investigated in this chapter. The formation control protocol for the designed aerial swarm is fully distributed. The communication topology of the network is modelled using graph theory. Robust feedback linearization [121] is used to handle the tri-rotor drone's highly coupled and nonlinear dynamics. It provides a systematic multi-input/multi-output (MIMO) method which linearises nonlinear dynamics geometrically to match the Jacobi linearization of the nonlinear system at the operating point of interest. In contrast to classic feedback linearization which does full nonlinear dynamic inversion to produce a linear system which is simply a chain of integrators, robust feedback linearization preserves the system information at the operating point of interest. It has been successfully demonstrated [122] to provide significant robustness to both model uncertainty and external dynamics. An output feedback formation control protocol is also applied to the networked tri-rotor UAV swarm, which consists of an optimal state observer and a Linear Quadratic Regulator (LQR)-based distributed state feedback formation protocol. It is shown that LQR based optimal design provides a straightforward way to construct fully distributed controllers and observers that ensure stabilization and synchronization of the swarm [123].

The chapter is organized as follows. The nonlinear dynamical model of the tri-rotor drone is described in Section 5.2. Robust feedback linearization of a single tri-rotor drone is first given in Section 5.3 and then an optimal distributed formation controller is designed at the end of Section 5.3 to control a swarm of tri-rotor drones. Section 5.4 is devoted to the

presentation of simulation results when the proposed control architecture is applied to the aerial swarm of tri-rotor drones. Conclusions are given in Section 5.5.

5.2 Mathematical Modeling

In this section, we dynamically modeling the proposed tri-rotor UAV.

5.2.1 System Description

The configuration of the tri-rotor UAV was first proposed in [2]. The UAV has a triangular structure with three arms and a force generating unit plus a revolute joint at the end of each arm. All three arms have identical length l. Each force generating unit includes a fixed pitch propeller driven by a brushless DC motor to provide thrust. The motors can be powered by a single battery pack located at the centre of mass or by three separate battery packs located at an equal distance from the centre of mass and each other. The propeller-motor assembly is attached to the body arm via a servo motor that can rotate in a vertical plane to tilt the propeller-motor assembly with an angle α_{si} (the subscript 's' denotes servo) in order to produce a horizontal component of the generated force.

All three propellers can be tilted independently to give full thrust vectoring authority. Then the UAV becomes a full six-degrees-of-freedom (6-DOF) vehicle in which all motions can be achieved independently by changing speed of the propellers and tilting angles of the servo motor directly. This configuration enables vehicle attitude (i.e. 3D orientation) and vehicle translation (i.e. 3D movement) to be independently controlled.

In order to develop the dynamic model of the proposed tri-rotor UAV, the following right hand coordinate systems shown in Fig. 5.1 are considered: (X_e, Y_e, Z_e) represents the earth coordinate system, which is assumed to be inertial (i.e. fixed). (X_b, Y_b, Z_b) denotes the body coordinate system, where the origin O_b is fixed to the center of mass of the vehicle. This coordinate system moves with the vehicle. (X_{li}, Y_{li}, Z_{li}) with $i \in \{1,2,3\}$ is the local coordinate system of each propeller-motor assembly. The location of the origin of each local

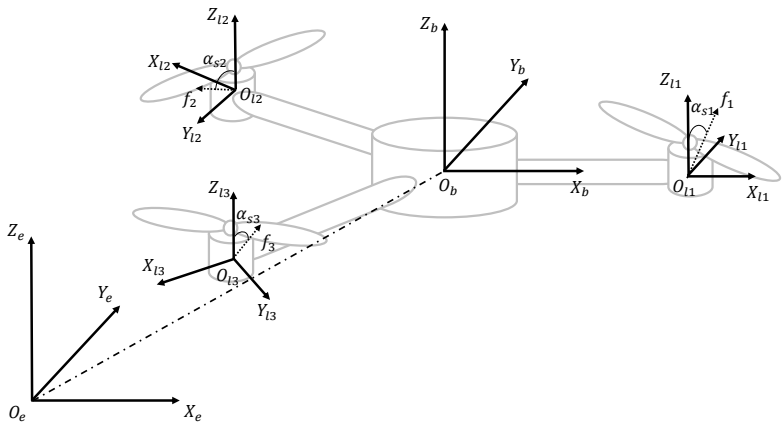

Figure 5.1: Coordinate systems of the tri-rotor UAV [2].

coordinate system coincides with the intersection of the UAV arm and the propeller-motor assembly, where X_{li} is extended outside the ith arm of UAV along the same line as the arm and Z_{li} is along the direction of the motor shaft axis when the servo angle is zero.

In this section, the superscript b, e and l_i are used to denote the corresponding coordinate system in which vectors are expressed. The subscript i refers to the ith propeller, servo motor or brushless DC motor with $i \in \{1,2,3\}$. The nominal mathematical model is based on the following assumptions:

1) Fast actuators are assumed, so the dynamics of actuators are neglected.

2) Propellers are considered to be rigid, thus blade flapping is not considered in the model.

3) The body structure is rigid and the mass is fixed.

It should be noted that although we do not consider these factors in model design, they can still be included as perturbations and uncertainties when carrying out simulation or experiment to test the robustness of the proposed control system in the next section.

5.2.2 Dynamic Model

The dynamic model of the tri-rotor can be described by

$$\dot{v}_v^b = g\Theta - S(\omega_v^b)v_v^b + \frac{k_f}{m}H_f\rho, \tag{5.1}$$

Table 5.1: Notation of the tri-rotor UAV model

Symbol	Defination
ω_{mi}	Rotational speed of the ith DC motor
α_{si}	Tilting angle of the ith servo motor
k_f	Thrust-to-speed constant of the propeller
k_d	Torque-to-speed constant of the propeller
g	Gravitational acceleration
m	Total mass of the UAV
I_v^b	Inertia matrix of the UAV
κ_v^b	The transitional velocity of the UAV
u_b, v_b, w_b	The Cartesian coordinates of the UAV transitional velocity
ω_v^b	Angular velocity of the UAV
p, q, r	The Cartesian coordinates of the UAV angular velocity
η_v	Attitude vector of the UAV related to the earth frame
λ_v^e	Position vector of the UAV (earth frame)
ϕ	Roll angle of the UAV related to the earth frame
θ	Pitch angle of the UAV related to the earth frame
ψ	Yaw angle of the UAV related to the earth frame
x_v	The x coordinate position of the UAV in the earth frame
y_v	The y coordinate position of the UAV in the earth frame
z_v	The z coordinate position of the UAV in the earth frame
R_b^e	The rotational matrix from frame b to frame e

$$\dot{\omega}_v^b = -(I_v^b)^{-1} S(\omega_v^b) I_v^b \omega_v^b + (I_v^b)^{-1}(k_f H_t - k_d H_f)\rho, \tag{5.2}$$

$$\dot{\eta}_v = \Psi \omega_v^b, \tag{5.3}$$

$$\dot{\lambda}_v^e = R_b^e v_v^b, \tag{5.4}$$

where all terms used in the model of the UAV are described in Table 5.1 and

$$v_v^b = \begin{bmatrix} u_b \\ v_b \\ w_b \end{bmatrix}, \ \omega_v^b = \begin{bmatrix} p \\ q \\ r \end{bmatrix}, \ \eta_v = \begin{bmatrix} \phi \\ \theta \\ \psi \end{bmatrix} \text{ and } \lambda_v^e = \begin{bmatrix} x_v \\ y_v \\ z_v \end{bmatrix}.$$

The vehicle's inertia matrix expressed in the body coordinate frame and the skew matrix constructed from the vector $\omega_v^b = [p\ q\ r]^T$ are given by

$$I_v^b = \begin{bmatrix} I_{xx} & 0 & 0 \\ 0 & I_{yy} & -I_{yz} \\ 0 & -I_{yz} & I_{zz} \end{bmatrix} \tag{5.5}$$

and

$$S(\omega_v^b) = \begin{bmatrix} 0 & -r & q \\ r & 0 & -p \\ -q & p & 0 \end{bmatrix}. \tag{5.6}$$

More details of modeling process and the construction of parameters are defined in [2, 13].

Choosing the state vector as

$$\begin{aligned} x &= [x_1 \;\; x_2 \;\; x_3 \;\; x_4 \;\; x_5 \;\; x_6 \;\; x_7 \;\; x_8 \;\; x_9 \;\; x_{10} \;\; x_{11} \;\; x_{12}]^T \\ &= [u_b \;\; v_b \;\; w_b \;\; p \;\; q \;\; r \;\; \phi \;\; \theta \;\; \psi \;\; x_v \;\; y_v \;\; z_v]^T, \end{aligned} \tag{5.7}$$

and the input vector as

$$u = \rho = \begin{bmatrix} u_1 \\ u_2 \\ u_3 \\ u_4 \\ u_5 \\ u_6 \end{bmatrix} = \begin{bmatrix} \omega_{m1}^2 \sin(\alpha_{s1}) \\ \omega_{m2}^2 \sin(\alpha_{s2}) \\ \omega_{m3}^2 \sin(\alpha_{s3}) \\ \omega_{m1}^2 \cos(\alpha_{s1}) \\ \omega_{m2}^2 \cos(\alpha_{s2}) \\ \omega_{m3}^2 \cos(\alpha_{s3}) \end{bmatrix}, \tag{5.8}$$

then the set of (5.1)-(5.4) can be written in the state-space form as

$$\dot{x}_1 = x_2x_6 - x_3x_5 + g\sin(x_8) - \frac{\sqrt{3}k_f}{2m}u_2 + \frac{\sqrt{3}k_f}{2m}u_3, \tag{5.9}$$

$$\dot{x}_2 = x_3x_4 - x_1x_6 - g\sin(x_7)\cos(x_8) + \frac{k_f}{m}u_1 - \frac{k_f}{2m}u_2 - \frac{k_f}{2m}u_3, \tag{5.10}$$

$$\dot{x}_3 = x_1x_5 - x_2x_4 - g\cos(x_7)\cos(x_8) + \frac{k_f}{m}u_4 + \frac{k_f}{m}u_5 + \frac{k_f}{m}u_6, \tag{5.11}$$

$$\dot{x}_4 = \frac{x_5x_6(I_{yy} - I_{zz}) + I_{yz}(x_5^2 - x_6^2)}{I_{xx}} + \frac{\sqrt{3}k_d}{2I_{xx}}u_2 - \frac{\sqrt{3}k_d}{2I_{xx}}u_3 + \frac{\sqrt{3}lk_f}{2I_{xx}}u_5 - \frac{\sqrt{3}lk_f}{2I_{xx}}u_6, \tag{5.12}$$

$$\begin{aligned}\dot{x}_5 = {} & \frac{x_4x_5(I_{xx}I_{yz} - I_{yy}I_{yz} - I_{zz}I_{yz})}{I_{yy}I_{zz} - I_{yz}^2} + \frac{x_4x_6(I_{yz}^2 + I_{zz}^2 - I_{xx}I_{zz})}{I_{yy}I_{zz} - I_{yz}^2} + \frac{I_{yz}k_fl - I_{zz}k_d}{I_{yy}I_{zz} - I_{yz}^2}u_1 \\ & + \frac{2I_{yz}k_fl + I_{zz}k_d}{2(I_{yy}I_{zz} - I_{yz}^2)}u_2 + \frac{2I_{yz}k_fl + I_{zz}k_d}{2(I_{yy}I_{zz} - I_{yz}^2)}u_3 - \frac{I_{zz}k_fl + I_{yz}k_d}{I_{yy}I_{zz} - I_{yz}^2}u_4 \\ & + \frac{I_{zz}k_fl - 2I_{yz}k_d}{2(I_{yy}I_{zz} - I_{yz}^2)}u_5 + \frac{I_{zz}k_fl - 2I_{yz}k_d}{2(I_{yy}I_{zz} - I_{yz}^2)}u_6,\end{aligned} \tag{5.13}$$

$$\begin{aligned}\dot{x}_6 = {} & \frac{x_4x_6(I_{yy}I_{yz} + I_{zz}I_{yz} - I_{xx}I_{yz})}{I_{yy}I_{zz} - I_{yz}^2} + \frac{x_4x_5(I_{xx}I_{yy} - I_{yz}^2 - I_{yy}^2)}{I_{yy}I_{zz} - I_{yz}^2} + \frac{I_{yy}k_fl - I_{yz}k_d}{I_{yy}I_{zz} - I_{yz}^2}u_1 \\ & + \frac{2I_{yy}k_fl + I_{yz}k_d}{2(I_{yy}I_{zz} - I_{yz}^2)}u_2 + \frac{2I_{yy}k_fl + I_{yz}k_d}{2(I_{yy}I_{zz} - I_{yz}^2)}u_3 - \frac{I_{yz}k_fl + I_{yy}k_d}{I_{yy}I_{zz} - I_{yz}^2}u_4 \\ & + \frac{I_{yz}k_fl - 2I_{yy}k_d}{2(I_{yy}I_{zz} - I_{yz}^2)}u_5 + \frac{I_{yz}k_fl - 2I_{yy}k_d}{2(I_{yy}I_{zz} - I_{yz}^2)}u_6,\end{aligned} \tag{5.14}$$

$$\dot{x}_7 = x_4 + x_5\sin(x_7)\tan(x_8) + x_6\cos(x_7)\tan(x_8), \tag{5.15}$$

$$\dot{x}_8 = x_5\cos(x_7) - x_6\sin(x_7), \tag{5.16}$$

$$\dot{x}_9 = x_5\sin(x_7)\sec(x_8) + x_6\cos(x_7)\sec(x_8), \tag{5.17}$$

$$\begin{aligned}\dot{x}_{10} = {} & x_1\cos(x_8)\cos(x_9) + x_2(\sin(x_7)\sin(x_8)\cos(x_9) - \cos(x_7)\sin(x_9)) \\ & + x_3(\cos(x_7)\sin(x_8)\cos(x_9) + \sin(x_7)\sin(x_9)),\end{aligned} \tag{5.18}$$

$$\begin{aligned}\dot{x}_{11} = {} & x_1\cos(x_8)\sin(x_9) + x_2(\sin(x_7)\sin(x_8)\sin(x_9) + \cos(x_7)\cos(x_9)) \\ & + x_3(\cos(x_7)\sin(x_8)\sin(x_9) - \sin(x_7)\cos(x_9)),\end{aligned} \tag{5.19}$$

$$\dot{x}_{12} = -x_1\sin(x_8) + x_2\sin(x_7)\cos(x_8) + x_3\cos(x_7)\cos(x_8). \tag{5.20}$$

The output vector is chosen as

$$y = \begin{bmatrix} \phi \\ \theta \\ \psi \\ x_v \\ y_v \\ z_v \end{bmatrix} = \begin{bmatrix} x_7 \\ x_8 \\ x_9 \\ x_{10} \\ x_{11} \\ x_{12} \end{bmatrix}. \tag{5.21}$$

Remark 5.2.1. Note that the real inputs (ω_{mi} and α_{si}) are mapped into the control inputs u_i via the nonlinear mapping (5.8). It can be shown that this nonlinear mapping is invertible thus giving actuator signals ω_{mi} and α_{si} for use in real application. The physical actuator inputs ω_{mi} and α_{si} can be calculated back from the control inputs u_i via

$$\alpha_{si} = \arctan\left(\frac{u_i}{u_{i+3}}\right) \text{ and } \omega_{mi} = \sqrt[4]{u_i^2 + u_{i+3}^2}\ \forall i \in \{1,2,3\}.$$

5.3 Control System Design

The objective of this section is to design a robust distributed formation control protocol for swarms of the proposed tri-rotor UAV. Since the dynamical model of a single tri-rotor UAV is highly coupled and nonlinear, a robust feedback linearization technique is first applied to each tri-rotor to obtain simpler closed-loop dynamics. Then the swarm of identical tri-rotor UAVs is controlled through an optimal distributed formation control protocol which solves the time-varying formation tracking problem for tri-rotor robotic swarms.

5.3.1 Robust Feedback Linearization

Consider a single nonlinear system with n states, m inputs, and m outputs described by

$$\dot{x} = F(x) + G(x)u = F(x) + \sum_{i=1}^{m} G_i(x)u_i, \tag{5.22}$$

$$y = [H_1(x), \ldots, H_m(x)]^T, \tag{5.23}$$

where $x(t) \in \mathbb{R}^n$ denotes the state vector, $u(t) \in \mathbb{R}^m$ is the control input, $y(t) \in \mathbb{R}^m$ is the output vector, and $F(x)$, $G_1(x), \ldots, G_m(x)$, y are smooth vector fields defined on an open subset of $\mathbb{R}^n$.

Suppose that this system satisfies the well-known conditions for feedback linearization [124]: The relative degree of H_i is equal to r_i for $i \in \{1, \ldots, m\}$ such that $r_1 + \cdots + r_m = n$, and the decoupling matrix

$$M(x) = \begin{bmatrix} L_{G_1} L_f^{r_1-1} H_1(x) & \ldots & L_{G_m} L_f^{r_1-1} H_1(x) \\ \vdots & \ddots & \vdots \\ L_{G_1} L_f^{r_m-1} H_m(x) & \ldots & L_{G_m} L_f^{r_m-1} H_m(x) \end{bmatrix} \tag{5.24}$$

is invertible, where $L_{(.)}(.)$ denotes the Lie derivative operator [124]. It is then possible to find a feedback linearizing control law of the form

$$u(x, w) = \alpha_c(x) + \beta_c(x) w, \tag{5.25}$$

where $w(t)$ is a new control input, and $\alpha_c(x) = -M^{-1}(x) \begin{bmatrix} L_f^{r_1} H_1(x) & \ldots & L_f^{r_m} H_m(x) \end{bmatrix}^T$, $\beta_c(x) = M^{-1}(x)$, such that on application of the control law in (5.25), the nonlinear state-equation (5.22) reduces into the linear state-equation

$$\dot{x}_c = A_c x_c + B_c w, \tag{5.26}$$

where A_c and B_c are matrices of the Brunovsky canonical form [124], and a change of coordinates is given by $x_c = \phi_c(x)$ with $\phi_{ci}^T(x) = \left[H_i(x),\ L_f H_i(x),\ \ldots,\ L_f^{r_i-1} H_i(x)\right]$ and $\phi_c^T(x) = \left[\phi_{c1}^T(x),\ \ldots,\ \phi_{cm}^T(x)\right]$.

The robust feedback linearization technique [121], on the other hand, exactly transforms the nonlinear state-equation into a linear state-equation that is equal to the Jacobi linear approximation of the original nonlinear state-equation around the origin. This can then be controlled using linear techniques [122]. In the robust feedback linearization case, the linearized state-equation becomes

$$\dot{x}_r = A_r x_r + B_r v, \tag{5.27}$$

where $A_r = \partial_x F(0)$ and $B_r = G(0)$. The nonlinear state-equation (5.22) is geometrically transformed into the linear state-equation of any operating point, not only in a small neighborhood of the origin point. [121] argues that classical feedback linearization may be non

robust in the presence of uncertainties as any system is transformed into a chain of integrators (i.e. Brunovsky form) whereas robust feedback linearization preserves some system information.

The robust feedback linearization control law is

$$u(x,v) = \alpha(x) + \beta(x)v, \tag{5.28}$$

where

$$\alpha(x) = \alpha_c(x) + \beta_c(x)LU^{-1}\phi_c(x), \tag{5.29}$$

$$\beta(x) = \beta_c(x)R^{-1}, \tag{5.30}$$

$$\phi_r(x) = U^{-1}\phi_c(x), \tag{5.31}$$

$$L = -M(0)\partial_x\alpha_c(0), \tag{5.32}$$

$$R = M^{-1}(0), \tag{5.33}$$

$$U = \partial_x\phi_c(0), \tag{5.34}$$

$$x_r = \phi_r(x). \tag{5.35}$$

Now we apply the robust feedback linearization to the dynamics of tri-rotor UAV system. The relative degrees $r_1 = 2$, $r_2 = 2$, $r_3 = 2$, $r_4 = 2$, $r_5 = 2$ and $r_6 = 2$ are computed from the output (5.21), resulting in a vector relative degree $r = 12$, which is equal to the number of states. The decoupling matrix $M(x)$ can also be written in a compact form as given in [2]:

$$M(x) = \begin{bmatrix} \Psi(I_v^b)^{-1}(k_f H_t - k_d H_f) \\ \frac{k_f}{m} R_b^e H_f \end{bmatrix}. \tag{5.36}$$

It can be verified that $\det[M(x)] \neq 0$ as the pitch angle is assumed to be in the range of $-\pi/2 < \theta < \pi/2$, such that $M(x)$ is always invertible in this case. As a result, the conditions for feedback linearization are satisfied.

After calculating the classic Brunowski form linearizing input (5.25) and applying the formulas for the robust feeedback linearization (5.28)-(5.35), the system can then be robust feedback linearized into

$$\dot{x}_r = A_r x_r + B_r v, \tag{5.37}$$

$$y = C_r x_r. \tag{5.38}$$

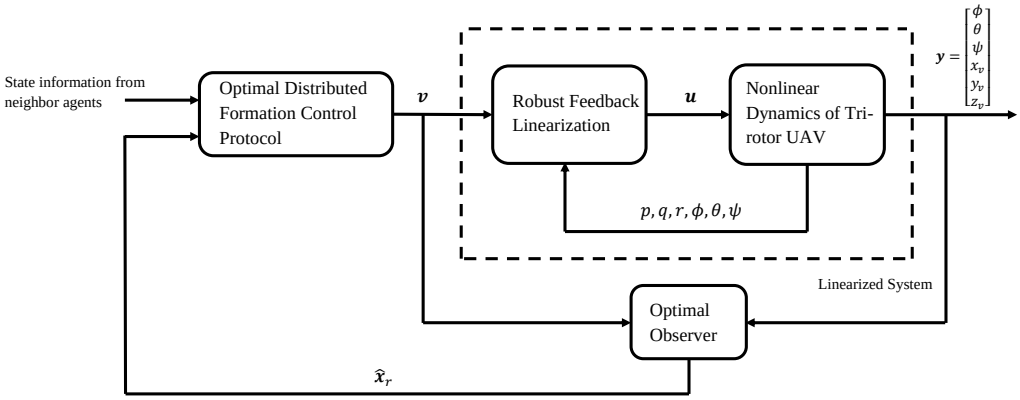

Figure 5.2: Control system scheme: Distributed optimal formation control law and robust feedback linearization combining linear and nonlinear parts

The state space matrix A_r, B_r and C_r are given by

$$A_r = \begin{bmatrix} 0&0&0&0&0&0&0&g&0&0&0&0 \\ 0&0&0&0&0&0&-g&0&0&0&0&0 \\ 0&0&0&0&0&0&0&0&0&0&0&0 \\ 0&0&0&0&0&0&0&0&0&0&0&0 \\ 0&0&0&0&0&0&0&0&0&0&0&0 \\ 0&0&0&0&0&0&0&0&0&0&0&0 \\ 0&0&0&1&0&0&0&0&0&0&0&0 \\ 0&0&0&0&1&0&0&0&0&0&0&0 \\ 0&0&0&0&0&1&0&0&0&0&0&0 \\ 1&0&0&0&0&0&0&0&0&0&0&0 \\ 0&1&0&0&0&0&0&0&0&0&0&0 \\ 0&0&1&0&0&0&0&0&0&0&0&0 \end{bmatrix}, \tag{5.39}$$

$$B_r = \begin{bmatrix} 0 & -\frac{\sqrt{3}k_f}{2m} & \frac{\sqrt{3}k_f}{2m} & 0 & 0 & 0 \\ \frac{k_f}{m} & -\frac{k_f}{2m} & -\frac{k_f}{2m} & 0 & 0 & 0 \\ 0 & 0 & 0 & \frac{k_f}{m} & \frac{k_f}{m} & \frac{k_f}{m} \\ 0 & \frac{\sqrt{3}k_d}{2I_{xx}} & -\frac{\sqrt{3}k_d}{2I_{xx}} & 0 & \frac{\sqrt{3}lk_f}{2I_{xx}} & -\frac{\sqrt{3}lk_f}{2I_{xx}} \\ \frac{I_{yz}k_f l - I_{zz}k_d}{I_{yy}I_{zz}-I_{yz}^2} & \frac{2I_{yz}k_f l + I_{zz}k_d}{2(I_{yy}I_{zz}-I_{yz}^2)} & \frac{2I_{yz}k_f l + I_{zz}k_d}{2(I_{yy}I_{zz}-I_{yz}^2)} & -\frac{I_{zz}k_f l + I_{yz}k_d}{I_{yy}I_{zz}-I_{yz}^2} & \frac{I_{zz}k_f l - 2I_{yz}k_d}{2(I_{yy}I_{zz}-I_{yz}^2)} & \frac{I_{zz}k_f l - 2I_{yz}k_d}{2(I_{yy}I_{zz}-I_{yz}^2)} \\ \frac{I_{yy}k_f l - I_{yz}k_d}{I_{yy}I_{zz}-I_{yz}^2} & \frac{2I_{yy}k_f l + I_{yz}k_d}{2(I_{yy}I_{zz}-I_{yz}^2)} & \frac{2I_{yy}k_f l + I_{yz}k_d}{2(I_{yy}I_{zz}-I_{yz}^2)} & -\frac{I_{yz}k_f l + I_{yy}k_d}{I_{yy}I_{zz}-I_{yz}^2} & \frac{I_{yz}k_f l - 2I_{yy}k_d}{2(I_{yy}I_{zz}-I_{yz}^2)} & \frac{I_{yz}k_f l - 2I_{yy}k_d}{2(I_{yy}I_{zz}-I_{yz}^2)} \\ 0 & 0 & 0 & 0 & 0 & 0 \\ 0 & 0 & 0 & 0 & 0 & 0 \\ 0 & 0 & 0 & 0 & 0 & 0 \\ 0 & 0 & 0 & 0 & 0 & 0 \\ 0 & 0 & 0 & 0 & 0 & 0 \\ 0 & 0 & 0 & 0 & 0 & 0 \end{bmatrix}, \tag{5.40}$$

$$C_r = \begin{bmatrix} 0&0&0&0&0&0&1&0&0&0&0&0 \\ 0&0&0&0&0&0&0&1&0&0&0&0 \\ 0&0&0&0&0&0&0&0&1&0&0&0 \\ 0&0&0&0&0&0&0&0&0&1&0&0 \\ 0&0&0&0&0&0&0&0&0&0&1&0 \\ 0&0&0&0&0&0&0&0&0&0&0&1 \end{bmatrix}. \tag{5.41}$$

Furthermore, L, R and U are calculated by

$$L = \begin{bmatrix} 0&0&0&0&0&0&0&0&0&0&0&0 \\ 0&0&0&0&0&0&0&0&0&0&0&0 \\ 0&0&0&0&0&0&0&0&0&0&0&0 \\ 0&0&0&0&0&0&0&g&0&0&0&0 \\ 0&0&0&0&0&0&-g&0&0&0&0&0 \\ 0&0&0&0&0&0&0&0&0&0&0&0 \end{bmatrix}, \tag{5.42}$$

$$R = \begin{bmatrix} 0 & -\frac{I_{yz}}{3k_f l} & \frac{I_{zz}}{3k_f l} & 0 & \frac{2m}{3k_f} & \frac{k_d m}{3k_f^2 l} \\ 0 & -\frac{I_{yz}}{3k_f l} & \frac{I_{zz}}{3k_f l} & -\frac{\sqrt{3}m}{3k_f} & -\frac{m}{3k_f} & \frac{k_d m}{3k_f^2 l} \\ 0 & -\frac{I_{yz}}{3k_f l} & \frac{I_{zz}}{3k_f l} & \frac{\sqrt{3}m}{3k_f} & -\frac{m}{3k_f} & \frac{k_d m}{3k_f^2 l} \\ 0 & -\frac{2I_{yy}}{3k_f l} & \frac{2I_{yz}}{3k_f l} & 0 & -\frac{2k_d m}{3k_f^2 l} & \frac{m}{3k_f} \\ \frac{\sqrt{3}I_{xx}}{3k_f l} & \frac{I_{yy}}{3k_f l} & -\frac{I_{yz}}{3k_f l} & \frac{\sqrt{3}k_d m}{3k_f^2 l} & \frac{k_d m}{3k_f^2 l} & \frac{m}{3k_f} \\ -\frac{\sqrt{3}I_{xx}}{3k_f l} & \frac{I_{yy}}{3k_f l} & -\frac{I_{yz}}{3k_f l} & -\frac{\sqrt{3}k_d m}{3k_f^2 l} & \frac{k_d m}{3k_f^2 l} & \frac{m}{3k_f} \end{bmatrix}, \tag{5.43}$$

$$U = \begin{bmatrix} 0&0&0&0&0&0&1&0&0&0&0&0 \\ 0&0&0&0&0&0&0&1&0&0&0&0 \\ 0&0&0&0&0&0&0&0&1&0&0&0 \\ 0&0&0&0&0&0&0&0&0&1&0&0 \\ 0&0&0&0&0&0&0&0&0&0&1&0 \\ 0&0&0&0&0&0&0&0&0&0&0&1 \\ 0&0&0&1&0&0&0&0&0&0&0&0 \\ 0&0&0&0&1&0&0&0&0&0&0&0 \\ 0&0&0&0&0&1&0&0&0&0&0&0 \\ 1&0&0&0&0&0&0&0&0&0&0&0 \\ 0&1&0&0&0&0&0&0&0&0&0&0 \\ 0&0&1&0&0&0&0&0&0&0&0&0 \end{bmatrix}, \tag{5.44}$$

and ϕ_c and ϕ_r are given by

$$\phi_c = [x_7\ x_8\ x_9\ x_{10}\ x_{11}\ x_{12}\ \dot{x}_7\ \dot{x}_8\ \dot{x}_9\ \dot{x}_{10}\ \dot{x}_{11}\ \dot{x}_{12}]^T, \tag{5.45}$$

$$\phi_r = [\dot{x}_{10}\ \dot{x}_{11}\ \dot{x}_{12}\ \dot{x}_7\ \dot{x}_8\ \dot{x}_9\ x_7\ x_8\ x_9\ x_{10}\ x_{11}\ x_{12}]^T. \tag{5.46}$$

From (5.35) we know $x_r = \phi_r(x)$. Finally, $\alpha(x)$ and $\beta(x)$ can then be computed from (5.29) and (5.30) directly.

5.3.2 Distributed Optimal Formation Protocol Design

In practical applications, some states do not need to be measured by sensors for controller design. For example, the vehicle's translational velocity in the body coordinate frame v_v^b is not used in the robust feedback linearization controller. It can hence be obtained by using an observer on input and output information of the feedback linearized system. In this section, we propose a distributed optimal formation protocol which uses the neighbourhood state estimation information for controller design and the local output estimation error information for the observer design. The scheme for controlling the dynamics of attitude and position of each tri-rotor UAV, based on robust feedback linearization and distributed optimal output feedback formation protocol, is illustrated in Fig. 5.2.

Assumption 5.3.1. The directed graph $\mathcal{G}$ contains a spanning tree and the root node i can obtain information from the leader node.

Consider a set of N tri-rotor UAVs. Suppose that each tri-rotor UAV has the identical linearized dynamics described by

$$\dot{x}_{ri} = A_r x_{ri} + B_r v_i, \tag{5.47}$$

$$y_i = C_r x_{ri}. \tag{5.48}$$

It can be easily verified that (A_r, B_r, C_r) is stabilizable and detectable.

The dynamics of the leader node, labeled 0, is given by

$$\dot{x}_0 = A_r x_0, \tag{5.49}$$

$$y_0 = C_r x_0. \tag{5.50}$$

where $x_0 \in \mathbb{R}^n$ is the state, $y_0 \in \mathbb{R}^p$ is the output. It can be considered as a command generator, which generates the desired target trajectory. The leader can be observed from a subset of agents in a graph. If node i observes the leader, an edge $(0,i)$ is said to exist with weighting gain $g_i > 0$ as a pinned node. We denote the pinning matrix as $G = \text{diag}\{g_i\} \in \mathbb{R}^{N\times N}$.

The desired formation is specified by the vector $h = \left[h_1^T, h_2^T, \ldots, h_N^T\right]^T$ with $h_i \in \mathbb{R}^n$ being a preset vector known by the corresponding i^{th} agent. It should be noted that the formation problem reduces to a consensus problem when $h_i = 0 \; \forall \; i \in \{1, \ldots, N\}$.

Denote the estimate of the state x_{ri} by $\hat{x}_{ri} \in \mathbb{R}^n$ and let the state estimation error be $\tilde{x}_{ri} = x_{ri} - \hat{x}_{ri}$. Then the consequent estimate of the output y_i is given by $\hat{y}_i = C_r \hat{x}_{ri}$ and the output estimation error for node i is given by $\tilde{y}_i = y_i - \hat{y}_i$. Consider the following distributed optimal formation protocol

$$v_i = cK \sum_{j\in N_i} a_{ij} \left(\left(\hat{x}_{rj} - h_j\right) - \left(\hat{x}_{ri} - h_i\right) \right) + cKg_i \left(x_0 - \left(\hat{x}_{ri} - h_i\right)\right) + \gamma_i, \tag{5.51}$$

$$\dot{\hat{x}}_{ri} = A_r \hat{x}_{ri} + B_r v_i - cF\tilde{y}_i, \tag{5.52}$$

where $c > 0$ is the scalar coupling gain, $K \in \mathbb{R}^{m\times n}$ is the feedback control gain matrix, $F \in \mathbb{R}^{n\times m}$ is the observer gain, and $\gamma_i \in \mathbb{R}^m$ represents the formation compensation signal to be designed.

Let $x = \left[x_{r1}^T, x_{r2}^T, \ldots, x_{rN}^T\right]^T$, $\hat{x} = \left[\hat{x}_{r1}^T, \hat{x}_{r2}^T, \ldots, \hat{x}_{rN}^T\right]^T$, $\tilde{x} = \left[\tilde{x}_{r1}^T, \tilde{x}_{r2}^T, \ldots, \tilde{x}_{rN}^T\right]^T$, $\underline{x}_0 = \mathbf{1}_N \otimes x_0$, and $\gamma = \left[\gamma_1^T, \gamma_2^T, \ldots, \gamma_N^T\right]^T$. Under a control protocol with directed topology, the tri-rotor

UAV swarm can be written in a compact form as

$$\dot{x} = (I_N \otimes A_r)x - c[(L+G) \otimes B_r K](\hat{x} - \underline{x}_0) + c[(L+G) \otimes B_r K]h + (I_N \otimes B_r)\gamma, \tag{5.53}$$

$$\begin{aligned} \dot{\hat{x}} =& (I_N \otimes A_r)\hat{x} - (I_N \otimes cFC_r)(x - \hat{x}) - c[(L+G) \otimes B_r K](\hat{x} - \underline{x}_0) \\ &+ c[(L+G) \otimes B_r K]h + (I_N \otimes B_r)\gamma. \end{aligned} \tag{5.54}$$

It follows the fact that matrix B_r given in (5.40) is of full rank, there always exists a nonsingular matrix $[\tilde{B}^T, \bar{B}^T]^T$ with $\tilde{B} \in \mathbb{R}^{m \times n}$ and $\bar{B} \in \mathbb{R}^{(n-m) \times n}$ such that $\tilde{B}B_r = I_m$ and $\bar{B}B_r = 0$. The following theorem which is motivated by [125], has been improved to deal with output feedback tracking of multi-agent systems.

Theorem 5.3.1. Let $\lambda_i\,(i \in \{1, \ldots, N\})$ be the eigenvalues of $(L+G)$. If Assumption 5.3.1 is satisfied, then the tri-rotor UAV swarm with directed interaction topology asymptotically converges to the formation specified by $(x_0 + h_i) \in \mathbb{R}^n\ \forall i \in \{1, \ldots, N\}$ if the following conditions hold for all $i \in \{1, \ldots, N\}$

$$\bar{B}A_r h_i - \bar{B}\dot{h}_i = 0, \tag{5.55}$$

$$A_r - c\lambda_i B_r K \text{ and } A_r + cFC_r \text{ are Hurwitz}, \tag{5.56}$$

$$\text{and } \gamma_i = \tilde{B}\dot{h}_i - \tilde{B}A_r h_i \text{ for all } i \in \{1, \ldots, N\}. \tag{5.57}$$

Proof. Let formation tracking error be $\Phi_i = x_{ri} - h_i - x_0$ and $\Phi = [\Phi_1^T, \ldots, \Phi_N^T]^T$. Then the global formation error dynamics with directed interaction topology can be written as

$$\begin{aligned} \dot{\Phi} =& [I_N \otimes A_r - c\,(L+G) \otimes B_r K]\Phi + c[(L+G) \otimes B_r K]\tilde{x} \\ &+ (I_N \otimes A_r)\,h - (I_N \otimes I_N)\dot{h} + (I_N \otimes B_r)\,\gamma. \end{aligned} \tag{5.58}$$

The global observer error dynamics is

$$\dot{\tilde{x}} = I_N \otimes (A_r + cFC_r)\tilde{x}. \tag{5.59}$$

In view of Assumption 5.3.1, all the eigenvalues of matrix $(L+G)$ have positive real parts [126]. It is well known that there exists a nonsingular T such that $T^{-1}\,(L+G)\,T$ is in the

Jordan canonical form J. Let $\vartheta = \left(T^{-1} \otimes I_n\right) \Phi = \left[\vartheta_1^T, \vartheta_2^T, \ldots, \vartheta_N^T\right]^T$. Then the multi-agent system can be represented in terms of ϑ as

$$\begin{aligned} \dot{\vartheta} = &(I_N \otimes A_r - cJ \otimes B_r K)\,\vartheta + c[T^{-1}(L+G) \otimes B_r K]\tilde{x} \\ &+ \left(T^{-1} \otimes A_r\right) h - (T^{-1} \otimes I_N)\dot{h} + \left(T^{-1} \otimes B_r\right)\gamma. \end{aligned} \tag{5.60}$$

If condition (5.55) holds, then for all $i \in \{1, \ldots, N\}$

$$\bar{B}A_r h_i - \bar{B}\dot{h}_i + \bar{B}B_r\gamma_i = 0. \tag{5.61}$$

By letting $\gamma_i = \tilde{B}\dot{h}_i - \tilde{B}A_r h_i$, it follows that

$$\tilde{B}A_r h_i - \tilde{B}\dot{h}_i + \tilde{B}B_r\gamma_i = 0. \tag{5.62}$$

From (5.61) and (5.62) and the fact that $\left[\tilde{B}^T, \bar{B}^T\right]^T$ is nonsingular, one gets

$$A_r h_i - \dot{h}_i + B_r\gamma_i = 0, \tag{5.63}$$

which means that

$$(I_N \otimes A_r)\,h - (I_N \otimes I_N)\dot{h} + (I_N \otimes B_r)\,\gamma = 0. \tag{5.64}$$

Pre-multiplying the both sides of (5.64) by $T^{-1} \otimes I_N$ yields

$$\left(T^{-1} \otimes A_r\right) h - (T^{-1} \otimes I_N)\dot{h} + \left(T^{-1} \otimes B_r\right)\gamma = 0. \tag{5.65}$$

Then (5.60) reduces to the following dynamics

$$\dot{\vartheta} = (I_N \otimes A_r - cJ \otimes B_r K)\,\vartheta + c[T^{-1}(L+G) \otimes B_r K]\tilde{x}. \tag{5.66}$$

From (5.66) and (5.59), it can be obtained that

$$\begin{bmatrix} \dot{\vartheta} \\ \dot{\tilde{x}} \end{bmatrix} = \begin{bmatrix} A_e & B_e \\ 0 & I_N \otimes (A_r + cFC_r) \end{bmatrix} \begin{bmatrix} \vartheta \\ \tilde{x} \end{bmatrix}, \tag{5.67}$$

where

$$A_e = I_N \otimes A_r - cJ \otimes B_r K,$$

$$B_e = cT^{-1}(L+G) \otimes B_r K.$$

Therefore, the global error system in (5.67) is asymptotically stable if and only if both A_e and $I_N \otimes (A_r + cFC_r)$ are Hurwitz, and the latter can be satisfied due to the detectability of

(C_r, A_r). Note that the the state matrix A_e is either block diagonal or block upper-triangular. Hence the stability of (5.67) is equivalent to the stability of the N subsystems defined with the diagonal blocks. Therefore, $A_r - c\lambda_i B_r K$ is Hurwitz $\forall\ i \in \{1,\ldots,N\}$ if and only if $I_N \otimes A_r - cJ \otimes B_r K$ is Hurwitz. Therefore, ϑ converges asymptotically to the origin which is equivalent to stating that x_{ri} converges asymptotically to $x_0 + h_i$ for all $i \in \{1,\ldots,N\}$. □

Next we will show how to select state variable feedback control gain K to guarantee stability on arbitrary directed graphs containing a spanning tree by using LQR based optimal design and proper choice of the coupling gain c. The following theorem is an extension of a result in [123], which only considers the consensus problem. In the case where $h = 0$, the optimal formation tracking protocol (5.51) becomes the optimal consensus tracking protocol of [123], so it can be viewed as a special case of the result in the current chapter.

Theorem 5.3.2. Let $Q = Q^T \in \mathbb{R}^{n\times n}$ and $R = R^T \in \mathbb{R}^{m\times m}$ be positive definite matrices. Let P be the unique positive definite solution of the algebraic Riccati equation

$$A_r^T P + PA_r + Q - PB_r R^{-1} B_r^T P = 0. \tag{5.68}$$

Then, under Assumption 5.3.1 and condition (5.55), the distributed formation tracking control protocol (5.51) with

$$K = R^{-1} B_r^T P \tag{5.69}$$

and γ_i set as in (5.57) ensures that the tri-rotor UAV swarm with directed interaction topology asymptotically converges to the formation specified by $(x_0 + h_i) \in \mathbb{R}^n\ \forall i \in \{1,\ldots,N\}$ if the coupling gain

$$c \geq \frac{1}{2\lambda_R} \tag{5.70}$$

with $\lambda_R = \min_{i\in\{1,\ldots,N\}} \mathrm{Re}\,(\lambda_i)$, where λ_i are the eigenvalues of $(L+G)$.

Proof. Consider the stability of the following subsystem

$$\dot{\delta}_i = (A_r - c\lambda_i B_r K)\,\delta_i, \tag{5.71}$$

where δ denotes the formation tracking closed-loop error. Construct the following Lyapunov candidate function

$$V_i = \delta_i^* P \delta_i. \tag{5.72}$$

Taking the derivative of V_i along the trajectory of subsystem gives

$$\dot{V}_i = \delta_i^* \left(PA_r + A_r^T P - c\lambda_i^* (B_r K)^T P - c\lambda_i PB_r K\right)\delta_i. \tag{5.73}$$

Substituting $K = R^{-1}B_r^T P$ and $A_r^T P + PA_r = -Q + PB_r R^{-1} B_r^T P$ into (5.71) one has

$$\dot{V}_i = \left[1 - 2c\mathrm{Re}\left(\lambda_i\right)\right]\delta_i^* \left(PB_r R^{-1} B_r^T P\right)\delta_i - \delta_i^* Q\delta_i. \tag{5.74}$$

It can be seen that if condition (5.70) holds, then $\dot{V}_i < 0$. Therefore, $A_r - c\lambda_i B_r K$ is Hurwitz for all $i \in \{1, \ldots, N\}$ by Lyapunov theory [127]. This completes the proof. □

The ARE in (5.68) is extracted by minimizing the following performance index for each tri-rotor UAV

$$J_i = \frac{1}{2}\int_0^\infty (\delta_i^T Q\delta_i + v_i^T R v_i)dt. \tag{5.75}$$

The design Riccati matrices Q and R can be selected to adjust the relative cost of formation tracking error and control effort. This allows the cooperative control system to be tuned to trade-off between the speed of formation tracking and the speed of DC motors to achieve it.

Remark 5.3.1. In order to enhance the robustness of our tri-rotor UAV, suppose external white noises ε_1 and ε_2 are added to (5.47) and (5.48) respectively, which satisfy that

$$E[\varepsilon_1 {\varepsilon_1}^T] = \bar{Q}, E[\varepsilon_2 {\varepsilon_2}^T] = \bar{R}, E[\varepsilon_1 {\varepsilon_2}^T] = 0, \tag{5.76}$$

where E donates the expected value, and $\bar{Q}$ and $\bar{R}$ are positive definite matrices. Then a local optimal observer gain F can be calculated by a similar approach (see [128] for further details) as

$$F = \bar{P}C_r^T \bar{R}^{-1}, \tag{5.77}$$

where $\bar{P}$ is the unique positive definite solution of ARE

$$A_r\bar{P} + \bar{P}A_r^T - \bar{P}C_r^T \bar{R}^{-1} C_r \bar{P} + \bar{Q} = 0. \tag{5.78}$$

This optimal observer is also known as Kalman-Bucy filter [129], which has been widely used in system state estimation. It has been demonstrated [130] to have many advantages, including optimality of state estimation in the presence of white noise and external disturbance [131].

Algorithm 3 Procedure for construction of the control law of a tri-rotor UAV robotic swarm

1: initialize state variables for a tri-rotor UAV robotic swarm;
2: **for** each vehicle $i \in \{1, \ldots, N\}$ **do**
3: select the desired formation reference $h_i \in \mathbb{R}^n$;
4: **if** formation feasibility condition (5.55) is satisfied **then**
5: compute distributed feedback gain K using (5.69) and (5.68);
6: select coupling gain c according to condition (5.70);
7: compute local optimal observer gain F using (5.77) and (5.78);
8: set $\gamma_i \in \mathbb{R}^n$ according to (5.57);
9: set the distributed optimal formation control protocol v_i as in (5.51) and (5.52);
10: set the robust feedback control law u_i as in (5.28).
11: **else**
12: back to Step 3;
13: **end if**
14: **end for**

With the above analysis, the procedure to construct the control law u_i is given in Algorithm 3.

Validation of internal stability using closed-loop data from experiments can be performed using technique described in [132]. This is useful as one would also expect unmodelled dynamics.

5.4 Simulation Results

The electric propulsion unit of the tri-rotor UAV includes energy storage units (battery packs), electronic speed control units (ESC), electric motors (brushless DC motors), and propellers. Also, an embedded system is installed on the main body, which includes an on-board microcontroller (OBM), a data acquisition module (DAQ) and a sensor module (IMU). The measured model parameters of the tri-rotor UAV are given in Table 5.2.

The simulation environment has been designed and implemented in Simscape Multibody™ and Simulink® for more realistic results as this provides a 3D graphical display of physical devices. Simscape Multibody™ is used to develop the dynamic model of the tri-rotor UAV based on physical components such as joints, constraints, force elements, and sensors. The designed control system is implemented in Simulink®. Furthermore, a time delay of 0.01s in servo motor responses and a maximum speed saturation constraint of 12000 RPM on the electric motors are considered in the simulation model to mimic real physical considerations.

Table 5.2: Tri-rotor UAV and controller parameters

	Value	Unit	Description
m	0.5	kg	Tri-rotor mass
g	9.81	$\mathrm{m/s^2}$	Gravity acceleration
l	0.23	m	Arm length
I_{xx}	6.8×10^{-3}	$\mathrm{kg \cdot m^2}$	Moment of inertia along X_b
I_{yy}	5.3×10^{-3}	$\mathrm{kg \cdot m^2}$	Moment of inertia along Y_b
I_{zz}	1.7×10^{-3}	$\mathrm{kg \cdot m^2}$	Moment of inertia along Z_b
I_{yz}	3.1×10^{-4}	$\mathrm{kg \cdot m^2}$	Product of inertia about Y_b and Z_b
k_f	1.97×10^{-5}	$\mathrm{kg \cdot m/rad^2}$	Thrust to speed coefficient
k_d	2.88×10^{-7}	$\mathrm{kg \cdot m^2/rad^2}$	Drag to speed coefficient

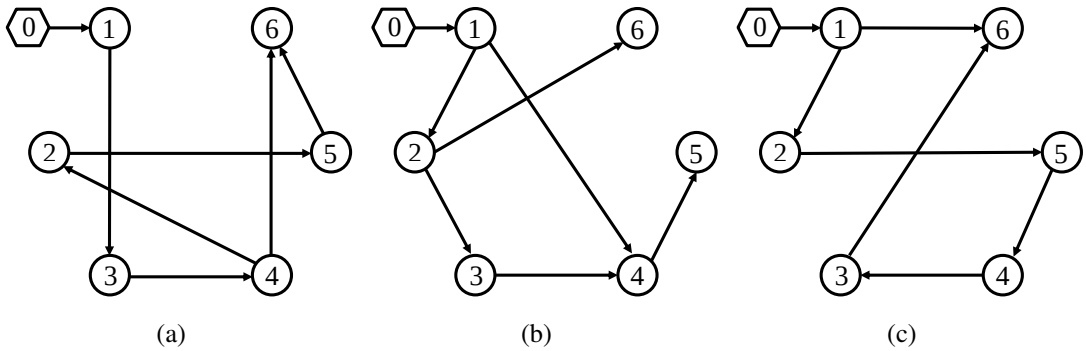

Figure 5.3: Directed interaction topologies

For this case study, consider a set of six tri-rotor UAVs performing a target surveillance task, whose goal is to track a predefined time-varying formation while maintaining different attitudes individually for monitoring the full range of target activity. The directed interaction topology among the six vehicles is shown in Fig. 5.3, where the leader agent 0 provides the formation reference signal and the directed topology is switched every 5 seconds in sequence. Recall that $h_i \in \mathbb{R}^n$ is the formation offset vector with respect to the formation reference $x_0 \in \mathbb{R}^n$. The 3D attitude and 3D position of each UAV are chosen independently.

The matrix $\bar{B}$ can be chosen as

$$\bar{B} = \begin{bmatrix} 0&0&0&0&0&0&1&0&0&0&0&0 \\ 0&0&0&0&0&0&0&1&0&0&0&0 \\ 0&0&0&0&0&0&0&0&1&0&0&0 \\ 0&0&0&0&0&0&0&0&0&1&0&0 \\ 0&0&0&0&0&0&0&0&0&0&1&0 \\ 0&0&0&0&0&0&0&0&0&0&0&1 \end{bmatrix},$$

and $\tilde{B}$ can be calculated as a left generalized inverse of B_r, which is given by

$$\tilde{B} = \begin{bmatrix} 0 & 406.09 & 29.68 & 0 & -0.05 & 0.28 & 0&0&0&0&0&0 \\ -351.68 & -203.04 & 29.68 & 0 & -0.05 & 0.28 & 0&0&0&0&0&0 \\ 351.68 & -203.04 & 29.68 & 0 & -0.05 & 0.28 & 0&0&0&0&0&0 \\ 0 & -59.36 & 203.04 & 0 & -1.79 & 0.10 & 0&0&0&0&0&0 \\ 51.41 & 29.68 & 203.04 & 1.99 & 0.89 & -0.05 & 0&0&0&0&0&0 \\ -51.41 & 29.68 & 203.04 & -1.99 & 0.89 & -0.05 & 0&0&0&0&0&0 \end{bmatrix}.$$

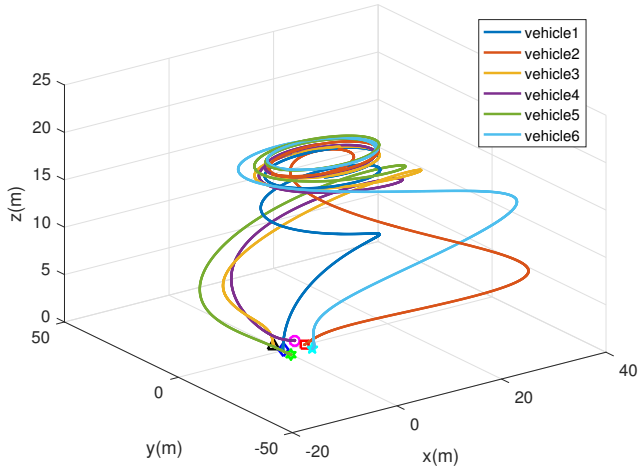

Figure 5.4: 3D trajectories of the tri-rotor swarm

In this case, the states of the leader node are given by

$$x_0 = [0 \;\; 0 \;\; 0 \;\; 0 \;\; 0 \;\; 0 \;\; 0 \;\; 0 \;\; 0 \;\; 5 \;\; -5 \;\; 0]^T,$$

which indicates that the reference position will be located at a static position $(5,-5,0)$ with roll, pitch and yaw angles being zero, and all the reference velocities and reference angular velocities are kept zero to maintain the static target position. It should however be pointed out that the individual attitudes and positions of each UAV are also effected by the choice of h_i, which will not be set to zero. The proposed control strategy is valid regardless of the target is static or time-varying. In this case, h_i is selected as

$$h_i = \begin{bmatrix} 10\cos(t+\frac{(i-1)\pi}{3}) \\ -10\sin(t+\frac{(i-1)\pi}{3}) \\ 0 \\ 0 \\ 0 \\ 0 \\ -0.5\times(-1)^i \\ -0.5\times(-1)^i \\ 0.5\times(-1)^i \\ 10\sin(t+\frac{(i-1)\pi}{3}) \\ 10\cos(t+\frac{(i-1)\pi}{3}) \\ 20 \end{bmatrix} \quad (\text{for } i \in \{1,2,\ldots,6\}),$$

where the desired offsets of 3D attitude and 3D position with respect to the reference signal for each agent are represented by last six rows, and the first six rows are the derivatives of them according to the change of coordinates given in (5.46).

It can be verified that the formation tracking feasibility condition (5.55) in Theorem 5.3.1 is satisfied. Then the optimal state-feedback gain K and coupling gain c can be obtained using

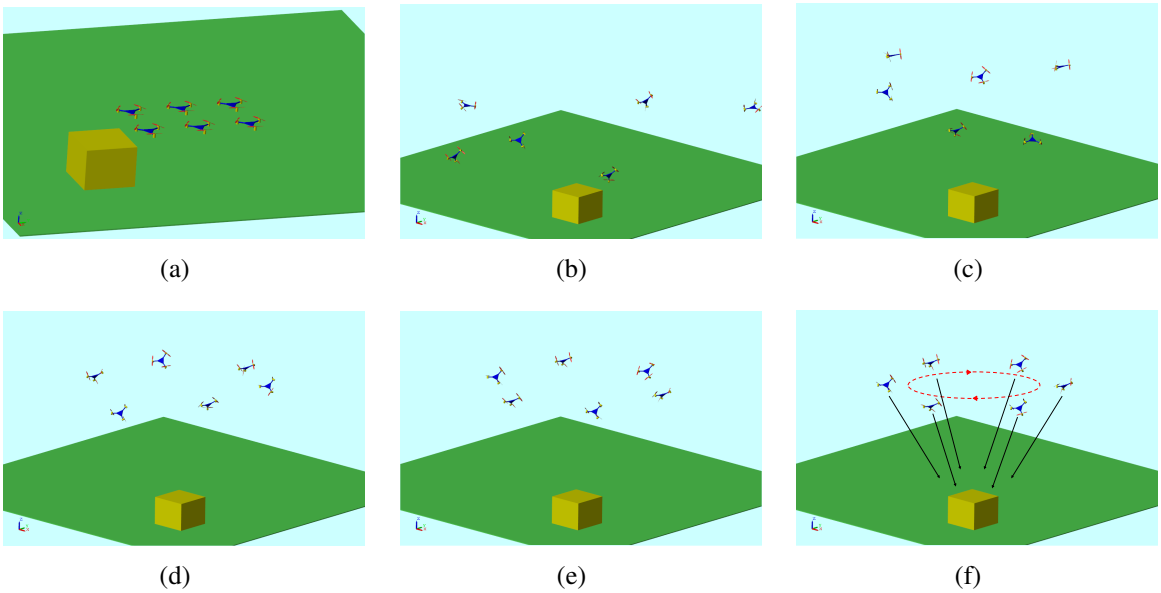

Figure 5.5: 3D shots of the tri-rotor swarm. (a) $t = 0$ s. (b) $t = 5$ s. (c) $t = 10$ s. (d) $t = 15$ s. (e) $t = 25$ s. (f) $t = 50$ s.

the approach in Theorem 5.3.2. The local optimal observer gain F for each UAV can also be selected easily by solving the corresponding ARE based on the estimation of noise. These design gains are hence given by

$$c = 5,$$

$$K = \begin{bmatrix} -2.1 & 0.3 & 12 & -0.1 & -2.3 & 3.2 & -0.9 & -9.4 & 18 & -2.2 & 0.5 & 2.6 \\ 2.1 & -2.9 & 12 & 2.6 & 1.2 & 3.1 & 11 & 7.6 & 17 & 2.8 & -3.5 & 2.6 \\ 2.6 & 2.5 & 12 & -2.4 & 1.3 & 3.1 & -11 & 8.9 & 17 & 3.7 & 2.9 & 2.6 \\ -20 & 0 & 85 & 0 & -17 & 0.3 & 0.1 & -81 & -0.5 & -25 & 0 & 18 \\ 10 & -18 & 85 & 17 & 8.4 & -0.8 & 77 & 40 & -3.6 & 12 & -22 & 18 \\ 10 & 18 & 85 & -17 & 8.4 & -0.8 & -77 & 40 & -3.6 & 12 & 22 & 18 \end{bmatrix},$$

$$F = \begin{bmatrix} -0.12 & 10.08 & -0.01 & 9.83 & 0 & 0 \\ -10.14 & -0.12 & 0 & 0 & 9.83 & 0 \\ 0 & 0 & -0.18 & 0 & 0 & 1.25 \\ 160.26 & 0 & 0 & -0.12 & 5.57 & 0 \\ 0 & 208.61 & 50.72 & -6.01 & -0.12 & 0 \\ 0 & 50.72 & 916.32 & -0.13 & 0 & -0.18 \\ 17.90 & 0 & 0 & -0.01 & -0.20 & 0 \\ 0 & 20.36 & 1.60 & 0.16 & -0.01 & 0 \\ 0 & 1.60 & 42.77 & 0 & 0 & 0 \\ -0.01 & 0.16 & 0 & 4.43 & 0 & 0 \\ -0.20 & -0.01 & 0 & 0 & 4.43 & 0 \\ 0 & 0 & 0 & 0 & 0 & 1.5864 \end{bmatrix}.$$

On using robust control law (5.28) with optimal distributed formation control protocol (5.51) and (5.52), the trajectory of each tri-rotor UAV is given by Fig. 5.4. The 3D visualisation of distributed formation of the tri-rotor UAV swarm are illustrated in Fig. 5.5. The attitude tracking performance with respect to roll, pitch and yaw angles is shown in Fig. 5.6. The position tracking of hovering is shown in Fig. 5.7. From all these figures, it can be seen that the tri-rotor swarm forms a regular hexagonal formation with circular time-variation in the x-y plane after 25s and the surveilled target lies in the middle of the circular rotation at ground

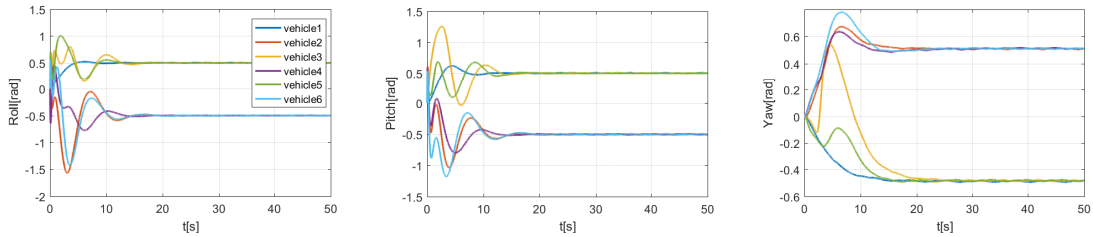

(a) (b) (c)

Figure 5.6: Attitude response of the tri-rotor swarm system. (a) Roll angle ϕ. (b) Pitch angle θ. (c) Yaw angle ψ.

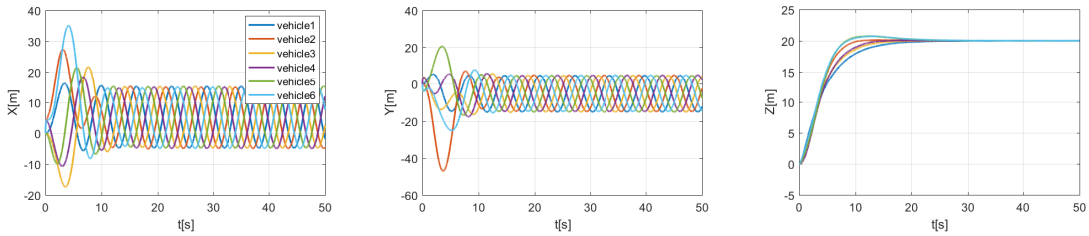

(a) (b) (c)

Figure 5.7: Position response of the tri-rotor swarm system. (a) Longitudinal displacement x_v. (b) Lateral displacement y_v. (c) Vertical displacement z_v

level. The attitude of each tri-rotor UAV varies with time along the circular trajectory so that each tri-rotor points (e.g. its onboard camera) to the target located at the centre of the circle. It is concluded that the desired formation and attitude tracking of the UAV swarm is achieved independently, and the designed control system preserves good robustness properties when subjected to simulated aerodynamic disturbances and model uncertainties.

5.5 Conclusion

In this chapter, we have proposed a new tri-rotor unmanned aerial vehicle which is more efficient and flexible than a quadrotor UAV. A formation tracking problem of a networked tri-rotor UAV swarm has also been solved using a distributed formation control protocol.

To achieve this, the dynamical model was first derived based on force and torque kinematic analysis and subsequent translational and rotational dynamic modelling. A robust feedback linearization controller was then developed to deal with this highly coupled and nonlinear tri-rotor UAV to achieve a feedback linearized system through geometric transformation that

is valid at any operating point but matches the Jacobi linearization of the system at the operating point of interest. The technique preserves robustness as it does not invert all nonlinear dynamics, unlike classic feedback linearization. An distributed optimal formation tracking control protocol was then developed for the tri-rotor robotic swarm, which guarantees that the target time-varying position and time-varying attitude of each UAV can be achieved independently. Finally, simulation results were given in a realistic environment based on 3D graphical display and physical visualisations. It has been shown that the proposed tri-rotor UAV swarm is able to track a desired time-varying formation whilst independently tracking different time-varying attitudes. A target surveillance task was performed effectively by these tri-rotor UAVs, which lays the foundation for some more complex collaborative tasks to be explored.

Future work will take obstacle avoidance and power management as shown in [133] into consideration, the proposed distributed controller will be applied to real hardware, and robust methods such as [134], [135] will be exploited in the design of the distributed control protocol.

Chapter 6

Cooperative Control of Heterogeneous Connected Vehicle Platoons

6.1 Introduction

The notion of Intelligent Highway Vehicle Systems was introduced more than two decades ago and has attracted considerable attention of the transportation engineering communities to accommodate exponentially increasing number of highway traffic in today's life along with minimizing the risk of traffic accidents [136]. The key strategy to implement IHVSs is to employ automatic or semi-automatic cruise control mechanisms for highway vehicles and thereby reducing human intervention in driving the vehicles.

The fundamental issue in controlling a string (also called platoon) of connected vehicles is how to ensure platoon stability when the lead vehicle in a platoon suddenly accelerates or decelerates due to exogenous disturbances. platoon stability of automated vehicles guarantees that the spacing and velocity errors between the successive vehicles do not grow or amplify upstream along the platoon [137]. Efficacy of a platoon control scheme depends highly on the vehicular information available for feedback and on the spacing policy used. For instance, the acceleration feedback via Vehicle-to-Vehicle (V2V) communication (such as DSRC and VANET [138]) in addition to position and velocity feedback information enhances the relative platoon stability of a platoon [139]. Spacing policy also plays a major

Figure 6.1: A platoon of driverless vehicles in an automated highway system.

role in deciding a particular platoon control strategy. Constant spacing policy is quite popular in the literature since it ensures constant inter-vehicular spacing independent of the cruising velocity of the platoon and also offers high traffic capacity and easier implementation. (as portrayed in Fig. 6.1).

A Cooperative Adaptive Cruise Control technique was proposed in [140] for heterogeneous vehicle platoon along with practical validation results and also examined the platoon stability of the practical setup. The article [141] has introduced the concept of $\mathcal{L}_p$ platoon stability for connected vehicles and analysed platoon stability properties of cooperative adaptive cruise control strategies for vehicle platoons with experimental validation results. In [142], platoon stability of homogeneous and heterogeneous vehicle platoons with constant time headway spacing policy has been investigated considering time delays in sensors and actuators.An adaptive bidirectional platoon control scheme using a coupled sliding-mode control technique is proposed in [143] to ensure platoon stability of the platoon and to improve its performance. In [144], a distributed finite-time adaptive integral sliding-mode control framework is designed for a platoon of vehicles subjected to bounded exogenous disturbances. However, these studies have considered fixed interaction topology among the vehicles which reduces the flexibility and reliability of a platoon control scheme. Of late, in [145], a fully decentralized control scheme is developed including obstacle avoidance feature for a platoon of car-like vehicles equipped with on-board cameras to detect the obstacles. In the present context, the experimental work done in [146] is a major contribution in the area of cooperative driving in which a fleet of miniature robotic cars is developed for conducting platoon control activities.

With the advent of multi-agent consensus theory and formation control techniques [13, 147, 148], cooperative control of connected vehicles platoons has started emerging in the recent years [149–151]. The major objective of cooperative control of connected vehicle platoon is to maintain uniform velocity of all the vehicles in a platoon moving in one dimension on a straight flat road alongside ensuring a desired inter-vehicular spacing at the steady-state. Pioneering research works have been carried out in [149] and [150] to apply the consensus based cooperative control techniques in developing distributed control schemes for connected vehicle platoons moving in one dimension. While [149] have developed the control schemes for homogeneous vehicle platoons, [150] have extended their previous results for heterogeneous platoons. However, in [149] and [150], the proposed cooperative control protocols are not adaptive and the case of communication link failure have not been explored.

Motivated by the ongoing developments and existing challenges in the area of cooperative control of multiple connected vehicle platoon, in this chapter, we consider the problem of designing a distributed control scheme for a platoon of heterogeneous connected vehicles moving in one dimension considering constant spacing policy and constant longitudinal velocity of the lead vehicle. Below, we summarize the contributions of this chapter:

- A two-layer distributed and adaptive control architecture is developed for a heterogeneous platoon of bidirectionally connected vehicles to maintain same cruising velocity of all vehicles in the platoon and to keep equal inter-vehicular spacing between any two successive vehicles, which together preserve platoon stability of the platoon in presence of exogenous input applied to the lead vehicle.

- The proposed scheme takes into account the complete nonlinear vehicle dynamics during the controller design, hence, the heterogeneity of the vehicles due to different parameters are directly considered in this scheme.

- The proposed platoon control design being distributed and adaptive facilitates uninterrupted and reliable control of the platoon despite any bounded disturbance on the lead vehicle and also in the event of communication link failure.

- Effectiveness of the proposed method has been validated through affordable real robot

experiments on a two-lane platoon of six connected vehicles, represented by autonomous, miniature Mona robots [1], in a real-time laboratory environment equipped with low-cost over-head camera tracking system.

6.2 Technical Background and Problem Formulation

In this chapter, we aim to establish the platoon stability of a heterogeneous vehicle platoon and thereby to ensure that all the vehicles in the platoon remain equidistant even when the lead vehicle is affected by exogenous input (e.g. sudden acceleration/deceleration). In order to achieve this, we developed a two-layer platoon control scheme which exploits the feedback linearization technique to first linearize the nonlinear vehicle dynamics and then applies a distributed cooperative control technique to develop a rectilinear static formation of the connected vehicles to keep them equidistant assuming that the leader vehicle has constant velocity.

6.2.1 Communication Topology

Suppose that the information links among following vehicles are bidirectional and there exists at least one directional link from the leader to followers. If the ith following vehicle observes the lead vehicle then an edge $(0,i)$ between them is said to exist with the pinning gain $g_i > 0$. We denote the pinning matrix as $G = \text{diag}\{g_i\} \in \mathbb{R}^{N\times N}$. It is assumed that at least one follower is connected to the leader. In virtue of the bidirectional communication topology among the followers, all the eigenvalues of the matrix $L+G$ (denoted by λ_i for $1,2,\ldots,N$) are real and positive.

6.2.2 Modelling of Heterogeneous Vehicles

We consider a platoon of connected vehicles with non-identical dynamics that forms a platoon running through dense traffic on a straight highway assuming there is no overtaking. In each platoon, the vehicle at the front is considered as the leader that moves at a constant

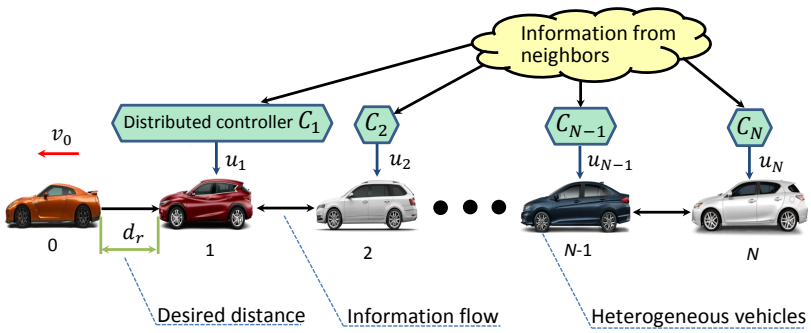

Figure 6.2: Cooperative control architecture of a heterogeneous and connected vehicle platoon in which the vehicle labelled with 0 acts as the leader while the rest $1,2,\ldots,N$ vehicles are considered as followers.

velocity while rest of the downstream vehicles are considered as followers. A schematic diagram of the platoon is depicted in Fig. 6.2 where all the following vehicles try to maintain equal spacing between any two of them. In this chapter, we will use the following notations: position, velocity and acceleration of the ith following vehicle are denoted by $p_i(t)$, $v_i(t)$, $a_i(t)$ for all $i \in \{1,2,\ldots,N\}$, while those of the lead vehicle are denoted by $p_0(t)$, $v_0(t)$ and $a_0(t)$. In rest of the chapter, explicit dependence on time $t \geq 0$ has been omitted. Now, the dynamics of each vehicle can be modelled, as shown in [137], by the following nonlinear input-affine differential equation

$$\dot{a}_i = f_i(v_i, a_i) + g_i(v_i) b_i \qquad \forall i \tag{6.1}$$

which encompasses the engine dynamics, brake system and aerodynamics drag. In (6.1), b_i is the input to the engine of the ith vehicle and the nonlinear functions $f_i(v_i, a_i)$ and $g_i(v_i)$ are given by

$$f_i(v_i, a_i) = -\frac{1}{\tau_i}\left(a_i + \frac{\sigma\phi_i c_{di}}{2m_i} v_i^2 + \frac{d_{mi}}{m_i}\right) - \frac{\sigma\phi_i c_{di}}{m_i} v_i a_i,$$
$$g_i(v_i) = \frac{1}{\tau_i m_i},$$

where σ denotes the specific mass of the air, ϕ_i is the cross-sectional area, c_{di} indicates the drag coefficient, m_i denotes the mass, d_{mi} represents the mechanical drag and τ_i symbolizes the engine time constant (also called the inertial time-lag). The group of terms $\frac{\sigma\phi_i c_{di}}{2m_i}$ models the air resistance [137]. Note that since most of the parameters mentioned in (6.1) are not identical for all vehicles, hence, the present work deals with control of heterogeneous vehicle platoon. Now, we can use the following feedback linearizing control law

$$b_i = u_i m_i + 0.5\sigma\phi_i c_{di} v_i^2 + d_{mi} + \tau_i \sigma\phi_i c_{di} v_i a_i \tag{6.2}$$

for all $i \in \{1,2,\ldots,N\}$ to transform the nonlinear vehicle dynamics into a linearized model. Note that the feedback linearized controller constitutes the inner layer of the proposed two-layer platoon control scheme and is implemented as a local controller available to each vehicle as shown in Fig. 6.5. In (6.2), u_i is the new control input to be designed. Now, substituting (6.2) into (6.1), the longitudinal dynamics of each vehicle in the platoon is obtained as

$$\begin{cases} \dot{p}_i = v_i, \\ \dot{v}_i = a_i, \\ \tau_i \dot{a}_i + a_i = u_i \qquad \forall i, \end{cases} \tag{6.3}$$

which is then expressed in the standard state-space form as

$$\dot{x}_i = A_i x_i + B_i u_i \qquad \forall i, \tag{6.4}$$

where

$$x_i(t) = \begin{bmatrix} p_i \\ v_i \\ a_i \end{bmatrix}, \; A_i = \begin{bmatrix} 0 & 1 & 0 \\ 0 & 0 & 1 \\ 0 & 0 & -\frac{1}{\tau_i} \end{bmatrix} \text{ and } B_i = \begin{bmatrix} 0 \\ 0 \\ \frac{1}{\tau_i} \end{bmatrix}.$$

It can be readily verified that the pair (A_i, B_i) is controllable for all $i \in \mathcal{F}$. The leader vehicle runs with constant velocity under the steady-state condition (i.e., $u_0 = 0$). Note that even though the nonlinear vehicle dynamics (6.1) is linearized to (6.4) but it is still heterogeneous due to the presence of the parameter τ_i. This makes the present problem non-trivial and challenging.

6.2.3 Problem Formulation

Cooperative control of a platoon of $N+1$ heterogeneous vehicles moving on a straight flat road is considered in this work, which includes a leader indexed by 0 and N followers indexed from 1 to N. Let $\mathcal{F} = \{1,2,\ldots,N\}$ be the set of the followers. The control objective is to ensure all the following vehicles maintains the same speed as the leader while keeping a constant inter-vehicular spacing, thereby potentially improving road throughput. This policy can provide advantages such as high vehicle density and low energy consumption.

The heterogeneous connected vehicles shown in Fig. 6.2 are said to achieve the desired platoon control objectives with the lead vehicle having constant velocity if for any given

bounded initial states

$$\begin{cases} \lim_{t\to\infty} \left\| p_i(t) - p_j(t) \right\| = (i-j)d_r, \\ \lim_{t\to\infty} \|v_i(t) - v_0(t)\| = 0 \quad \text{and} \\ \lim_{t\to\infty} \|a_i(t) - a_0(t)\| = 0, \end{cases} \tag{6.5}$$

for all $i, j \in \mathcal{F},\ j \neq i$. The platoon control activities including how to preserve platoon stability is formulated as a 'Leader-following' static formation of the connected vehicles in the platoon where the lead vehicle is considered as the root node. The desired static formation of the platoon is specified by the vector $d_i = [id_r, 0, 0]^T\ \forall i \in \{1, 2, \ldots, N\}$ known to the ith following vehicle, where d_r is a pre-specified gap between any two consecutive vehicles in the platoon. In case of implementing constant spacing policy, the desired gap d_r remains constant for all i. Note that any acceleration/deceleration in a vehicle happening due to taking sharp turns, climbing uphill or going downhill can be considered as a bounded disturbance acting on the vehicle temporarily. Platoon stability of a platoon ensures that the spacing error grows only during the period of disturbance but quickly decays to zero as soon as the disturbance (i.e. the acceleration/deceleration) disappears.

6.3 Control Protocol Design

This section develops distributed cooperative control scheme for a platoon of heterogeneous and connected vehicles, which is the main theoretical contribution of the chapter. The control objectives are i) to keep equal and constant inter-vehicular spacing between successive vehicles, ii) maintain the velocities of all the following vehicles same as that of the leader and iii) to maintain zero acceleration for all the vehicles in the platoon. Motivated by the adaptive control techniques developed in [15, 82, 152], we propose a distributed control protocol given in Theorem 6.3.1 to satisfy the aforementioned objectives and thereby to maintain platoon stability of the platoon.

Theorem 6.3.1. Consider a platoon of heterogeneous connected vehicles with the feedback linearized dynamics given in (6.4). Define $\delta = \frac{\tau_0}{\max_{i\in\mathcal{F}} \tau_i}$, $\rho = \frac{\tau_0}{\min_{i\in\mathcal{F}} \tau_i}$ and select $\varphi \geq \frac{1}{2\delta \min_{i\in\mathcal{F}} \lambda_i}$. Then, the cooperative control objectives of the heterogeneous platoon are achieved when the following adaptive control protocol is applied to each followers vehicles

$i \in \mathcal{F}$

$$\begin{cases} u_i = B_0^T \xi_i x_i + \varphi K \sum_{j=0}^{N} \alpha_{ij}\big((x_i - d_i) - (x_j - d_j)\big), \\ \dot{\xi}_i = \rho x_i^T B_0 K \sum_{j=0}^{N} \alpha_{ij}\big((x_i - d_i) - (x_j - d_j)\big), \end{cases} \tag{6.6}$$

with $K = -B_0^T P$ where $P > 0$ is a unique solution to the algebraic Riccati equation (ARE)

$$A_0^T P + P A_0 - P B_0 B_0^T P + \gamma I_3 = 0 \tag{6.7}$$

for a given $\gamma > 0$.

Proof. The closed-loop dynamics of the heterogeneous vehicle platoon given in (6.4) under the proposed distributed platoon control law (6.6) is obtained as

$$\dot{x}_i = \big(A_i + B_i B_0^T \xi_i\big) x_i + \varphi B_i K \sum_{j=0}^{N} \alpha_{ij}\big((x_i - d_i) - (x_j - d_j)\big). \tag{6.8}$$

For each connected vehicle, exploiting the controllable canonical structure of A_0, B_0, A_i and B_i for all i, it is always possible to find a constant scalar ζ_i such that the following relationship

$$A_0 = A_i + B_i B_0^T \zeta_i \tag{6.9}$$

holds for all $i \in \mathcal{F}$. Plugging (6.9) into (6.8), we get

$$\dot{x}_i = A_0 x_i + B_i B_0^T (\xi_i - \zeta_i) x_i + \varphi B_i K \sum_{j=0}^{N} \alpha_{ij}\big((x_i - d_i) - (x_j - d_j)\big). \tag{6.10}$$

Define the formation tracking error $\varepsilon_i = x_i - d_i - x_0$ for each following vehicle and let the vector $\varepsilon = \big[\varepsilon_1^T, \varepsilon_2^T, \ldots, \varepsilon_N^T\big]^T$. Then $\dot{\varepsilon}$ is calculated as:

$$\dot{\varepsilon}_i = A_0 \varepsilon_i + B_i B_0^T (\xi_i^T - \zeta_i) x_i + \varphi B_i K \sum_{j=0}^{N} \alpha_{ij}(\varepsilon_i - \varepsilon_j) \tag{6.11}$$

by using (6.4) and since $\dot{d}_i = [0\,0\,0]^T$. Then, (6.11) is expressed in the Kronecker product form as

$$\dot{\varepsilon} = (I \otimes A_0)\varepsilon + \varphi \mathrm{diag}\{B_i K\}\big((L+G) \otimes I\big)\varepsilon + \begin{bmatrix} B_1 B_0^T (\xi_1 - \zeta_1) x_1 \\ B_2 B_0^T (\xi_2 - \zeta_2) x_2 \\ \vdots \\ B_N B_0^T (\xi_N - \zeta_N) x_N \end{bmatrix}. \tag{6.12}$$

In this proof, the platoon control problem, and therefore ensuring platoon stability of the platoon, has been cast as an asymptotic stability problem of the closed-loop formation tracking error dynamics $\dot{\varepsilon}$. To approach this problem via Lyapunov's method, we consider the following Lyapunov function candidate

$$V = \varepsilon^T\big((L+G)\otimes P\big)\varepsilon + \sum_{i=1}^{N}(\xi_i-\zeta_i)^2. \tag{6.13}$$

Note $V>0$ since $L+G>0$ and $P>0$ for a given $\gamma>0$. The time derivative of V is computed along the trajectories of (6.11) as

$$\begin{aligned}
\dot{V} =& \varepsilon^T\big((L+G)\otimes(PA_0+A_0^TP)\big)\varepsilon + 2\varepsilon^T\big((L+G)\otimes I\big)\varphi\mathrm{diag}\{PB_iK\}\big((L+G)\otimes I\big)\varepsilon \\
&+2\varepsilon^T\big((L+G)\otimes P\big)\begin{bmatrix} B_1B_0^T(\xi_1-\zeta_1)x_1 \\ B_2B_0^T(\xi_2-\zeta_2)x_2 \\ \vdots \\ B_NB_0^T(\xi_N-\zeta_N)x_N \end{bmatrix} + 2\sum_{i=1}^{N}(\xi_i-\zeta_i)\dot{\xi}_i \\
=& \varepsilon^T\big((L+G)\otimes(PA_0+A_0^TP)\big)\varepsilon \\
&+2\varepsilon^T\big((L+G)\otimes I\big)\varphi\mathrm{diag}\{PB_iK\}\big((L+G)\otimes I\big)\varepsilon \\
&+2\sum_{i=1}^{N}\sum_{j=0}^{N}\alpha_{ij}(\varepsilon_i-\varepsilon_j)^TPB_iB_0^T(\xi_i-\zeta_i)x_i \\
&+2\rho\sum_{i=1}^{N}(\xi_i-\zeta_i)x_i^TB_0K\sum_{j=0}^{N}\alpha_{ij}\big((x_i-d_i)-(x_j-d_j)\big) \\
=& \varepsilon^T\big((L+G)\otimes(PA_0+A_0^TP)\big)\varepsilon \\
&+2\varepsilon^T\big((L+G)\otimes I\big)\varphi\mathrm{diag}\{PB_iK\}\big((L+G)\otimes I\big)\varepsilon \\
&+2\sum_{i=1}^{N}\sum_{j=0}^{N}\alpha_{ij}(\varepsilon_i-\varepsilon_j)^TPB_iB_0^T(\xi_i-\zeta_i)x_i \\
&-2\rho\sum_{i=1}^{N}\sum_{j=0}^{N}(\xi_i-\zeta_i)x_i^TB_0B_0^TP\alpha_{ij}\big(\varepsilon_i-\varepsilon_j\big) \\
=& \varepsilon^T\big((L+G)\otimes(PA_0+A_0^TP)\big)\varepsilon \\
&+2\varepsilon^T\big((L+G)\otimes I\big)\varphi\mathrm{diag}\{PB_iK\}\big((L+G)\otimes I\big)\varepsilon \\
&+2\sum_{i=1}^{N}\sum_{j=0}^{N}\alpha_{ij}(\varepsilon_i-\varepsilon_j)^TP\left(B_iB_0^T-\rho B_0B_0^T\right)(\xi_i-\zeta_i)x_i \\
&[\text{since } K=-B_0^TP \text{ and noting that } \varepsilon_i-\varepsilon_j=(x_i-d_i)-(x_j-d_j) \text{ for any } i,j\in\mathcal{F}].
\end{aligned}$$

Now exploiting the structures of B_0, B_i and the parameter $\rho=\frac{\tau_0}{\min_{i\in\mathcal{F}}\tau_i}$, we can readily obtain

the following relationship

$$B_i B_0^T - \rho B_0 B_0^T \leq 0. \tag{6.14}$$

Upon applying (6.14) into the last expression of $\dot{V}$, it gives

$$\dot{V} \leq \varepsilon^T \left[(L+G) \otimes (PA_0 + A_0^T P) \; - \; 2\varphi \left((L+G) \otimes I \right) \mathrm{diag}\{PB_i B_0^T P\} \left((L+G) \otimes I \right) \right] \varepsilon$$

which in turn implies

$$\dot{V} \leq \varepsilon^T \left[((L+G) \otimes (PA_0 + A_0^T P) - 2\varphi\delta (L+G)^2 \otimes PB_0 B_0^T P \right] \varepsilon, \tag{6.15}$$

since

$$B_i B_0^T - \delta B_0 B_0^T \geq 0 \qquad \forall i \in \mathcal{F} \tag{6.16}$$

due to a similar argument used to show (6.14). Now since $L+G > 0$, there always exists an unitary diagonalizing matrix $D \in \mathbb{R}^{N \times N}$ such that $\Lambda = D^T (L+G) D$ where $\Lambda = \mathrm{diag}\{\lambda_1, \lambda_2, \ldots, \lambda_N\}$. Replacing $L+G$ in (6.15) by $D^T \Lambda D$, we have

$$\begin{aligned} \dot{V} &\leq \varepsilon^T (D^T \otimes I) \left[\Lambda \otimes (PA_0 + A_0^T P) - \frac{1}{\min_{i \in \mathcal{F}} \lambda_i} \Lambda^2 \otimes PB_0 B_0^T P \right] (D \otimes I) \varepsilon \\ &\leq \varepsilon^T (D^T \otimes I) \left[\Lambda \otimes (PA_0 + A_0^T P - PB_0 B_0^T P) \right] (D \otimes I) \varepsilon. \end{aligned} \tag{6.17}$$

Then, (6.17) implies $\dot{V} \leq 0$ using the ARE given in (6.6) for a given $\gamma > 0$ and $\dot{V} = 0$ only when $\varepsilon = 0$. Hence invoking LaSalle's invariance principle [55], asymptotic stability of the closed-loop tracking error dynamics ($\dot{\varepsilon}$) given in (6.11) can be guaranteed. Therefore,

$$\lim_{t \to \infty} \varepsilon(t) = 0 \tag{6.18}$$

which implies

$$\lim_{t \to \infty} x_i(t) - d_i - x_0(t) = 0 \qquad \forall i \in \mathcal{F}. \tag{6.19}$$

This completes the proof. □

Remark 6.3.1. Different from the results shown in [139, 149] where only homogeneous vehicular platoons are considered (i.e., $A_i = A_0$, $B_i = B_0$, $\forall i \in \mathcal{F}$), the proposed control protocol in this work can deal with the heterogeneous dynamics of vehicles, which is more practical in real applications. Even though control of heterogeneous vehicle platoons is investigated in [143], it is required to know all the model information of the leader and followers before designing the control law, while in this work only the leader's model and the bound of the followers' models are needed, which largely reduces the computation complexity and thus provides more possibility in real hardware implementation.

Following the analysis presented above, the procedure to construct the control law u_i is given in Algorithm 4.

Algorithm 4 Procedure to design the control law for heterogeneous vehicle platoons

1: **for** each vehicle $i \in \{1, \ldots, N\}$ **do**
2: **initialize** p_i, v_i, a_i and ξ_i;
3: set a bidirectional communication graph;
4: set the desired distance d_r;
5: **if** all the vehicles are connected with the leader as the root node **then**
6: choose positive constants ρ and δ;
7: select the positive parameter φ;
8: compute controller parameter K by solving ARE (6.7) for a given γ;
9: construct the control protocol u_i given in (6.6);
10: **else**
11: back to Step 3;
12: **end if**
13: **end for**

6.4 Nonlinear Simulation Results

In this section, we provide a complete set of simulation results to show the usefulness and performance of the proposed cooperative platoon control scheme. We consider a heterogeneous platoon of six connected vehicles, of which one is leader while the rest five are followers, interconnected via three different communication topologies as shown in Fig. 6.3(a)-6.3(c). The parameters of each connected vehicle are arbitrarily selected and tabulated below in Table 6.1. Note that in the simulation study, the actual nonlinear vehicle dynamics as mentioned in (6.1) has been considered.

Table 6.1: Vehicle Parameters Used in the Simulations

Index	0	1	2	3	4	5
m_i (kg)	1753	1837	1942	1764	1029	1688
τ_i (s)	0.51	0.55	0.62	0.52	0.33	0.48

The initial state of the leader is arbitrarily assigned to $p_0(0) = 200$m, $v_0(0) = 8$m/s, and $a_0(0) = 0$m/s^2. Note that the acceleration or deceleration of the leader can be viewed as disturbances in a platoon. The initial position of the ith follower is given by $p_i(0) = (40 - 8i)$m. In the simulation study, the desired inter-vehicular spacing is set to $d_r = 5$m. Now based on the vehicle parameters given in Table 6.1, we calculate the controller parameters

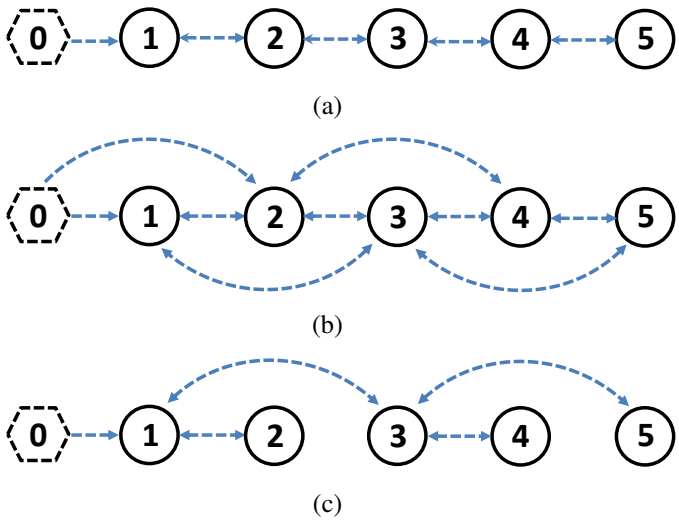

Figure 6.3: Variety of communication topologies used in the simulation case study on the platoon control mission. (a) Topology 1: predecessor-following (PF); (b) Topology 2: two-predecessor following (TPF) and (c) Topology 3: to examine the response of the platoon in the event of link failure.

as $\rho = 1.545$, $\delta = 0.823$ and $\varphi = 10$. Then, choosing $\gamma = 100$ and by solving the ARE (6.7), we get

$$P = \begin{bmatrix} 180.287 & 112.517 & 7.1 \\ 112.517 & 195.7535 & 12.8004 \\ 7.1 & 12.8004 & 7.2787 \end{bmatrix} > 0$$

which form the feedback gain matrix

$$K = -B_0^T P = -\begin{bmatrix} 10 & 18.0287 & 10.2517 \end{bmatrix}.$$

Three sets of simulation results are presented in Fig. 6.4(a), 6.4(b) and 6.4(c) corresponding to Topologies 1, 2 and 3 respectively as shown in Fig. 6.3(a), 6.3(b) and 6.3(c). Each set of results contains position (p_i) and velocity (v_i) trajectories of the vehicles, the coupling weights (ξ_i) designed for them and the spacing error (ε_i) corresponding to each vehicle. For the first 10 sec of the simulation, the vehicles in the platoon move all together at the same cruising velocity $v_0(0) = 8$ m/s as that of the leader, hence, the inter-vehicular spacing between any two consecutive vehicles remains zero. Distance traversed by the vehicles during this phase increases at a constant rate and the coupling weights also remain constant at their initial values. Then, in order to disturb the constant velocity movement of the platoon, an

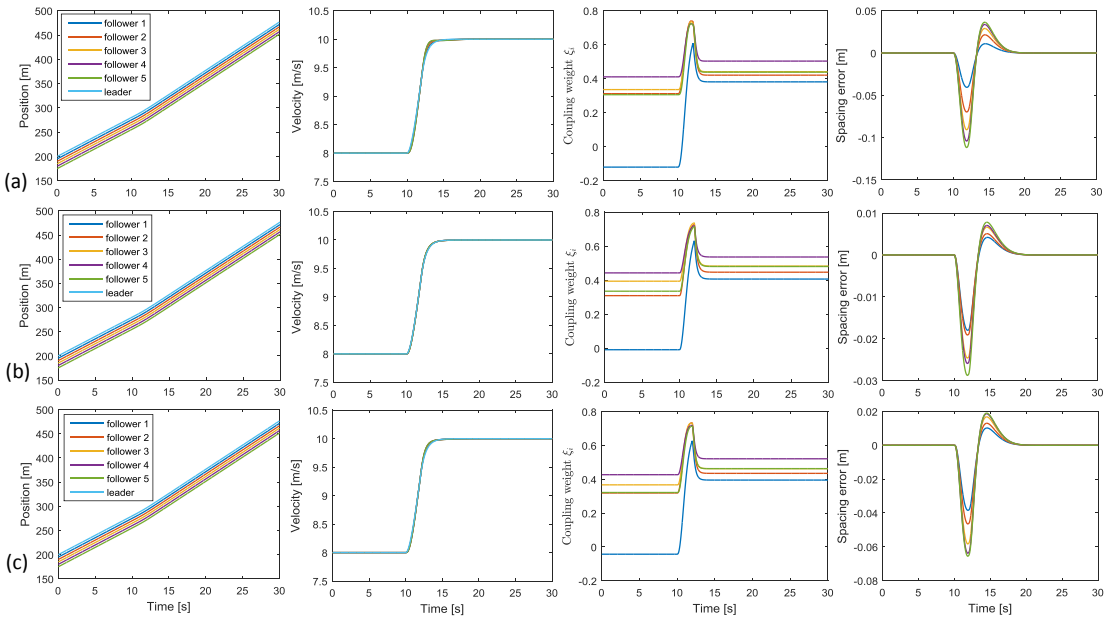

Figure 6.4: Simulation results shows the performance achieved by the proposed two-layer cooperative control scheme when applied to a platoon of six connected and heterogeneous vehicles of which one acts as the leader while rest five are followers. (a) Position $p_i(t)$, velocity $v_i(t)$, coupling weight $\xi_i(t)$ and spacing error $\varepsilon_i(t)$ for each of the vehicles in the platoon corresponding to Topology 1; (b) $p_i(t)$, $v_i(t)$, $\xi_i(t)$, $\varepsilon_i(t)$ corresponding to Topology 2; (c) $p_i(t)$, $v_i(t)$, $\xi_i(t)$, $\varepsilon_i(t)$ corresponding to Topology 3.

exogenous input

$$w_0(t) = \begin{cases} 0, & 0 \text{ s} \leq t < 10 \text{ s}; \\ 1, & 10 \text{ s} \leq t < 12 \text{ s}; \\ 0, & t \geq 12 \text{ s}; \end{cases} \tag{6.20}$$

is applied on the lead vehicle causing an acceleration in it followed by a steep rise in its velocity as portrayed in the velocity vs. time graph of Fig. 6.4(a). This figure also reveals that in response to the sudden increase in the velocity of the leader the following vehicles also try to synchronize with the new stable velocity of the leader and after $t = 12$s, all following vehicles attain the same velocity as that of the leader. This has been made possible due to the influence of the proposed platoon control scheme. The graph ξ_i vs. t in Fig. 6.4(a) shows that the coupling weights adapt to new values to tune the controller gains to counteract the disturbance in the platoon. From the spacing error vs. time graph given in Fig. 6.4(a), it is clear that during the transient period 10s $\leq t <$ 20s spacing error deviates from zero, exhibits bounded variation, then quickly decays to zero around $t = 20$ s and after that remains zero for all $t >$ 20s. This confirms that the designed cooperative control scheme has worked satisfactorily to sustain the disturbance in the platoon caused due to applying

an acceleration input to the lead vehicle and to restore normal operating condition after the disturbance is removed and thus the proposed controller has preserved platoon stability of the platoon. The same conclusion can be drawn in case of the other two sets of simulation results given in Fig. 6.4(b) and 6.4(c). Most importantly, Fig. 6.4(c) highlights that the proposed distributed platoon control scheme works even in presence of communication link failure as long as there exists a spanning tree in the topology, that is, all the following vehicles are either explicitly or implicitly connected to the lead vehicle. Furthermore, in contrast to the results reported in [150], the performance of the controller in Fig. 6.4(a) and 6.4(b) corresponding to Topologies 1 and 2 suggests that 'two-predecessor' topology is not necessary for the proposed scheme to work.

6.5 Experimental Validation

In order to establish the feasibility and effectiveness of the proposed two-layer distributed platoon control scheme, in this chapter, real-world experiments with mobile robots have been performed. Below we introduce the experimental setup in brief and subsequently, we will analyse the experimental results.

6.5.1 Experimental Setup

Vehicle Platform

In the experiment, we used real autonomous robots, Mona [1], that approximate the longitudinal dynamics of a vehicle. Mona is a low-cost, open-source, miniature robot which has been developed for swarm robotic applications and is used in this work. Mona houses two DC gear-head motors connected directly to its wheels having 32mm diameter and it has a circular chassis having diameter equal to 80mm. The main processor is an AVR microcontroller equipped with an external clock of 16MHz frequency. A NRF24l01 wireless transceiver module is equipped on each robot to achieve inter-communication. The robot is developed based on the Arduino Mini/Pro architecture that facilitates to use all existing open-source libraries associated with the Arduino boards.

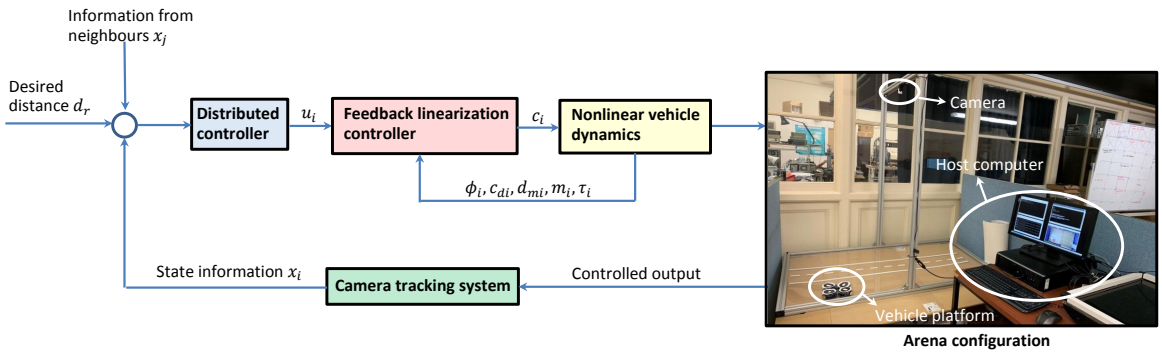

Figure 6.5: Hardware control loop associated with the experiment. Experimental arena includes overhead camera tracking system, base station (i.e. the desktop), aluminium framed glass platform and the Mona robots.

Experimental Platform

As shown in Fig. 6.5, the experimental platform includes a digital camera connected to a PC which runs the tracking system, arena frame and walls made of aluminium strut profile and wooden floor. The tracking system used in this work is an open-source multi-robotic localization system [98]. The tracking system can track the positions and orientations of the robots using their unique circular tags which are placed on top of the robots. The position information are transmitted to the controller via ROS communication framework. Note that the over-head camera can be easily removed in real implementation if the automated vehicles are equipped with on-board communication and positioning modules. For example, the road information (e.g., lane width, lane curvature) and the surrounding vehicles information (e.g., relative distance, relative speed) can be recorded by Mobileye used in [153].

6.5.2 Experimental Results

In the experiment, a platoon of six connected vehicles is considered which consists of two lanes as shown in Fig. 6.6. There are three vehicles in each lane which are bidirectionally connected. All vehicles are moving in one dimension from left to right direction on the glass board since only longitudinal motion has been considered. Fig. 6.6(a) shows the initial rest position of the robots (i.e. the vehicles) in the platoon. The platoon is then brought into motion at $t > 0$ by applying an external input to the leader as seen in Fig. 6.6(b). Note here that the initial acceleration in any vehicle can be considered as a temporary

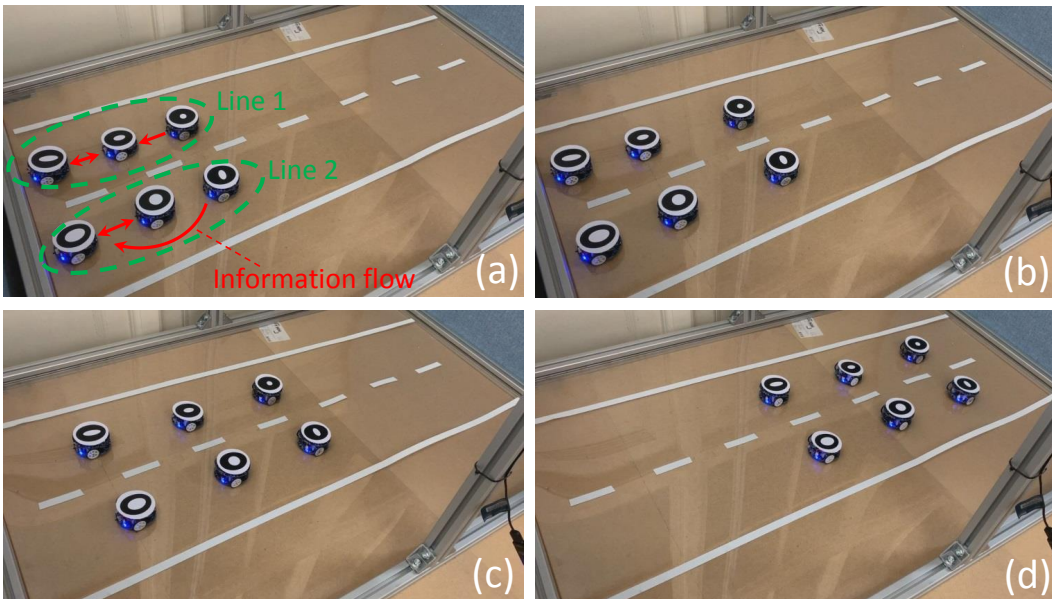

Figure 6.6: Experimental results: course of motion of a two-lane platoon containing six connected vehicles, all represented by Mona robots, in the experimental arena. (a) Initial rest position for all vehicles at $t = 0$s; (b) Lead vehicles has acquired the longitudinal motion from rest at $t > 0$; (c) Following vehicles gradually catch the velocity of the leaders and the desired inter-vehicular spacing is restored; and (d) At $t = 45$s, the platoon (both the lanes) reaches the other end of the arena – mission accomplished.

bounded disturbance input since the platoon as a whole has been shown to be platoon-stable under the influence of the proposed control scheme. Similar theoretical viewpoint was established in [150]. The notion remains applicable when a vehicle decelerates for taking a turn. Due to communication delay, the follower vehicles cannot catch up with the velocity of the leader instantaneously. As a result, at the beginning, spacing between the leader and the immediate follower becomes more than the desired spacing, but gradually the followers get synchronized with the leader and also restore equal inter-vehicular spacing at the steady-state. Fig. 6.6(c) reflects this situation. Fig. 6.6(d) indicates that the platoon has reached its destination (i.e. the right end of the glass board) at $t = 45$s satisfying all the platoon control objectives. Thus the mission is accomplished with the proposed platoon control scheme, which demonstrates the feasibility and effectiveness of the scheme in hardware experiment with real robots leading to its possible application in platoon control of real vehicles. Fig. 6.7(a) and 6.7(b) complement the experimental results shown in Fig. 6.6(a)-6.6(d) by providing the time variation of the positions $p_i(t)$ and velocities $v_i(t)$ of the vehicles and the associated spacing error $\varepsilon_i(t)$. We observe from Fig 6.7(a) that velocities of the followers in Lane 1 start rising in accordance with the leader from $t = 4$ s onwards,

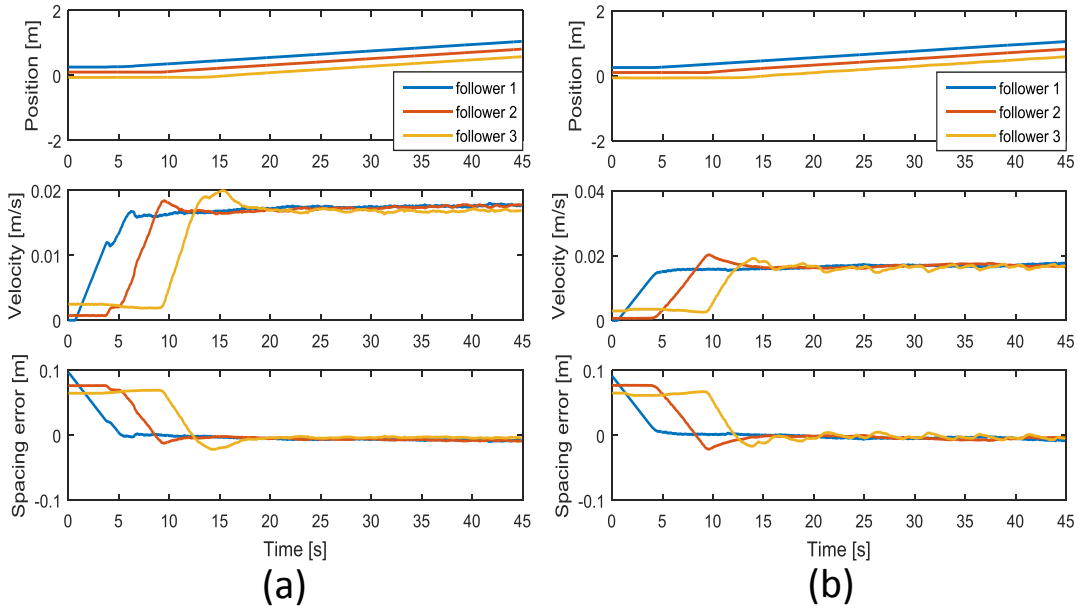

Figure 6.7: Time evolvement of position $p(t)$, velocity $v(t)$ and spacing error $\varepsilon(t)$ of the leader and following vehicles during the experiment with real Mona robots: (a) For the vehicles in Lane 1; (b) For the vehicles in Lane 2.

reach the leader around $t = 20$ s and remain synchronized until the end. The graph for the spacing error is in agreement with this fact. It shows that the spacing error between any two vehicles decays to zero at the same time around $t = 20$ s and remains zero throughout the rest of the experiment. The same conclusion can be drawn for the vehicles in Lane 2 as illustrated in Fig. 6.7(b).

6.6 Conclusions

In this chapter, we have introduced a two-layer decentralized and adaptive control scheme for heterogeneous connected vehicle platoon, which exploits first an input-output feedback linearization technique to linearize the nonlinear vehicle dynamics and then applies a distributed cooperative control law to serve the platoon control objectives. The proposed methodology ensures equal and constant inter-vehicular spacing between successive vehicles along with maintaining a desired cruising velocity of the platoon when the lead vehicle runs at constant velocity. Furthermore, the platoon stability of the platoon is preserved even when the lead vehicle is disturbed by exogenous disturbances (for example, due to acceleration/deceleration). It is investigated that the acceleration feedback, in addition to position

and velocity feedback, improves the platoon stability and reliability of the proposed scheme. Simulation results shows satisfactory performance of the platoon control scheme in presence of leader's disturbance which is then further validated by real-time hardware experiments with Mona robots.

In the future, more challenging and realistic situations (e.g. when the road is uneven or there is turning, when a vehicle at the middle of a platoon breaks down or starts malfunctioning due to hardware faults, when the vehicles move along uphill or downhill roads, etc.) shall be taken into account by improving the proposed platoon control scheme using outer-loop optimization, game theoretic and artificial intelligence techniques. Furthermore, the proposed scheme shall be validated with more sophisticated experimental platforms including full-sized real cars in a controlled environment.

Chapter 7

Conclusions

In this chapter the main contributions of this thesis are summarised and possible directions of future research are explored. The aim of this thesis is to generate advanced formation control techniques for multi-agent systems (MASs), and to find possible real world applications using the proposed distributed control algorithms.

7.1 Contributions

The main contributions of this thesis are summarised below.

- A distributed, adaptive and nonlinear control protocol has been introduced to achieve TGFT for linear MASs having directed communication topology. The control objectives also include sub-formation and tracking, that is, the followers are divided into several subgroups depending on the positions of the leaders and each subgroup reaches individual sub-formations while tracking the positions of the respective leaders attached to that subgroup. In contrast to existing literature, the proposed result addresses the group formation tracking problem where each subgroup can have multiple leaders and the leaders may have separate control inputs. The proposed control technique is fully distributed as it requires only the relative state information and does not need to calculate the eigenvalues of the graph Laplacian. The advantage of using

an appropriate blending of adaptive and nonlinear control techniques is to render the proposed control scheme robust to network topology changes and unknown inputs to the leaders.

- A fully distributed formation-containment problem for linear MASs with directed graphs has been investigated. A two-layer control architecture is proposed to solve the formation-containment problem, which consists of the leaders' formation layer and the followers' containment layer. To achieve formation-containment, distributed adaptive protocols are constructed based on relative state information, which made the proposed control design fully distributed without using global information about the interaction topology. Then, algorithms are presented to construct the control laws by testing formation feasibility condition and solving algebraic Riccati equation. The stability of the proposed scheme is proved by Lyapunov theory. Moreover, it is proved that the states of followers not only converge into the convex hull spanned by those of leaders but also maintain certain formation determined by the leaders and the virtual agent. Finally, the effectiveness of the proposed strategy is verified by numerical simulations with formation-containment tasks of networked satellites and real-hardware experiments with mobile robots.

- A formation tracking problem of a networked tri-rotor UAV swarm has been solved using a distributed formation control protocol. To achieve this, a robust feedback linearization controller was first developed to deal with this highly coupled and nonlinear tri-rotor UAV to achieve a feedback linearized system through geometric transformation that is valid at any operating point. The technique preserves robustness as it does not invert all nonlinear dynamics, unlike classic feedback linearization. An distributed optimal formation tracking control protocol was then developed for the tri-rotor robotic swarm, which guarantees that the target time-varying position and time-varying attitude of each UAV can be achieved independently. Finally, simulation results were given in a realistic environment based on 3D graphical display and physical visualisations. It has been shown that the proposed tri-rotor UAV swarm is able to track a desired time-varying formation whilst independently tracking different time-varying attitudes. A target surveillance task was performed effectively by these tri-rotor UAVs, which lays the foundation for some more complex collaborative tasks

to be explored.

- A decentralized and adaptive control scheme for heterogeneous connected vehicle platoon has been developed, which exploits first an input-output feedback linearization technique to linearize the nonlinear vehicle dynamics and then applies a distributed cooperative control law to serve the platoon control objectives. The proposed methodology ensures equal and constant inter-vehicular spacing between successive vehicles along with maintaining a desired cruising velocity of the platoon when the lead vehicle runs at constant velocity. Furthermore, the string stability of the platoon is preserved even when the lead vehicle is disturbed by exogenous disturbances (for example, due to acceleration/deceleration). It is investigated that the acceleration feedback, in addition to position and velocity feedback, improves the string stability and reliability of the proposed scheme. Simulation results shows satisfactory performance of the platoon control scheme in presence of leader's disturbance which is then further validated by real-time hardware experiments with mobile robots.

7.2 Future Works

Some possible future research directions are outlined below.

- In this thesis, most of the novel formation control techniques are developed for linear homogeneous/heterogeneous MASs. How to deal with the nonlinearities and external disturbances observed in the agent dynamics will be investigated.
- Some high-level swarm intelligence and decision making methods will be integrated with the current formation control framework such that the collaborative multi-agent system will become more smart.
- Robot localization, fault detection and obstacle avoidance are also very important in the experimental implementation. Outdoor experiments involving field robotics and full-size real car will be conducted in the future.
- The collaboration between aerial vehicles and ground vehicles for a complicated task is also an interesting direction.

Bibliography

[1] Farshad Arvin, Jose Espinosa, Benjamin Bird, Andrew West, Simon Watson, and Barry Lennox. Mona: an affordable open-source mobile robot for education and research. *Journal of Intelligent & Robotic Systems*, pages 1–15, 2018.

[2] Mohamed Kara Mohamed and Alexander Lanzon. Design and control of novel tri-rotor UAV. In *Proceedings of the 2012 UKACC International Conference on Control*, pages 304–309, Cardiff, UK, 2012.

[3] Ying Tan and Zhong-Yang Zheng. Research advance in swarm robotics. *Defense Technology*, 9:18–39, 2013.

[4] Manuele Brambilla, Eliseo Ferrante, Mauro Birattari, and Marco Dorigo. Swarm robotics: a review from the swarm engineering perspective. *Swarm Intelligence*, 7(1):1–41, 2013.

[5] Farshad Arvin, Ali Emre Turgut, Tomas Krajnik, and Shigang Yue. Investigation of cue-based aggregation in static and dynamic environments with a mobile robot swarm. *Adaptive Behaviour*, 24(2):102–118, 2016.

[6] Gianluca Antonelli, Filippo Arrichiello, and Stefano Chiaverini. The entrapment/escorting mission. *IEEE Robotics and Automation Magazine*, 15(1):22–29, 2008.

[7] Marco Dorigo, Dario Floreano, Luca Maria Gambardella, Francesco Mondada, Stefano Nolfi, Tarek Baaboura, Mauro Birattari, Michael Bonani, Manuele Brambilla, Arne Brutschy, et al. Swarmanoid: A novel concept for the study of heterogeneous robotic swarms. *IEEE Robotics and Automation Magazine*, 20(4):60–71, 2013.

[8] Farshad Arvin, Ali Emre Turgut, and Shigang Yue. Fuzzy-based aggregation with a mobile robot swarm. In *International Conference on Swarm Intelligence*, pages 346–347. Springer, 2012.

[9] Saptarshi Bandyopadhyay, Soon-Jo Chung, and Fred Y. Hadaegh. Probabilistic and distributed control of a large-scale swarm of autonomous agents. *IEEE Transactions on Robotics*, 33(5):1103–1123, 2017.

[10] Tomas Krajnik, Matias Nitsche, Jan Faigl, Petr Vanek, Martin Saska, Libor Preucil, Tom Duckett, and Marta Mejail. A practical multirobot localization system. *Journal of Intelligent and Robotic Systems*, 76(3-4):539–562, 2014.

[11] Eliseo Ferrante, Ali Emre Turgut, Marco Dorigo, and Cristian Huepe. Elasticity-based mechanism for the collective motion of self-propelled particles with springlike interactions: A model system for natural and artificial swarms. *Physical Review Letters*, 111(26):268302–1 – 268302–5, 2013.

[12] Ben Grocholsky, JAMES Keller, VIJAY Kumar, and GEORGE Pappas. Cooperative air and ground surveillance. *IEEE Robotics and Automation Magazine*, 13(3):16–25, 2006.

[13] Junyan Hu and Alexander Lanzon. An innovative tri-rotor drone and associated distributed aerial drone swarm control. *Robotics and Autonomous Systems*, 103:162–174, 2018.

[14] Jan Faigl, Tomas Krajnik, Vojtech Vonasek, and Libor Preucil. On localization uncertainty in an autonomous inspection. In *In: Proceedings of the IEEE International Conference on Robotics and Automation*, pages 1119–1124, 2012.

[15] Junyan Hu, Parijat Bhowmick, and Alexander Lanzon. Distributed adaptive time-varying group formation tracking for multi-agent systems with multiple leaders on directed graphs. *IEEE Transactions on Control of Network Systems*, Early Access. DOI:10.1109/TCNS.2019.2913619.

[16] Vojtech Spurny, Tomas Baca, Martin Saska, Robert Penicka, Tomas Krajnik, Justin

Thomas, Dinesh Thakur, Giuseppe Loianno, and Kumar Vijoy. Cooperative autonomous search, grasping, and delivering in a treasure hunt scenario by a team of unmanned aerial vehicles. *Journal of Field Robotics*, 36:125–148, 2018.

[17] Max Schwarz, Tobias Rodehutskors, David Droeschel, Marius Beul, Michael Schreiber, Nikita Araslanov, Ivan Ivanov, Christian Lenz, Jan Razlaw, Sebastian Schüller, et al. Nimbro rescue: Solving disaster-response tasks with the mobile manipulation robot momaro. *Journal of Field Robotics*, 34(2):400–425, 2017.

[18] Fernando Alfredo Auat Cheein and Ricardo Carelli. Agricultural robotics: Unmanned robotic service units in agricultural tasks. *IEEE Industrial Electronics Magazine*, 7(3):48–58, 2013.

[19] D. C. Slaughter, D. K. Giles, and D. Downey. Autonomous robotic weed control systems: A review. *Computers and Electronics in Agriculture*, 61(1):63–78, 2008.

[20] C. Zhang and J. M. Kovacs. The application of small unmanned aerial systems for precision agriculture: a review. *Precision Agriculture*, 13(6):693–712, 2012.

[21] Bruce Donaldson Grieve, Tom Duckett, Martin Collison, Lesley Boyd, Jon West, Hujun Yin, Farshad Arvin, and Simon Pearson. The challenges posed by global broadacre crops in delivering smart agri-robotic solutions: A fundamental rethink is required. *Global Food Security*, 23:116–124, 2019.

[22] Kazuya Yoshida. Achievements in space robotics. *IEEE Robotics and Automation Magazine*, 16(4):20–28, 2009.

[23] L. Yliniemi, A. K. Agogino, and K. Tumer. Multirobot coordination for space exploration. *AI Magazine*, 35(4):61–74, 2014.

[24] Jianing Chen, Melvin Gauci, Wei Li, Andreas Kolling, and Roderich Grob. Occlusion-based cooperative transport with a swarm of miniature mobile robots. *IEEE Transactions on Robotics*, 31(2):307–321, 2015.

[25] He Bai and John T. Wen. Cooperative load transport: A formation-control perspective. *IEEE Transactions on Robotics*, 26(4):742–750, 2010.

[26] Eliseo Ferrante, Ali Emre Turgut, Nithin Mathews, Mauro Birattari, and Marco Dorigo. Flocking in stationary and non-stationary environments: a novel communication strategy for heading alignment. In *International Conference on Parallel Problem Solving from Nature*, pages 331–340. Springer, 2010.

[27] Jianan Wang, Alexander Lanzon, and Ian R Petersen. Robust output feedback consensus for networked negative-imaginary systems. *IEEE Transactions on Automatic Control*, 60(9):2547–2552, 2015.

[28] Junyan Hu and Alexander Lanzon. Distributed finite-time consensus control for heterogeneous battery energy storage systems in droop-controlled microgrids. *IEEE Transactions on Smart Grid*, 10(5):4751–4761, 2019.

[29] Jianan Wang, Alexander Lanzon, and Ian R Petersen. Robust cooperative control of multiple heterogeneous negative-imaginary systems. *Automatica*, 61:64–72, 2015.

[30] Miguel Aranda, Gonzalo López-Nicolás, Carlos Sagüés, and Youcef Mezouar. Formation control of mobile robots using multiple aerial cameras. *IEEE Transactions on Robotics*, 31(4):1064–1071, 2015.

[31] Javier Alonso-Mora, Stuart Baker, and Daniela Rus. Multi-robot formation control and object transport in dynamic environments via constrained optimization. *The International Journal of Robotics Research*, 36(9):1000–1021, 2017.

[32] Gianluca Antonelli, Filippo Arrichiello, Fabrizio Caccavale, and Alessandro Marino. Decentralized time-varying formation control for multi-robot systems. *The International Journal of Robotics Research*, 33(7):1029–1043, 2014.

[33] Hector Garcia De Marina, Bayu Jayawardhana, and Ming Cao. Distributed rotational and translational maneuvering of rigid formations and their applications. *IEEE Transactions on Robotics*, 32(3):684–697, 2016.

[34] Javier Alonso-Mora, Eduardo Montijano, Tobias Nägeli, Otmar Hilliges, Mac Schwager, and Daniela Rus. Distributed multi-robot formation control in dynamic environments. *Autonomous Robots*, pages 1–22, 2018.

[35] Herbert G. Tanner, George J. Pappas, and Vijoy Kumar. Leader-to-formation stability. *IEEE Transactions on Robotics and Automation*, 20(3):443–455, 2004.

[36] Soon-Jo Chung and Jean-Jacques E. Slotine. Cooperative robot control and concurrent synchronization of lagrangian systems. *IEEE Transactions on Robotics*, 25(3):686–700, 2009.

[37] Jaydev P. Desai, James P. Ostrowski, and Vijay Kumar. Modeling and control of formations of nonholonomic mobile robots. *IEEE Transactions on Robotics and Automation*, 17(6):905–908, 2001.

[38] Javier Alonso-Mora, Paul Beardsley, and Roland Siegwart. Cooperative collision avoidance for nonholonomic robots. *IEEE Transactions on Robotics*, 34(2):404–420, 2018.

[39] Akshit Saradagi, Vijay Muralidharan, Vishaal Krishnan, Sandeep Menta, and Arun D Mahindrakar. Formation control and trajectory tracking of nonholonomic mobile robots. *IEEE Transactions on Control Systems Technology*, (99):1–9, 2017.

[40] Yongcan Cao, Daniel Stuart, Wei Ren, and Ziyang Meng. Distributed containment control for multiple autonomous vehicles with double-integrator dynamics: algorithms and experiments. *IEEE Transactions on Control Systems Technology*, 19(4):929–938, 2011.

[41] Zhongkui Li, Zhisheng Duan, Wei Ren, and Gang Feng. Containment control of linear multi-agent systems with multiple leaders of bounded inputs using distributed continuous controllers. *International Journal of Robust and Nonlinear Control*, 25(13):2101–2121, 2015.

[42] Ziyang Meng, Wei Ren, and Zheng You. Distributed finite-time attitude containment control for multiple rigid bodies. *Automatica*, 46(12):2092–2099, 2010.

[43] Reihane Rahimi, Farzaneh Abdollahi, and Karo Naqshi. Time-varying formation control of a collaborative heterogeneous multi agent system. *Robotics and Autonomous Systems*, 62(12):1799–1805, 2014.

[44] Ryuma Maeda, Takahiro Endo, and Fumitoshi Matsuno. Decentralized navigation for heterogeneous swarm robots with limited field of view. *IEEE Robotics and Automation Letters*, 2(2):904–911, 2017.

[45] Haibo Du, Wenwu Zhu, Guanghui Wen, Zhisheng Duan, and Jinhu Lü. Distributed formation control of multiple quadrotor aircraft based on nonsmooth consensus algorithms. *IEEE Transactions on Cybernetics*, (In press). DOI:10.1109/TCYB.2017.2777463.

[46] Xiwang Dong, Qingdong Li, Qilun Zhao, and Zhang Ren. Time-varying group formation analysis and design for general linear multi-agent systems with directed topologies. *International Journal of Robust and Nonlinear Control*, 27(9):1640–1652, 2017.

[47] Jiahu Qin and Changbin Yu. Cluster consensus control of generic linear multi-agent systems under directed topology with acyclic partition. *Automatica*, 49(9):2898–2905, 2013.

[48] Omur Arslan, Dan P Guralnik, and Daniel E Koditschek. Coordinated robot navigation via hierarchical clustering. *IEEE Transactions on Robotics*, 32(2):352–371, 2016.

[49] Junyan Hu, Parijat Bhowmick, Farshad Arvin, Alexander Lanzon, and Barry Lennox. Cooperative control of heterogeneous connected vehicle platoons: An adaptive leader-following approach. *IEEE Robotics and Automation Letters*, 5(2):977–984, 2020.

[50] Roger A Horn and Charles R Johnson. *Matrix analysis*. Cambridge university press, 2012.

[51] Hongwei Zhang, Frank L Lewis, and Zhihua Qu. Lyapunov, adaptive, and optimal design techniques for cooperative systems on directed communication graphs. *IEEE Transactions on Industrial Electronics*, 59(7):3026–3041, 2012.

[52] Dennis S Bernstein. *Matrix mathematics: Theory, facts, and formulas with application to linear systems theory*. Princeton University Press, Princeton, USA, 2005.

[53] Kemin Zhou, John Comstock Doyle, Keith Glover, et al. *Robust and optimal control*, volume 40. Prentice hall New Jersey, 1996.

[54] Z. Ding. *Nonlinear and Adaptive Control Systems*. IET CONTROL ENGINEERING SERIES. Institution of Engineering and Technology, 2013.

[55] Hassan K Khalil. *Noninear Systems*. Prentice-Hall, New Jersey, USA, 1996.

[56] Wei Ren and Randal W Beard. Consensus seeking in multiagent systems under dynamically changing interaction topologies. *IEEE Transactions on Automatic Control*, 50(5):655–661, 2005.

[57] Hasan A Poonawala, Aykut C Satici, Hazen Eckert, and Mark W Spong. Collision-free formation control with decentralized connectivity preservation for nonholonomic-wheeled mobile robots. *IEEE Transactions on Control of Network Systems*, 2(2):122–130, 2015.

[58] Arjun Nagendran, William Crowther, Martin Turner, Alexander Lanzon, and Robert Richardson. Design, control, and performance of the 'weed' 6 wheel robot in the UK MOD grand challenge. *Advanced Robotics*, 28(4):203–218, 2014.

[59] Bill Crowther, Alexander Lanzon, Martin Maya-Gonzalez, and David Langkamp. Kinematic analysis and control design for a nonplanar multirotor vehicle. *AIAA Journal of Guidance, Control, and Dynamics*, 34(4):1157–1171, 2011.

[60] G. Foderaro, P. Zhu, H. Wei, T. A. Wettergren, and S. Ferrari. Distributed optimal control of sensor networks for dynamic target tracking. *IEEE Transactions on Control of Network Systems*, 5(1):142–153, 2018.

[61] R. Deng, S. He, and J. Chen. An online algorithm for data collection by multiple sinks in wireless-sensor networks. *IEEE Transactions on Control of Network Systems*, 5(1):93–104, 2018.

[62] J. Sun, Z. Geng, Y. Lv, Z. Li, and Z. Ding. Distributed adaptive consensus disturbance rejection for multi-agent systems on directed graphs. *IEEE Transactions on Control of Network Systems*, 5(1):629–639, 2018.

[63] S. Zuo, Y. Song, F. L. Lewis, and A. Davoudi. Time-varying output formation-containment of general linear homogeneous and heterogeneous multi-agent systems. *IEEE Transactions on Control of Network Systems*, (in press), 2018. DOI:10.1109/TCNS.2018.2847039.

[64] Shiyu Zhao and Daniel Zelazo. Translational and scaling formation maneuver control via a bearing-based approach. *IEEE Transactions on Control of Network Systems*, 4(3):429–438, 2017.

[65] Matthew Turpin, Nathan Michael, and Vijay Kumar. Decentralized formation control with variable shapes for aerial robots. In *Proceedings of the IEEE International Conference on Robotics and Automation (ICRA)*, pages 23–30, 2012.

[66] Minh Hoang Trinh, Shiyu Zhao, Zhiyong Sun, Daniel Zelazo, Brian DO Anderson, and Hyo-Sung Ahn. Bearing-based formation control of a group of agents with leader-first follower structure. *IEEE Transactions on Automatic Control*, (In press), 2018. DOI:10.1109/TAC.2018.2836022.

[67] Chunyan Wang, Hilton Tnunay, Zongyu Zuo, Barry Lennox, and Zhengtao Ding. Fixed-time formation control of multi-robot systems: Design and experiments. *IEEE Transactions on Industrial Electronics*, (In press), 2018. DOI:10.1109/TIE.2018.2870409.

[68] Xiuxian Li and Lihua Xie. Dynamic formation control over directed networks using graphical laplacian approach. *IEEE Transactions on Automatic Control*, (In press), 2018. DOI:10.1109/TAC.2018.2798808.

[69] Shiyu Zhao. Affine formation maneuver control of multi-agent systems. *IEEE Transactions on Automatic Control*, (In press), 2018. DOI:10.1109/TAC.2018.2798805.

[70] Xiwang Dong, Bocheng Yu, Zongying Shi, and Yisheng Zhong. Time-varying formation control for unmanned aerial vehicles: Theories and applications. *IEEE Transactions on Control Systems Technology*, 23(1):340–348, 2015.

[71] Xiwang Dong, Yan Zhou, Zhang Ren, and Yisheng Zhong. Time-varying formation tracking for second-order multi-agent systems subjected to switching topologies with application to quadrotor formation flying. *IEEE Transactions on Industrial Electronics*, 64(6):5014–5024, 2017.

[72] Zhongkui Li and Zhisheng Duan. *Cooperative control of multi-agent systems: a consensus region approach*. CRC Press, 2014.

[73] Rui Wang, Xiwang Dong, Qingdong Li, and Zhang Ren. Distributed adaptive time-varying formation for multi-agent systems with general high-order linear time-invariant dynamics. *Journal of the Franklin Institute*, 353(10):2290–2304, 2016.

[74] Zhongkui Li, Michael ZQ Chen, and Zhengtao Ding. Distributed adaptive controllers for cooperative output regulation of heterogeneous agents over directed graphs. *Automatica*, 68:179–183, 2016.

[75] Weiguo Xia and Ming Cao. Clustering in diffusively coupled networks. *Automatica*, 47(11):2395–2405, 2011.

[76] Yuanzhen Feng, Shengyuan Xu, and Baoyong Zhang. Group consensus control for double-integrator dynamic multiagent systems with fixed communication topology. *International Journal of Robust and Nonlinear Control*, 24(3):532–547, 2014.

[77] Xiwang Dong, Qingdong Li, Qilun Zhao, and Zhang Ren. Time-varying group formation analysis and design for second-order multi-agent systems with directed topologies. *Neurocomputing*, 205:367–374, 2016.

[78] Yuezu Lv, Zhongkui Li, Zhisheng Duan, and Gang Feng. Novel distributed robust adaptive consensus protocols for linear multi-agent systems with directed graphs and external disturbances. *International Journal of Control*, 90(2):137–147, 2017.

[79] Fuzhen Zhang. *The Schur complement and its applications*. Springer Science & Business Media, 2006.

[80] Daniel Shevitz and Brad Paden. Lyapunov stability theory of nonsmooth systems. *IEEE Transactions on Automatic Control*, 39(9):1910–1914, 1994.

[81] Xiwang Dong and Guoqiang Hu. Time-varying formation tracking for linear multi-agent systems with multiple leaders. *IEEE Transactions on Automatic Control*, 62(7):3658–3664, 2017.

[82] Junyan Hu and Alexander Lanzon. Cooperative adaptive time-varying formation tracking for multi-agent systems with LQR performance index and switching directed topologies. pages 5102–5107. In: Proceedings of IEEE Conference on Decision and Control, 2018.

[83] Feng Xiao, Long Wang, Jie Chen, and Yanping Gao. Finite-time formation control for multi-agent systems. *Automatica*, 45(11):2605–2611, 2009.

[84] Wei Ren. Consensus strategies for cooperative control of vehicle formations. *IET Control Theory & Applications*, 1(2):505–512, 2007.

[85] Haibo Du, Shihua Li, and Xiangze Lin. Finite-time formation control of multiagent systems via dynamic output feedback. *International Journal of Robust and Nonlinear Control*, 23(14):1609–1628, 2013.

[86] J Alexander Fax and Richard M Murray. Information flow and cooperative control of vehicle formations. *IEEE Transactions on Automatic Control*, 49(9):1465–1476, 2004.

[87] Maurizio Porfiri, D Gray Roberson, and Daniel J Stilwell. Tracking and formation control of multiple autonomous agents: A two-level consensus approach. *Automatica*, 43(8):1318–1328, 2007.

[88] Zhongkui Li, Wei Ren, Xiangdong Liu, and Mengyin Fu. Distributed containment control of multi-agent systems with general linear dynamics in the presence of multiple leaders. *International Journal of Robust and Nonlinear Control*, 23(5):534–547, 2013.

[89] Yongcan Cao, Wei Ren, and Magnus Egerstedt. Distributed containment control with multiple stationary or dynamic leaders in fixed and switching directed networks. *Automatica*, 48(8):1586–1597, 2012.

[90] Jie Mei, Wei Ren, and Guangfu Ma. Distributed containment control for lagrangian networks with parametric uncertainties under a directed graph. *Automatica*, 48(4):653–659, 2012.

[91] Liang-Ming Chen, Chuan-Jiang Li, Jie Mei, and Guang-Fu Ma. Adaptive cooperative formation-containment control for networked euler–lagrange systems without using relative velocity information. *IET Control Theory & Applications*, 11(9):1450–1458, 2017.

[92] Chuanjiang Li, Liangming Chen, Yanning Guo, and Guangfu Ma. Formation–containment control for networked euler–lagrange systems with input saturation. *Nonlinear Dynamics*, 91(2):1307–1320, 2018.

[93] Liangming Chen, Chuanjiang Li, Bing Xiao, and Yanning Guo. Formation-containment control of networked euler–lagrange systems: An event-triggered framework. *ISA transactions*, 86:87–97, 2019.

[94] Huiyang Liu, Long Cheng, Min Tan, Zengguang Hou, Zhiqiang Cao, and Ming Wang. Containment control with multiple interacting leaders under switching topologies. *Proceedings of 32nd Chinese Control Conference (CCC)*, 1:7093–7098, 2013.

[95] Baojie Zheng and Xiaowu Mu. Formation-containment control of second-order multi-agent systems with only sampled position data. *International Journal of Systems Science*, 47(15):3609–3618, 2016.

[96] Xiwang Dong, Zongying Shi, Geng Lu, and Yisheng Zhong. Formation-containment analysis and design for high-order linear time-invariant swarm systems. *International Journal of Robust and Nonlinear Control*, 25(17):3439–3456, 2015.

[97] Yan-Wu Wang, Xiao-Kang Liu, Jiang-Wen Xiao, and Xiangning Lin. Output formation-containment of coupled heterogeneous linear systems under intermittent communication. *Journal of the Franklin Institute*, 354(1):392–414, 2017.

[98] Tomáš Krajník, Matías Nitsche, Jan Faigl, Petr Vaněk, Martin Saska, Libor Přeučil, Tom Duckett, and Marta Mejail. A practical multirobot localization system. *Journal of Intelligent & Robotic Systems*, 76(3-4):539–562, 2014.

[99] Alexander Lanzon and Hsueh-Ju Chen. Feedback stability of negative imaginary systems. *IEEE Transactions on Automatic Control*, 62(11):5620–5633, 2017.

[100] Zhuoyue Song, Alexander Lanzon, Sourav Patra, and Ian R Petersen. Robust performance analysis for uncertain negative-imaginary systems. *International Journal of Robust and Nonlinear Control*, 22(3):262–281, 2012.

[101] Robert Mahony, Vijay Kumar, and Peter Corke. Multirotor aerial vehicles: Modeling, estimation, and control of quadrotor. *IEEE Robotics & Automation Magazine*, 19(3):20–32, 2012.

[102] Madhubhashi Senanayake, Ilankaikone Senthooran, Jan Carlo Barca, Hoam Chung, Joarder Kamruzzaman, and Manzur Murshed. Search and tracking algorithms for swarms of robots: A survey. *Robotics and Autonomous Systems*, 75:422–434, 2016.

[103] Philipp Lottes, Raghav Khanna, Johannes Pfeifer, Roland Siegwart, and Cyrill Stachniss. UAV-based crop and weed classification for smart farming. In *Proceeding of the IEEE International Conference on Robotics and Automation (ICRA)*, pages 3024–3031, 2017.

[104] Amit Shukla and Hamad Karki. Application of robotics in onshore oil and gas industrya review part I. *Robotics and Autonomous Systems*, 75:490–507, 2016.

[105] Bill Crowther, Alexander Lanzon, Martin Maya-Gonzalez, and David Langkamp. Kinematic analysis and control design for a nonplanar multirotor vehicle. *AIAA Journal of Guidance, Control, and Dynamics*, 34(4):1157–1171, 2011.

[106] Mohamed Kara Mohamed and Alexander Lanzon. Effect of unmodelled actuator dynamics on feedback linearised systems and a two stage feedback linearisation method. In *Proceedings of the IEEE Conference on Decision and Control (CDC)*, pages 841–846, 2013.

[107] Scott Driessens and Paul Pounds. The triangular quadrotor: a more efficient quadrotor configuration. *IEEE Transactions on Robotics*, 31(6):1517–1526, 2015.

[108] Dong-Wan Yoo, Hyon-Dong Oh, Dae-Yeon Won, and Min-Jea Tahk. Dynamic modeling and stabilization techniques for tri-rotor unmanned aerial vehicles. *International Journal Aeronautical and Space Sciences*, 11(3):167–174, 2010.

[109] J Escareno, A Sanchez, O Garcia, and R Lozano. Triple tilting rotor mini-UAV: Modeling and embedded control of the attitude. In *Proceedings of the American Control Conference*, pages 3476–3481, 2008.

[110] Philippe Rongier, Erwann Lavarec, and François Pierrot. Kinematic and dynamic modeling and control of a 3-rotor aircraft. In *Proceedings of the IEEE International Conference on Robotics and Automation (ICRA)*, pages 2606–2611, 2005.

[111] Iñaki Navarro and Fernando Matía. An introduction to swarm robotics. *ISRN Robotics*, 2013, 2012.

[112] Rosario Aragues, Jorge Cortes, and C Sagues. Distributed consensus algorithms for merging feature-based maps with limited communication. *Robotics and Autonomous Systems*, 59(3):163–180, 2011.

[113] Jianan Wang and Ming Xin. Distributed optimal cooperative tracking control of multiple autonomous robots. *Robotics and Autonomous systems*, 60(4):572–583, 2012.

[114] Ruben Van Parys and Goele Pipeleers. Distributed mpc for multi-vehicle systems moving in formation. *Robotics and Autonomous Systems*, 97:144–152, 2017.

[115] Jianan Wang, Alexander Lanzon, and Ian R Petersen. Robust cooperative control of multiple heterogeneous negative-imaginary systems. *Automatica*, 61:64–72, 2015.

[116] Mohammad Hosseinzadeh Yamchi and Reza Mahboobi Esfanjani. Distributed predictive formation control of networked mobile robots subject to communication delay. *Robotics and Autonomous Systems*, 91:194–207, 2017.

[117] Wei Ren and Nathan Sorensen. Distributed coordination architecture for multi-robot formation control. *Robotics and Autonomous Systems*, 56(4):324–333, 2008.

[118] Kirill Ovchinnikov, Anna Semakova, and A Matveev. Cooperative surveillance of unknown environmental boundaries by multiple nonholonomic robots. *Robotics and Autonomous Systems*, 72:164–180, 2015.

[119] Masao Kubo, Hiroshi Sato, Tatsuro Yoshimura, Akihiro Yamaguchi, and Takahiro Tanaka. Multiple targets enclosure by robotic swarm. *Robotics and Autonomous Systems*, 62(9):1294–1304, 2014.

[120] Henrik Ebel, Ehsan Sharafian Ardakani, and Peter Eberhard. Distributed model predictive formation control with discretization-free path planning for transporting a load. *Robotics and Autonomous Systems*, 96:211–223, 2017.

[121] Ana Lùcia D Franco, Henri Bourlès, Edson R De Pieri, and Herve Guillard. Robust nonlinear control associating robust feedback linearization and H_∞ control. *IEEE Transactions on Automatic Control*, 51(7):1200–1207, 2006.

[122] Alexander Lanzon, Alessandro Freddi, and Sauro Longhi. Flight control of a quadrotor vehicle subsequent to a rotor failure. *AIAA Journal of Guidance, Control, and Dynamics*, 37(2):580–591, 2014.

[123] Hongwei Zhang, Frank L Lewis, and Abhijit Das. Optimal design for synchronization of cooperative systems: state feedback, observer and output feedback. *IEEE Transactions on Automatic Control*, 56(8):1948–1952, 2011.

[124] Alberto Isidori. *Nonlinear control systems*. Springer-Verlag, 1995.

[125] Xiwang Dong and Guoqiang Hu. Time-varying formation control for general linear multi-agent systems with switching directed topologies. *Automatica*, 73:47–55, 2016.

[126] Zhongkui Li, Zhisheng Duan, Guanrong Chen, and Lin Huang. Consensus of multi-agent systems and synchronization of complex networks: A unified viewpoint. *IEEE Transactions on Circuits and Systems I*, 57(1):213–224, 2010.

[127] Chi-Tsong Chen. *Linear system theory and design*. Oxford University Press, Inc., 1995.

[128] Dan Simon. *Optimal state estimation: Kalman, H infinity, and nonlinear approaches*. John Wiley & Sons, 2006.

[129] Rudolph E Kalman and Richard S Bucy. New results in linear filtering and prediction theory. *Journal of basic engineering*, 83(3):95–108, 1961.

[130] John C Doyle, Keith Glover, Pramod P Khargonekar, and Bruce A Francis. State-space solutions to standard H_2 and H_∞ control problems. *IEEE Transactions on Automatic Control*, 34(8):831–847, 1989.

[131] Mohinder S Grewal. Kalman filtering. In *International Encyclopedia of Statistical Science*, pages 705–708. Springer, 2011.

[132] Arvin Dehghani, Andrea Lecchini-Visintini, Alexander Lanzon, and Brian DO Anderson. Validating controllers for internal stability utilizing closed-loop data. *IEEE Transactions on Automatic Control*, 54(11):2719–2725, 2009.

[133] Madhav Patil, Tamer Abukhalil, Sarosh Patel, and Tarek Sobh. UB robot swarm – Design, implementation, and power management. In *proceedings of the IEEE International Conference on Control and Automation (ICCA)*, pages 577–582, 2016.

[134] Alexander Lanzon. Weight optimisation in H_∞ loop-shaping. *Automatica*, 41(7):1201–1208, 2005.

[135] Alexander Lanzon and George Papageorgiou. Distance measures for uncertain linear systems: A general theory. *IEEE Transactions on Automatic Control*, 54(7):1532–1547, 2009.

[136] Darbha Swaroop, J. Karl Hedrick, and S. B. Choi. Direct adaptive longitudinal control of vehicle platoons. *IEEE Transactions on Vehicular Technology*, 50(1):150–161, 2001.

[137] Ali Ghasemi, Reza Kazemi, and Shahram Azadi. Stable decentralized control of a platoon of vehicles with heterogeneous information feedback. *IEEE Transactions on Vehicular Technology*, 62(9):4299–4308, 2013.

[138] Theodore L Willke, Patcharinee Tientrakool, and Nicholas F Maxemchuk. A survey of inter-vehicle communication protocols and their applications. *IEEE Communications Surveys & Tutorials*, 11(2):3–20, 2009.

[139] Jeroen Ploeg, Dipan P Shukla, Nathan van de Wouw, and Henk Nijmeijer. Controller synthesis for string stability of vehicle platoons. *IEEE Transactions on Intelligent Transportation Systems*, 15(2):854–865, 2014.

[140] Gerrit J. L. Naus, Rene P. A. Vugts, Jeroen Ploeg, Marinus J. G. van de Molengraft, and Maarten Steinbuch. String-stable cacc design and experimental validation: A frequency-domain approach. *IEEE Transactions on Vehicular Technology*, 59(9):4268–4279, 2010.

[141] Jeroen Ploeg, Nathan van de Wouw, and Henk Nijmeijer. $\mathcal{L}_p$ string stability of cascaded systems: Application to vehicle platooning. *IEEE Transactions on Control Systems Technology*, 22(2):786–793, 2014.

[142] Lingyun Xiao and Feng Gao. Practical string stability of platoon of adaptive cruise control vehicles. *IEEE Transactions on Intelligent Transportation Systems*, 12(4):1183–1194, 2011.

[143] Ji-Wook Kwon and Dongkyoung Chwa. Adaptive bidirectional platoon control using a coupled sliding mode control method. *IEEE Transactions on Intelligent Transportation Systems*, 15(5):2040–2048, 2014.

[144] Xianggui Guo, Jianliang Wang, Fang Liao, and Rodney Swee Huat Teo. Distributed adaptive integrated-sliding-mode controller synthesis for string stability of vehicle platoons. *IEEE Transactions on Intelligent Transportation Systems*, 17(9):2419–2429, 2016.

[145] Ioannis M. Delimpaltadakis, Charalampos P. Bechlioulis, and Kostas J. Kyriakopoulos. Decentralized platooning with obstacle avoidance for car-like vehicles with limited sensing. *IEEE Robotics and Automation Letters*, 3(2):835–840, 2018.

[146] Nicholas Hyldmar, Yijun He, and Amanda Prorok. A fleet of miniature cars for experiments in cooperative driving. pages 1–7. In: Proceedings of IEEE International Conference on Robotics and Automation, 2019.

[147] Hsueh-Ju Chen, Alexander Lanzon, and Ian R Petersen. Conditions for preserving negative imaginary properties in feedback interconnections and an application to multi-agent systems. pages 1143–1147. In: Proceedings of 25th Mediterranean Conference on Control and Automation, 2017.

[148] Junyan Hu and Alexander Lanzon. Cooperative control of innovative tri-rotor drones using robust feedback linearization. pages 347–352. In: Proceedings of 12th UKACC International Conference on Control, 2018.

[149] Yang Zheng, Shengbo Eben Li, Keqiang Li, and Wei Ren. Platooning of connected vehicles with undirected topologies: Robustness analysis and distributed h-infinity controller synthesis. *IEEE Transactions on Intelligent Transportation Systems*, 19(5):1353–1364, 2018.

[150] Yang Zheng, Yougang Bian, Shengbo Eben Li, and Shen Li. Cooperative control of heterogeneous connected vehicles with directed acyclic interactions. *IEEE Intelligent Transportation Systems Magazine*, pages 1–16, 2019. DOI:10.1109/MITS.2018.2889654.

[151] Yuanheng Zhu, Dongbin Zhao, and Zhiguang Zhong. Adaptive optimal control of heterogeneous CACC system with uncertain dynamics. *IEEE Transactions on Control Systems Technology*, pages 1–8, 2019. DOI:10.1109/TCST.2018.2811376.

[152] Feng Xiao and Tongwen Chen. Adaptive consensus in leader-following networks of heterogeneous linear systems. *IEEE Transactions on Control of Network Systems*, 5(3):1169–1176, 2018.

[153] Wenshuo Wang and Ding Zhao. Extracting traffic primitives directly from naturalistically logged data for self-driving applications. *IEEE Robotics and Automation Letters*, 3(2):1223–1229, 2018.